# Site characterization and foundation design for the emplacement of radio telescope antennas at the Matjiesfontein Space Geodesy Observatory

by
Cornel Janse van Rensburg

*Thesis presented in fulfilment of the requirements for the degree of*
*Master of Engineering in the Faculty of Engineering at Stellenbosch University*

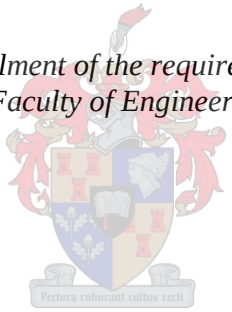


Supervisor: Mr Leon Croukamp

March 2017

## Declaration

By submitting this thesis electronically, I declare that the entirety of the work contained therein is my own, original work, that I am the authorship owner thereof (unless to the extent explicitly otherwise stated) and that I have not previously in its entirety or in part submitted it for obtaining any qualification.

Cornel Janse van Rensburg

March 2017

## Abstract

The suitability of the Matjiesfontein Space Geodesy Observatory (MSGO) site for hosting radio telescope antennas is partially dictated by certain civil engineering considerations. These include the investigated geotechnical and hydrological site characteristics. The engineering properties of different soil and rock types in the surrounding area were also investigated as their use as construction material may have cost implications for the project.

A GPS survey was carried out on the area earmarked for radio telescopes, which gave the researcher an opportunity to familiarize himself with the terrain and use the data for creating a digital terrain model (DTM) of the area. The geotechnical investigation followed and has shown encouraging results indicating shallow bedrock generally of hard to very hard rock consistency. This is a favourable founding condition for structures, but is particularly important in geodesy where instruments rely on stability to produce accurate results. The hydrological investigation has shown that, with even a very conservative steady flow analysis, the discharge in channels will not put infrastructure at risk of flooding in the event of heavy rainfall. Standard tests performed on local soil indicated a variety of soil types, mostly due to the different geomorphic processes in their origin as well as the varying geology in the area. Six disturbed samples of colluvial, alluvial and residual material were tested using the TMH1 (Technical Methods for Highways) to produce indicative characteristics of untreated local soil. They were then classified using the Unified Soil Classification System and the three main samples were classified for quality using TRH14 (Technical Recommendations for Highways). The materials were also evaluated as fine aggregate for concrete, selected fill for services and patching material for improving eroded sections of the access road. Petrographic results from a previous study indicated the presence of strained quartz in quartzitic sandstone from the site, rendering aggregate potentially susceptible to alkali-silica reaction. Tillite (Diamictite) of the Dwyka Formation in KwaZulu-Natal has also been identified as potentially reactive by laboratory testing. Quartzitic sandstone and tillite samples were subsequently collected from site and tested for alkali-silica reaction (ASR), resulting in almost none to innocuous expansion. These rocks were also tested for compressive strength, yielding strengths in excess of 70MPa. Based on these results and if found to be feasible, the possibility exists for loose boulders to be sourced, crushed and sorted locally for use as coarse aggregate in concrete, without causing any aesthetically displeasing affects to the environment.

A limit state design (LSD) approach for a SKA-type radio telescope foundation was undertaken using nominal loads obtained from the organization and characteristic material properties obtained from this study. The foundation was designed as a circular spread gravity footing with a diameter of 5.5m, the size being governed by equilibrium at the ultimate limit state (ULS). The most important conclusion is that the site is, in terms of its engineering properties, certainly suitable for conducting radio astronomy and geodetic experiments.

# Opsomming

Die geskiktheid van die “Matjiesfontein Space Geodesy Observatory” (MSGO) terrein vir die huisvesting van radioteleskoop antennas word gedeeltelik bepaal deur sekere siviele ingenieursoorwegings. Dit sluit die ondersoekde geotegniese en hidrologiese eienskappe van die terrein in. Die ingenieurseienskappe van verskillende grond- en rotstipes in die omliggende gebied was ook ondersoek aangesien die gebruik daarvan as konstruksiemateriaal koste-implikasies vir die projek mag inhou.

’n “GPS” opname was uitgevoer in die area geoormerk vir radioteleskope, wat die navorser die geleentheid gebied het om homself te vergewis met die terrein en die data te gebruik om ’n digitale terrein model (DTM) van die terrein te skep. Die geotegniese ondersoek het daarna gevolg en het goeie resultate opgelewer wat dui op ’n goeie gehalte vlak rotsbedding van harde tot baie harde materiaal. Dit is 'n gunstige toestand vir strukture, maar is veral belangrik vir geodesie waar instrumente staatmaak op stabiliteit om akkurate resultate op te lewer. Die hidrologiese ondersoek het getoon dat, selfs met ’n baie konserwatiewe bestendige vloei analise, die afloop in kanale nie infrastruktuur in gevaar van oorstroming sal plaas in die geval van swaar reënval nie. Standaard toetse op plaaslike grond het gedui op ’n verskeidenheid van grondtipes, as gevolg van die verskillende geomorfologiese prosesse sowel as die wisselende geologie in die gebied. Ses versteurde monsters van kolluviale, alluviale en residuele grond is getoets met behulp van die TMH1 (“Technical Methods for Highways”) om voorlopige eienskappe van onbehandelde plaaslike grond te verkry. Daarna was dit geklassifiseer met behulp van die “Unified Soil Classification” sisteem en die drie belangrikste monsters is verder geklassifiseer met behulp van die TRH14 (“Technical Recommendations for Highways”). Die materiaal was geëvalueer as fyn aggregaat vir beton, opvulmateriaal vir dienste en pleister-materiaal vir die verbetering van geërodeerde dele van die toegangspad. Petrografiese resultate uit ’n vorige studie het die teenwoordigheid van gespanne kwarts aangedui in die sandsteen van die terrein, wat aggregaat moontlik vatbaar maak vir alkali-silika reaksie. Tilliet (Diamiktiet) van die Dwyka Formasie in KwaZulu-Natal is in die literatuur geïdentifiseer as potensieel reaktief. Kwartsitiese sandsteen en tilliet monsters is gevolglik versamel en getoets vir alkali-silika reaktiwiteit (ASR), met byna geen tot weglaatbare uitsetting. Dié rots was ook getoets vir druksterkte, met sterktes bo 70MPa. Op grond van hierdie resultate en indien dit uitvoerbaar is, kan los rotse plaaslik versamel, gebreek en sorteer word vir gebruik as growwe aggregaat in beton, sonder enige negatiewe ongewensde effekte op die omgewing.

’n Limietstaat ontwerp (LSD) benadering vir die fondasie van ’n SKA-tipe radioteleskoop was gedoen met behulp van nominale laste verkry vanaf die organisasie en karakteristieke materiaaleienskappe vanuit dié studie. Die fondasie is ontwerp as ’n ronde plat voetstuk met 'n diameter van 5.5m, bepaal deur ewewig by die uiteindelike limietstaat (ULS). Die hoof gevolgtrekking is dat die terrein geskik is, in terme van sy ingenieurseienskappe, vir die uitvoer van radio-astronomie en geodetiese eksperimente.

## Acknowledgements

I would like to express my deepest gratitude to Mr Leon Croukamp as my supervisor and for allowing me to take part in this project. I also want to thank Inkaba Ye'Afrika for the financial support they have offered me during this study.

I further want to extend my gratitude to Dr Marius de Wet and Mrs Chantal Rudman for always being available to offer advice when needed. I want to thank Ms Susan Bothma for her aid in gathering and compiling the different survey datasets. I am very thankful towards Mrs Nanine Fouché for sharing her experience in core logging, which contributed greatly to this study. I want to thank Ms Danél van Tonder for her descriptions of the rock and mortar samples and for giving me the opportunity to look at the thin sections through the petrographic microscope. I want to thank Mr Salhin Alaud for introducing me to and letting me use his experimental setup for testing alkali-silica reactivity of aggregates and Mr Johan van der Merwe for his assistance in the design and production of the moulds. I would also like to thank Dr Bertie Oberholster and Mr Bertus Fonternel for their constructive discussions on the interpretation of the mortar-bar test and soil results, respectively. Furthermore, I want to express appreciation to Mr Pierre van der Spuy for sharing his knowledge on foundation design and Dr Peter Day for his review of the design along with the invaluable comments he made. The assistance provided by the geotechnical and transport laboratory staff is greatly appreciated. I also want to thank Roelof Lategan from Roadlab in Upington and Marjo Hofman from Geoscience Laboratories in Cape Town for their technical assistance and allowing me to use their facilities free of charge.

I finally wish to thank the people from Matjiesfontein for their hospitality and everyone else who were kind enough to lend their support.

# Dedications

It is with great gratitude that I dedicate this work and the degree that accompanies it to my loving parents, Louis and Luise Janse van Rensburg, whom have always supported me unconditionally.

# Table of Contents

# List of Figures

# List of Tables

# List of Abbreviations

| | |
|---|---|
| ASR | Alkali-Silica Reaction |
| AT-LBA | Australia Telescope - Long Baseline Array |
| BH | Borehole |
| CBR | California Bearing Ratio |
| DCP | Dynamic Cone Penetrometer |
| DTM | Digital Terrain Model |
| EVN | European VLBI Network |
| GNSS | Global Navigation Satellite System |
| GPS | Global Positioning System |
| HartRAO | Hartebeesthoek Radio Astronomy Observatory |
| HEC-RAS | Hydrologic Engineering Center - River Analysis System |
| IVS | International VLBI Service for Geodesy and Astrometry |
| KAT | Karoo Array Telescope |
| LCF | Load Concentration Factors |
| LL | Liquid Limit |
| LSD | Limit State Design |
| MAP | Mean Annual Precipitation |
| MeerKAT | Successor to KAT |
| MOD | Modified AASHTO (higher compaction effort) |
| MSA | Main Study Area |
| MSGO | Matjiesfontein Space Geodesy Observatory |
| NEMA | National Environmental Management Act |
| NGL | Natural Ground Level |
| NP | Non-plastic |
| NRB | National Road Board (intermediate compaction effort) |
| NTS | Not To Scale |
| NWA | National Water Act |
| PI | Plasticity Index |
| PL | Plastic Limit |
| RD | Relative Density |
| RMR | Rock Mass Rating |
| RQD | Rock Quality Designation |
| SDF | Standard Design Flood |
| SKA | Square Kilometer Array |
| S/LLR | Satellite/Lunar Laser Ranger |

| | |
|---|---|
| SLS | Serviceability Limit State |
| STD | Standard Proctor (lower compaction effort) |
| TOC | Top of Concrete |
| UCS | Unconfined Compressive Strength |
| ULS | Ultimate Limit State |
| VGOS | VLBI2010 Global Observing System |
| VLBA | Very Long Baseline Array |
| VLBI | Very Long Baseline Interferometry |
| WT | Water Table |

*"Remember to look up at the stars and not down at your feet. Try to make sense of what you see and wonder about what makes the universe exist. Be curious. And however difficult life may seem, there is always something you can do and succeed at. It matters that you don't just give up."*

~ Stephen Hawking ~

# Chapter 1

# Introduction

## 1.1 The town of Matjiesfontein

The town of Matjiesfontein is located approximately 240km inland to the north-east of Cape Town along the N1 national route between the towns of Touws River and Laingsburg, with Sutherland located about 120km to the north along the R354 regional route. Figure 1-1 shows the location of Matjiesfontein in relation to Cape Town and other major and minor towns in the Western Cape. The original inhabitants of the area called Matjiesfontein were Khoikhoi people to which Matjiesfontein owes its name. It falls within the Laingsburg Local Municipality and had a total population of only 422 people in 2011 (Statistics South Africa, 2011).

The road that connected Cape Town with the diamond fields of Kimberley ran directly via Matjiesfontein during the mid-nineteenth century, with a railway station only built in 1878. James Logan, who was superintendent of this stretch of rail at the time, bought land which included Matjiesfontein around 1884. The Scotsman opened a refreshment station for passengers of passing trains, which thrived so well that the business expanded into a luxurious health and holiday resort and eventually a self-sufficient village. During the Anglo-Boer War, the town was used as headquarters for British soldiers and the Hotel Milner, as it was initially named, was furnished to serve as a hospital. The renowned town was often visited by numerous influential personalities the likes of Cecil John Rhodes, Olive Schreiner and Randolph Churchill. Schreiner even took up residency in Matjiesfontein

with the house she once lived in now named in honour of the activist. The town started to deteriorate after the death of Logan in 1920.


**Figure 1-1: Locality of Matjiesfontein**

The hotelier David Rawdon bought Matjiesfontein in 1968 and steadily started to restore the town to its original Victorian charm. It was declared a national monument in 1975 under the direction of Rawdon, the railway station in 1989 and the cemetery somewhat later in 1994. Many of the local people are employed as staff of the Lord Milner, shown in Figure 1-2.

**Figure 1-2: The Lord Milner in Matjiesfontein (L Croukamp)**

The local community might also benefit from projects such as the MSGO, as it would have to employ a number of people during the construction and operational phases. It also has the potential to generate interest in science at young people and to get them involved in educational programs.

## 1.2 The Matjiesfontein Space Geodesy Observatory

The Matjiesfontein Space Geodesy Observatory (MSGO) is situated on the Matjiesfontein farm about 5km south of the town in a small valley at the foot of the Witteberg Mountains. An aerial view of the site is shown in Figure 1-3 below indicating the main study. The MSGO is to serve as an extension of the Hartebeesthoek Radio Astronomy Observatory (HartRAO) in Gauteng, as agreed upon between stakeholders of the project and the late Rawdon. The site is considered favourable for space geodetic observations due to several reasons such as protection offered against radio frequency interference by its remoteness and topography, low humidity with clear skies and the relative concealed nature of the site. The MSGO is currently equipped with a permanent GPS station and a vault housing instruments such as a gravimeter, seismometer and accelerometer. It is envisaged for a Satellite/Lunar Laser Ranger (S/LLR), currently operating at HartRAO, to be installed at the observatory. These and other instruments will be used to perform advanced space geodetic techniques as part of a global network.


**Figure 1-3: The MSGO site (Google Earth)**

## 1.3 Site description

The fauna and flora around Matjiesfontein are typical of the Karoo. Some indigenous antelope include Springbok, Steenbok, Klipspringer, Duiker and Grey Rhebok. Other mammals present are the Small Grey Mongoose, Rooikat and porcupine. The area is also home to the Spring hare and Riverine rabbit, the latter being classified as critically endangered. Succulent shrubs make out most of the surrounding terrain, with plants like proteas, ericas and gladioli flourishing higher up the mountain. The area is unique in terms of geology, as the contact zone between the Cape and Karoo supergroups lies between the town and site. This gives rise to a variety of rock types with formations including sedimentary rocks such as sandstone, shale and tillite and the metamorphic rock quartzite. The variety of soil can also be attributed in part to the varying geological conditions.

## 1.4 Problem statement

Radio telescope structures are high-tech instruments and their emplacement is a complex problem since it has to comply with a set of strict requirements. The structures need to be exceptionally stable for performing accurate VLBI (Very Long Baseline Interferometry) studies, such as calculating plate tectonic velocities, determining the rotational rate and orientation of the earth's axis and keeping track of the earth's celestial reference frame. The site conditions and local material need to be investigated, tested and evaluated with respect to their engineering properties. This include investigating the founding conditions and drainage capacity over the main study area for possible impact on structures and testing local soil and rock for potential use as construction material. The methods for acquiring this information is henceforth collectively referred to as site characterization. A site-specific foundation design for a SKA-type radio telescope was further undertaken with the loading requirements obtained from SKA South Africa and the geotechnical properties based on the relevant results obtained in site characterization. The problem can thus be formulated as the need to cognitively evaluate the suitability of the site for the emplacement of radio telescope antennas and their services such that the structures will conform to serviceability requirements.

## 1.5 Motivation for research

The research is motivated by the aspiration of conducting geodetic VLBI as part of the operations at the MSGO. This means that radio telescope structures and their services are to be built, resulting in a need for acquiring new information in terms of the civil engineering characteristics of the site. Figure 1-4 shows the initial model of the site with proposed positions for four radio telescope antennas. It also shows proposed positions for other structures like the S/LLR, automated SLR2000 system and administration buildings.

**Figure 1-4: Model of proposed positions for structures by Fourie *et al.* (2007)**

Several research studies have been done at the MSGO in the form of bachelor's and master's projects in civil engineering. Funding for the MSGO project is strained and studies are therefore generally aimed at presenting alternative solutions to various engineering problems in the development of the observatory. It is in the same regard that this study has been undertaken to provide new information which would be useful to the project.

## 1.6 Research aim

The research aim of this study is to serve as an alternative source of information for decision makers in the development of the observatory. The results are presented to give insight into the natural site characteristics and present alternative solutions to a number of civil engineering problems on site. The study can therefore be used to address these issues and, needless to say, the information can contribute to other applications not necessarily addressed in this thesis.

## 1.7 Research objectives

The research objectives can in a sense be regarded as the steps taken to reach the research aim and are practical, specific and narrow in scope. The objectives of the research can be summarised as follows:

- Review relevant pieces of literature in the form of a literature study;
- Perform a site inspection in which a GPS survey is conducted to create a digital terrain model of the main study area and in which local soil and rock are sampled for laboratory testing;
- Investigate the geotechnical and hydrological characteristics of the main study area in view of the placement of radio telescope structures in that area;
- Test sampled material in the laboratory to identify some engineering properties and potential for use as construction material;
- Design a suitable foundation for a SKA-type radio telescope;
- Draw conclusions and make recommendations based on the outcomes of this study.

## 1.8 Limitations

There are some major and minor limitations in this study. The influence sphere below a foundation is considered acting to a depth of one and a half times its width for a square footing according to Craig (2011). If one is to use the foundation size of the Karoo Array Telescope antennas as reference, which are 5.5m, it equates to a depth of 8.25m. Core drilling is a very expensive practise and as a result of this financial burden, drilling could not be performed to the required depth. Drilling was done however beyond founding level, but drilling through the influence sphere is important as discontinuities such as shear zones or unexpected changes in the profile may occur, which might threaten the long-term integrity of the structure. A limitation in terms of experience in performing laboratory tests on soil was

perceived, as these tests are particularly subjective. For this reason, special care was taken to follow the prescribed methods as closely as possible and tests were repeated as a form of practice. Another limitation is the absence of specifically prescribed instruments in the laboratories. One such instrument is the 250mm strain gauge as prescribed for the test of alkali-silica reactivity of aggregates. A 200mm strain gauge was used instead, but was not considered a problem, as expansion limits are given as percentages of gauge length. Where other necessary equipment was lacking, external laboratories were approached for permission to use their facilities.

## 1.9 Layout of report

This thesis consists of six chapters supported by seven appendices. Table 1-1 gives an overview of the report outlay with the title and brief description of each chapter and appendix. The introductory section at the beginning of each chapter provides a more detailed overview of its contents. More detail is also given on the supporting content of appendices whenever referenced in chapters.

**Table 1-1: Brief layout of report**

| Title | | Brief description |
|---|---|---|
| Chapter 1 | Introduction | Background to the research project |
| Chapter 2 | Literature Review | Desktop study on relevant pieces of literature |
| Chapter 3 | Methodology for Site Characterization | Description of the methods followed for the site investigation and laboratory tests performed |
| Chapter 4 | Results | Reports and interprets the results from the site investigation and laboratory tests performed as detailed in the methodology |
| Chapter 5 | Foundation Design | Foundation design for a SKA-type radio telescope based on actual loads and the results from the previous chapter |
| Chapter 6 | Closure | Final conclusions and recommendations |
| Appendix A | Subsurface Data | Contains the core logging sheets for each borehole |
| Appendix B | Hydraulic Data | Contains the flood calculation sheets for each drainage channel |
| Appendix C | Petrographic Results | Contains the petrographic images taken with the petrographic microscope accompanied by detailed descriptions |
| Appendix D | Miscellaneous Results | Contains the raw data of the results to avoid excess information and repetitiveness in the main report |
| Appendix E | Design Calculations | Contains the calculation sheets compiled in the foundation design |
| Appendix F | Drawings | Drawings for the production of the mortar-bar moulds and for the sizing and other details of the foundation design |
| Appendix G | Photo Report | Contains a gallery of additional photographs not included within the main report |

# Chapter 2

# Literature Review

## 2.1 Introduction

The literature review is done as a desktop study on information considered relevant to the following research. It commences with a background on radio telescopes followed by details on the instrument with reference to those at HartRAO. A look at Very Long Baseline Interferometry (VLBI) is then undertaken with the measurements made in geodesy. The review then takes a closer look at geology, starting with a review on one of the basic yet most important geological concepts, namely the rock cycle. The scope narrows down to a discussion on the local geology and potential geohazards. The general soil profile of the site is discussed with an overview of standard soil and rock profiling nomenclature in South Africa. Some of the engineering properties of soil with respect to particle size distribution, plasticity and compaction properties are discussed. A review on alkali-silica reaction follows paying particular attention to quartzitic sandstone and tillite. Literature on flooding and the methods for determining peak floods in South Africa are briefly reviewed. Different types of foundations are then discussed and the basic design methodologies for design are reviewed. Lastly, a short summary is included at the end of the chapter to provide the necessary link to the experimental phase of the research project. Previous research done at the Matjiesfontein Space Geodesy Observatory are reviewed when relevant to the particular discussion.

## 2.2 The radio telescope

This section contains an overview of radio telescopes, very long baseline interferometry and the measurements made from geodetic experiments.

### 2.2.1 Background

Radio telescopes are astronomical instruments used in the scientific fields of radio astronomy and space geodesy. They are typically built as large structures supporting parabolic dishes that perform as directional radio antennas to detect radio-frequency radiation of wavelengths between about 10m to 1mm at 30MHz to 300GHz, respectively (Encyclopaedia Britannica, 2016). Radio telescopes differ from optical telescopes in the sense that they receive and collect data from the radio frequency portion (also microwave frequency portion) of the electromagnetic spectrum illustrated in Figure 2-1, as oppose to the visible part.

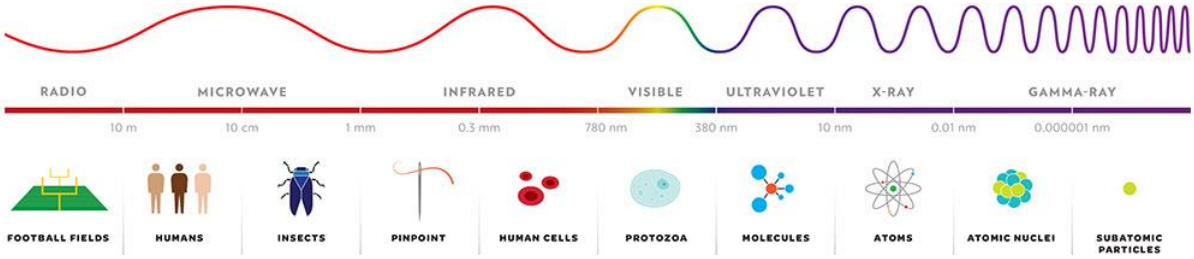


**Figure 2-1: The electromagnetic spectrum**

These detectable radio waves are emitted from astronomical radio sources such as quasars and pulsars, which are so far from the earth that they appear fixed in space and can thus be used as reference points. Radio telescopes are often situated in remote areas and valleys so as to shield them from electromagnetic interference emitted from devices such as microwaves, cell phones, radios, televisions etc., making the location of the Matjiesfontein Geodesy Observatory ideal for the addition of a radio telescope.

### 2.2.2 Radio telescopes in South Africa

The two radio telescopes shown in Figure 2-2 are situated at HartRAO and are both used for astronomy and geodesy. The main telescope at the observatory has a dish of 26m in diameter and the total structure weighs about 260 tons, of which 200 tons is movable. The telescope is equipped with radio receivers that operate in microwave bands at wavelengths of 18cm, 13cm, 6cm, 5cm, 4.5cm, 3.5cm, 2.5cm and 1.3cm (HartRAO, [s.a.]). The telescope was used to establish the absolute reference point, known as the Hartebeesthoek94 Datum, for South Africa's National Survey system. The smaller telescope has a dish of 15m in diameter and was fitted with receivers working in the 18cm to 21cm wavelength bands. It was built for developing technologies for the Square Kilometre Array (SKA) radio telescope located near Carnarvon in the Northern Cape. After completion of its test programme, a new receiver system was built operating at 13cm and 3.5cm, designed primarily for geodetic VLBI (HartRAO, [s.a.]).

Although being an astronomy observatory, it also runs a space geodesy programme that sees both its radio telescopes participating in geodetic VLBI experiments as part of the International VLBI Service for Geodesy and Astrometry (IVS).

**Figure 2-2: The radio telescopes at HartRAO (M Gaylard)**

Figure 2-3 shows the global VLBI networks in which HartRAO co-operates with radio-telescopes from other continents to form a virtual telescope nearly the size of the earth. HartRAO is a member of the European VLBI Network (EVN), the Australia Telescope Long Baseline Array (AT-LBA) and the Very Long Baseline Array (VLBA) in the United States. HartRAO was the only major radio astronomy observatory in Africa until the Square Kilometre Array started, which will be the largest in the world.

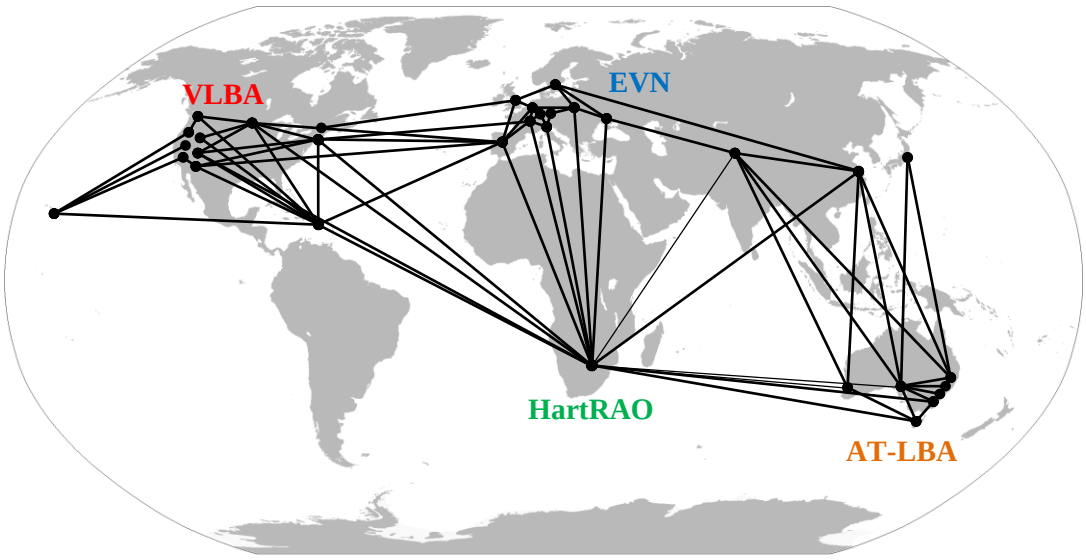


**Figure 2-3: Map of global VLBI networks with HartRAO**

### 2.2.3 Very long baseline interferometry

The spatial resolution that can be obtained when using a single telescope depends on the size of its main reflector, i.e. the diameter of the dish. Since better resolution is continuously desired and the construction of increasingly larger telescopes becomes expensive, difficult and impractical, the technique of very long baseline interferometry (VLBI) was developed to overcome this problem. The use of VLBI allows higher resolution, as the resolving power of the interferometer depends on the distance, called the baseline, between the individual telescopes and not their size. This concept is very basically illustrated in Figure 2-4. VLBI emulates a single radio telescope, as explained by Botha (2014), with an effective dish diameter of dimension equal to the baseline, achieving better resolution.

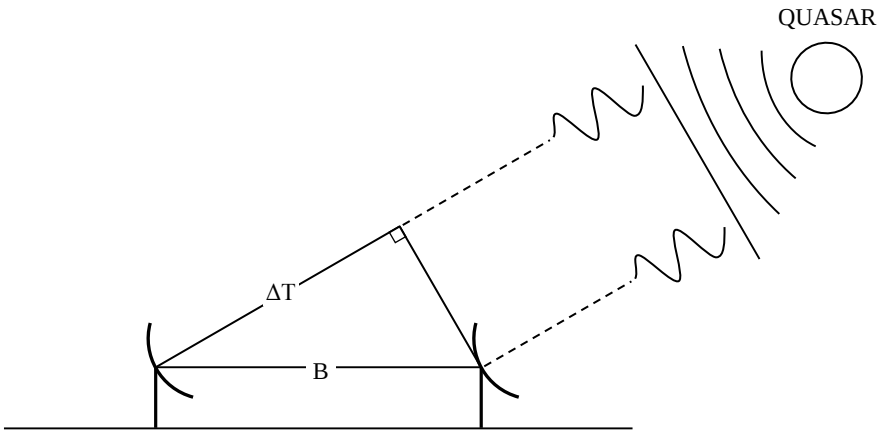


**Figure 2-4: The concept of VLBI**

By observing a cosmic source (such as a quasar) with a VLBI network, radio signals are collected at multiple radio telescope antennas on earth. The time difference (ΔT) between the arrival of the same signal at different antennas is measured from which the length of the baselines (B) can be calculated. According to Clark (2003), the accuracy of VLBI baseline determinations makes it the best long-distance technique, with VLBI being the only one to accurately give the absolute orientation of the earth in an inertial coordinate system. The technique of VLBI is known for mapping cosmic sources in astronomy, but are also used in geodesy for studying, inter alia, the following:

- Rotational rate of the earth;
- Orientation of the earth's axis;
- Velocities of plate tectonics and;
- Earth's celestial reference frame.

The Hartebeesthoek radio telescope moves at a pace of 2.5cm per year in the North-East direction, as shown by the vector lines in Figure 2-5. The movement of other radio telescope antennas around the

world is also shown, as measured by geodetic VLBI, with tectonic plate boundaries shown as brown lines. The VLBI2010 is the next generation VLBI system according to Schuh & Behrend (2012) with goals of achieving, on scales as big as the earth, an accuracy of 1mm in position and of 0.1mm/year in velocity. It is understood from Botha (2015) that HartRAO will take part in this system and are in the process of emplacing a VGOS (VLBI2010 Global Observing System) radio telescope.

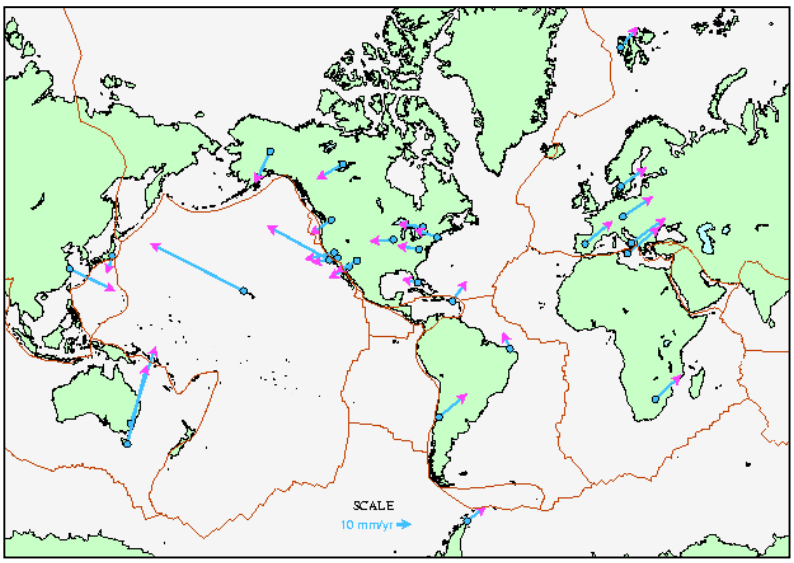


**Figure 2-5: Annual movement of radio telescopes measured by geodetic VLBI (HartRAO, [s.a.])**

The new VLBI2010 technology involves a complete reworking of the legacy S/X-band systems including the introduction of very fast slewing antennas, broadband observing systems, and a software correlator according to Petrachenko *et al.* (2013).

## 2.3 Geology

Geology, or engineering geology to be more specific, is the foundation of geotechnical engineering and since all material on site, soil and rock, are related to the surrounding geology, it is necessary to include a review of literature related to the local geology and the properties of these materials.

### 2.3.1 The rock cycle

A good reference point before discussing the local geology is perhaps to review the model of the rock cycle. The rock cycle, as illustrated in Figure 2-6, demonstrates the relationship between the three rock types, namely igneous, sedimentary and metamorphic. It also entails the formation of soil through the external processes of weathering, mass wasting and erosion that is driven by power from the sun, as explained by Tarbuck *et al.* (2011). Rock at or close to the surface of the earth is exposed to mechanical and chemical weathering, movement to lower levels under gravity and transported by erosion agents like water, wind and ice. The rock cycle is presented with varying detail in the literature and the one shown in Figure 2-6 is used for simplicity.

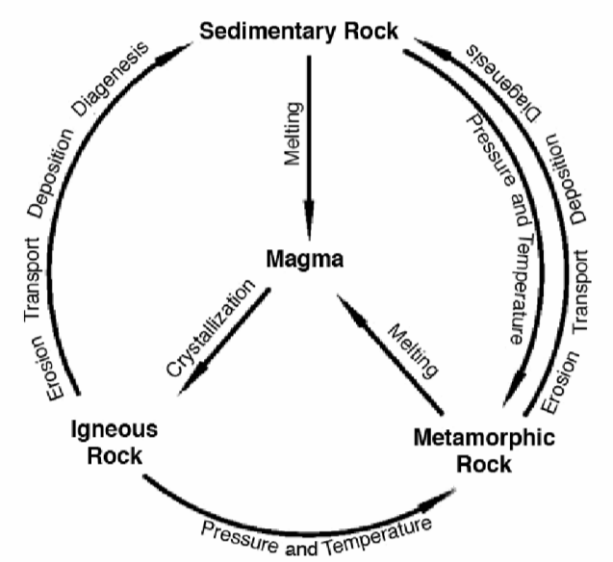


**Figure 2-6: The rock cycle**

### 2.3.2 The local geology

Brink (1979) reinforced the description of a stratigraphic unit as a stratum or assemblage of strata recognisable as a unit within the classification of the rock sequence with respect to any specific rock character, property or attribute, with the main stratigraphic units for engineering defined in lithostratigraphy. The Karoo Supergroup is the most widespread stratigraphic unit on the African continent south of the Saharan desert and is divided into five successions namely the Dwyka, Ecca, Beaufort, Stormberg and Drakensberg Groups. The Cape Supergroup are divided into three successions namely the Table Mountain Group, the Bokkeveld Group and the Witteberg Group. Sandstones and mudrocks are what mostly comprise the Witteberg Group according to Johnson *et al.* (2006). Table 2-1 is a summary of the formations present at the MSGO.

**Table 2-1: Stratigraphy obtained from Brink (1981)**

| Supergroup | Group | Formation | Dominant rock |
|---|---|---|---|
| Karoo | Dwyka | Dwyka (CPd) | Tillite |
| Cape | Witteberg | Waaipoort (Cw) | Grey shale |
| Cape | Witteberg | Floriskraal (Cf) | Shale and quartzitic sandstone |
| Cape | Witteberg | Kweekvlei (Ck) | Shale |
| Cape | Witteberg | Witpoort (Dwi) | Sandstone |

The stratigraphy of the Formations in Table 2-1 is listed from youngest to oldest. Sediments that created the Witteberg rocks were deposited approximately 370 to 330 million years ago, after which the glacial deposits from ice sheets were laid down to the north of the Cape Fold belt at the time that Gondwana drifted over the South Pole. The symbols within brackets next to each Formation in Table 2-1 refer to the field geology shown in Figure 2-7. These rocks are all sedimentary in origin with some metamorphism indicated by the presence of quartzitic sandstone, which is to be expected from mountain-building areas.

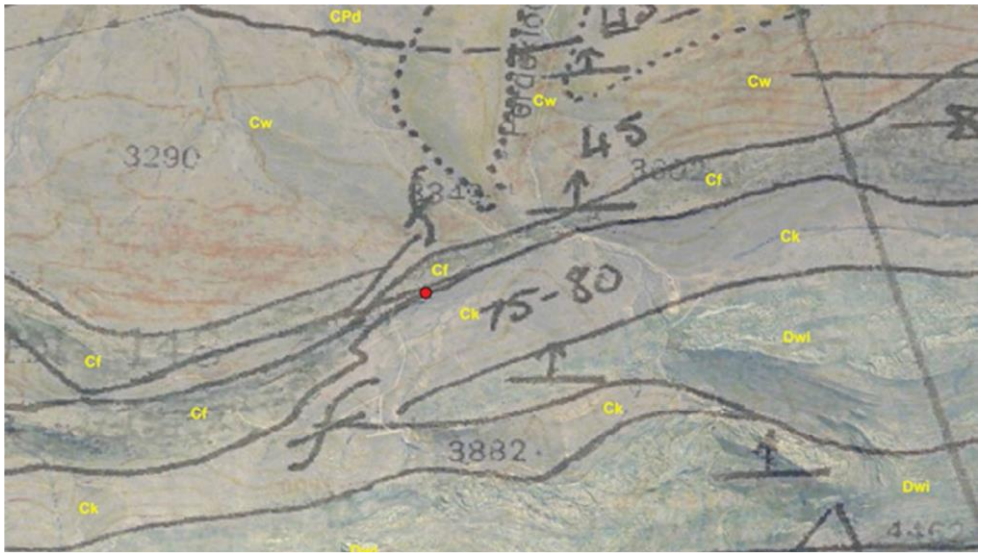


**Figure 2-7: Field geology (scale 1:50 000) (Council for Geoscience)**

Tillite of the Dwyka Formation is present north of the site and is visible by the tombstone weathered outcrops, shown in Figure 2-8, of which the rock has been steeply tilted, resulting from the mechanical disintegration along subvertical cleavage planes according to Brink (1983). It is a sedimentary rock formed by the lithification of unsorted glacial sediment called till. The Dwyka Group is the oldest and lowermost unit of the Karoo Supergroup deposited in the Karoo Basin of Southern Africa and consists mainly of tillite. This deposition took place during the Late Carboniferous and possibly extending into the Asselian of the early Permian. Results on Unconfined Compressive Strength (UCS) of tillite samples were summarised by Brink (1983) with unweathered tillite having a mean UCS of 225MPa. Slightly weathered tillite had a mean UCS of 107MPa, while moderately weathered tillite had a mean UCS of only 28MPa.

Only a short background to the Witteberg Group is given by Brink (1981) stating that no major engineering works are located on these rocks, apart from cuttings for road construction. Even though this statement was made a couple of decades ago, it appears that information on the Witteberg Group is still not as comprehensive in literature as that of the Table Mountain and Bokkeveld Groups. Subgroups exist for the Witteberg Group and the Waaipoort, Floriskraal and Kweekvlei Formations at Matjiesfontein fall under the Lake Mentz Subgroup West of 22°E.

**Figure 2-8: Tombstone weathered outcrops of Dwyka tillite**

Sandstone at the MSGO constitutes the Witpoort formation of the Witteberg group. This rock type is very common and consists mostly of quartz grains, but feldspar, mica or other minerals are also often present according to Pellant (2000). The strength of sandstones depends more on the amount of cementing material, with poorly cemented sandstones having strengths less than 3.5MPa and exceeding 240MPa for sandstones with voids filled by siliceous material according to Bell (1980). Sandstone is the most abundant sedimentary rock after shale making up about 20% of this rock group according to Tarbuck *et al.* (2011). It is able to be formed by various geological situations, the majority of which are accumulated in water or as windblown deposits in arid continental areas according to Pellant (2000). Quartzite is formed from sandstone by either contact metamorphism near large igneous intrusions or by regional metamorphism as explained by Pellant (2000). It is a very hard rock that might break through its quartz grains rather than along the grain boundaries according to Tarbuck *et al.* (2011) as a result of the recrystallization often being complete. During the process of contact metamorphism, sandstone is altered by heat alone to become a more crystalline and none-porous rock, composed of an interlocking mosaic of quartz crystals according to Pellant (2000). Regional metamorphism on the other hand refers to the altering of rock due to both heat and pressure and generally occurs in mountain-building areas. Van Wyk (2013) has shown quartzite to be the most durable rock at the MSGO site, followed by tillite. Shales at the MSGO can be from the Floriskraal, Kweekvlei or Waaipoort formations. It consists of a mixture of clay minerals, sometimes calcite and compounds of iron which gives the rock its colour according to Harvey (1982). It is a fine-grained sedimentary rock typically found deposited in bedding planes that are easily breakable. Weathering of shale when exposed to the atmosphere occurs rapidly, without much assistance of weathering agents such as water and wind. Since the underlying formation in the main study area is mostly shale according to Figure 2-7, its in-situ behaviour is important for review and typical data is given in Table 2-2.

**Table 2-2: Physical properties and probable in-situ behaviour of shale by Bell (1980)**

| Laboratory tests and in-situ observations | Average range of numbers | | High pore pressure | Low bearing capacity | Tendency to rebound | Slope stability problems | Rapid sinking | Rapid erosion | Tunnel support problems |
|---|---|---|---|---|---|---|---|---|---|
| | Unfavourable | Favourable | | | | | | | |
| Compressive strength (kPa) | 350 - 2 070 | 2 070 - 3 500 | ✓ | ✓ | | | | | |
| Modulus of elasticity (MPa) | 140 - 1 400 | 1 400 - 14 000 | | ✓ | | | | | ✓ |
| Cohesive strength (kPa) | 35 - 700 | 700 - > 10 500 | | | ✓ | ✓ | | | ✓ |
| Angle of internal friction (degrees) | 10 - 20 | 20 - 65 | | | ✓ | ✓ | | | ✓ |
| Dry density ($Mg/m^3$) | 1.12 - 1.78 | 1.78 - 2.56 | ✓ | | | | | ✓ | |
| Potential swell (%) | 3 - 15 | 1 - 3 | | | ✓ | ✓ | | ✓ | ✓ |
| Natural moisture content (%) | 20 - 35 | 5 - 15 | ✓ | | | ✓ | | | |
| Coefficient of permeability (m/s) | $10^{-7}$ - $10^{-12}$ | > $10^{-7}$ | ✓ | | | ✓ | ✓ | | |
| Predominant clay minerals | Montmorillonite or illite | Kaolinite and chlorite | ✓ | | | ✓ | | | |
| Activity ratio | 0.75 - > 2.0 | 0.35 - 0.75 | | | | ✓ | | | |
| Wetting and drying cycles | Reduces to grain sizes | Reduces to flakes | | | | | ✓ | ✓ | |
| Spacing of rock defects | Closely spaced | Widely spaced | | ✓ | | ✓ | | ✓ | ✓ |
| Orientation of rock defects | Adversely oriented | Favourable oriented | | ✓ | | ✓ | | | ✓ |
| State of stress | > Existing overburden | ≅ Overburden | | | ✓ | ✓ | | | ✓ |

### 2.3.3 Geohazards

South Africa is known to be relatively stable in terms of its natural seismic activity. Most earth tremors are generally mining induced taking place in the northern parts of the country, although tremors have been recorded in the Western Cape since the early seventeenth century (Historical Earthquakes, 2012). There is no sufficient record of seismic activity in Matjiesfontein itself, hence the addition of a seismometer and accelerometer to the MSGO. Matjiesfontein is in close proximity of places that have been hit by earthquakes in the past. Table 2-3 gives a short summary of the most significant events exceeding magnitudes of 5.0 on the Richter scale, which have occurred in the Western Cape relatively near Matjiesfontein. The most notable event in the Western Cape and most destructive in South Africa in recorded history was the 1969 earthquake in the Tulbach-Ceres-Wolseley area. The catastrophic earthquake occurred on 29 September 1969 and was responsible for the death of twelve people with some sustaining series injuries.

**Table 2-3: Earthquakes in the relative vicinity of Matjiesfontein (Historic Earthquakes, 2012)**

| Year | Locations | Magnitude | Intensity | Comments |
|---|---|---|---|---|
| 1970 | Ceres Tulbagh | 5.7 | VII | Trembling felt all over the Western Cape |
| 1969 | Ceres Tulbagh Wolseley | 6.3 | VIII - IX | Marked tremor all over Western Cape resulting in fatalities and extensive damage |
| 1969 | Oudtshoorn | 5.4 | IV - V | Strong shock felt all over the Western Cape from Cape Town to George |
| 1963 | De Doorns Worcester Ceres | 5.0 | VI | Sharp shock felt all over the Western Cape that woke and frightened people with buildings that heaved |

The event caused extensive to almost total destruction of both old and poorly constructed buildings, with very large cracks and structural damage in the more modern structures. It triggered numerous landslides and rockfalls along the surrounding mountain slopes, some leading to brushfires. The mainshock had a magnitude of 6.3 and was followed by frequent aftershocks for months, the greatest having a magnitude of 5.7 that caused even further damage in the area. The cost of damage was reported to be an estimated $24 million (Damaging Earthquakes, 2012). The seismic instruments installed at the MSGO have recorded an earthquake in 2015 having a magnitude of 3.7 on the Richter scale.

The MSGO site is confined by the Witteberg Mountain to the southern side, where a paleo-slope failure was noticed by Fourie *et al.* (2007). It is difficult to determine the age of the failure from the limited data available but it is believed not to be recent. Excessive rain and disturbance of the toe of the failure could potentially result in re-activation of the feature.

Four different types of slope failure are given by Wyllie & Mah (2004) associated with different geological structures shows the four types of failure:

- Plane failure;
- Wedge failure;
- Toppling failure and;
- Circular failure.

### 2.3.4 The soil profile

A geotechnical and geophysical investigation by Fourie *et al.* (2007) included excavating eight equally spaced trial pits and the soil profiling each of these trial pits. The investigation found that all of them either refused on weathered rock at shallow depth or that the cover material was very rough resembling scree. There was no water encountered in any of the trial pits and the general soil profile of the valley can be described as that seen in Table 2-4 below.

**Table 2-4: Typical soil profile of main study area by Fourie *et al.* (2007)**

| Depth | Description |
|---|---|
| 0.2 | Dry, light brown, loose, intact, boulders and gravel in a sandy matrix. Hill wash. |
| 0.5 | Slightly moist, dark reddish-orange, dense, intact, boulders and gravel with limited sandy matrix. Hill wash. |
| 0.6 - 1.0 | Refusal on highly to moderately weathered thinly bedded shale or mudstone. Bedding planes sub-vertical. |

The profiling was done in accordance with the extensively used MCCSSO system proposed by Jennings *et al*. (1973), which is done by recording the following properties of each soil layer:

- Moisture condition
- Colour
- Consistency
- Structure
- Soil type
- Origin

This method has been modified and adapted for application in the description of rock, which is compatible with the soil profiling system above, but varies greatly in detail. The following properties have been chosen by the Association of Engineering Geologists (1976) to describe a rock mass:

- Colour
- Weathering
- Fabric and discontinuity surface spacing
- Hardness
- Rock name
- Stratigraphic horizon

Not only did the site investigation by Fourie *et al.* (2009) show solid bedrock in the valley to be shallow, but also stated that the bedding planes of shale are folded or inclined to be sub-vertical, as can be seen on site by looking at the rocky outcrops at the surface and at the weathered rock exposed in the drainage channels. The phenomena of sedimentary layers being folded under crustal forces were first recognised by Nicolaus Steno, a Danish geologist considered as one of the founders of modern stratigraphy, and is called the principle of original horizontality. Tarbuck *et al.* (2011) explains the principle by simply stating that layers of sediment are generally deposited horizontally, and when found as such, they have not been disturbed and thereby have maintained their original horizontality. But if they are folded they must have been distorted by crustal disturbances after being deposited.

## 2.4 Engineering properties of soil

The discussion on the engineering properties of soil is one on the general properties of soil about the particle distribution, plasticity and compaction of soil.

### 2.4.1 Particle distribution of soil

When the properties of a soil are mostly influenced by sand and gravel size particles it is termed coarse soil, whereas if the properties are mostly influenced by clay and silt size particles it is termed fine soil. The soil types are classified on the basis of the particle sizes shown in Figure 2-9.

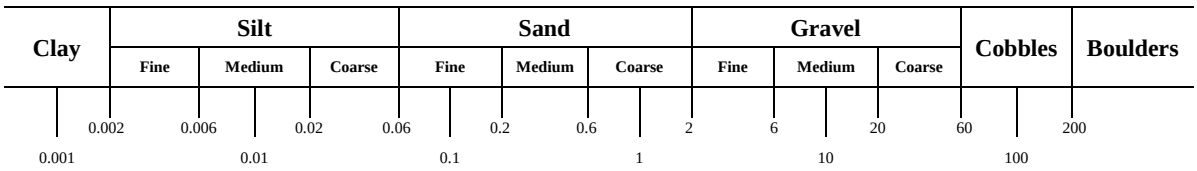


**Figure 2-9: Particle size ranges in millimetre from Craig (2004)**

In the grading of soil, the coarse fraction is graded by the method of sieving, while the fine fraction is separated by the method of sedimentation. In a sieve analysis the particles are separated by means of a series of standard sieves having successively smaller openings. The material on each sieve is weighed and the cumulative percentage passing by mass is then calculated. The method of sedimentation is based on Stokes' law which governs the velocity at which spherical particles settle in a suspension, i.e. the larger the particles the greater the velocity at which it settles, as explained by Craig (2004).

### 2.4.2 Plasticity of soil

The Atterberg limits can be described as a measure of the critical water contents of a soil. They are the liquid, plastic and shrinkage limits. These limits separate the soil in four states generally known as the liquid, plastic, semi-solid and solid states, shown diagrammatically in Figure 2-10 below.

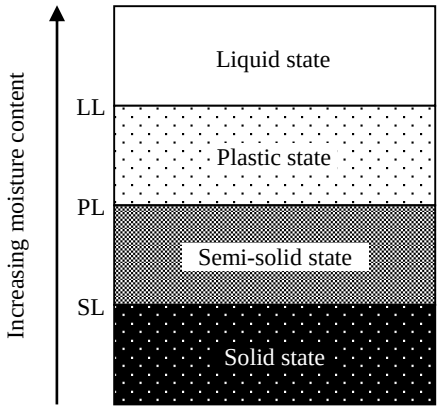


**Figure 2-10: The Atterberg limits**

The liquid limit (LL) is defined as the moisture content at which the behaviour of a soil changes from the liquid to the plastic state and is expressed as a percentage of the dry mass. The plastic limit (PL) is defined as the moisture content at which the behaviour of a soil changes from the plastic to the semi-solid state and is expressed as a percentage of the dry mass. The shrinkage limit (SL) is less used in engineering than the other two, but is defined as the moisture content at which the volume of the soil has reached its minimum value where the behaviour of a soil changes from the semi-solid to the solid state. The soil behaviour is different for each of these states, and therefore the engineering properties differ as well. The plasticity index (PI) is the range of water contents in which the soil behaves plastic and is the numerical difference between the liquid and plastic limits. Higher PI-values are indicative of clayey soils, lower PI-values of silty soils and those with a PI of zero are referred to as non-plastic and are usually the case in clean sands.

### 2.4.3 Compaction

Soil compaction is the process in which air is removed from the pores between individual grains in a soil, increasing the density and generally causing an increase in shear strength. Consolidation on the other hand is the process in which an applied stress causes densification as a result of water being removed from the pores between individual grains. An engineered fill in terms of Craig (2004) is a selected soil that has been placed in a certain thickness, typically in layers ranging from 75mm to 450mm, and compacted to a certain specification with the aim of achieving some sort of engineering performance. The laboratory compaction results are not directly relatable to field compaction, as heavy machinery such as rollers, rammers and vibrators are used to compact the soil on a larger scale.

Factors affecting the degree of soil compaction are the following:

- Moisture content
- Compactive effort/energy
- Type of soil

The main reasons for compacting soil for construction purposes are summarized as follows (Soil Compaction Handbook, 2016):

- Increase in load-bearing capacity
- Reduce settlement
- Reduce frost damage
- Provides stability
- Reduce water seepage, swelling and contraction

The Proctor compaction test is a laboratory method for determining the optimal moisture content at which a given soil type will become densest and achieve its maximum dry density. The dry density of a soil for a given compactive effort depends on the amount of water the soil contains during compaction. The original test is called the standard Proctor compaction test and another has since been used called the modified Proctor compaction test, the only difference being the amount of compactive effort applied during compaction. Table 2-5 gives typical values of maximum dry density and optimum moisture content for a range of soil types under standard compaction.

**Table 2-5: Typical densities (Fundamentals of Soil Compaction, 2016)**

| Soil type | Maximum dry density (kN/m$^3$) | Optimum moisture content (%) |
|---|---|---|
| Well-graded sand (SW) | 22 | 7 |
| Sandy clay (SC) | 19 | 12 |
| Poorly graded sand (SP) | 18 | 15 |
| Low plasticity clay (CL) | 18 | 15 |
| Non-plastic silt (ML) | 17 | 17 |
| High plasticity clay (CH) | 15 | 25 |

Generally speaking, the coarser the soil, the higher the dry densities obtained and lower the moisture content required and vice versa for finer soil. Increasing density by compaction usually increases the shearing resistance of the material, allowing for example the use of a thinner pavement structure over a compacted subgrade or the use of steeper side slopes for an embankment than would otherwise be possible (Soil Compaction, 2016). Figure 2-11 shows the results of a visual inspection by Kloos (2014) on the access road to the MSGO. The road was divided into three equal sections with section 1 starting in the town and section 3 ending on the site. It is clear that erosion is generally a problem as this causes gullies along the access road.

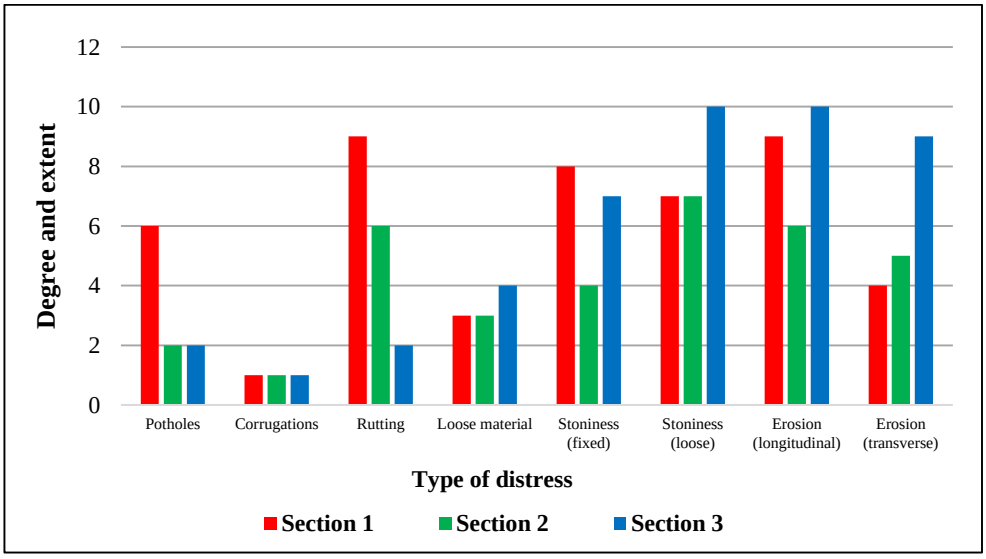


**Figure 2-11: Visual inspection on the access road by Kloos (2014)**

Both the standard and modified compaction tests are used in determining the California bearing ratio for a material. The CBR is a penetration test for evaluating the mechanical strength of material by measuring the force required to penetrate soil or crushed rock with a plunger of standard area. The measured force is divided by the force required to attain an equal penetration on the standard material.

## 2.5 Alkali-silica reaction

Certain minerals may react with alkaline substances to form a gel paste known as Alkali-silica reaction (ASR). This may result in expansion within concrete when the aggregate and cement reacts with one another resulting in cracking of the concrete element. Cracking of the concrete does not only cause an aesthetically displeasing effect, but its engineering properties deteriorates. Reinforcement becomes exposed to the elements and thus susceptible to corrosion, which can compromise the integrity of the element and even result in failure. The risk should be higher for concrete in foundations, since ground water may be present for long periods of time and deterioration may go unnoticed. Reaction leading to deleterious expansion may only occur when the following conditions are true for the concrete, and sometimes even needed in a specific combination, according to Oberholster (2009):

- Pore solution has sufficiently high alkalinity;
- Aggregate has a sufficient amount of deleteriously reactive minerals and;
- Environmental conditions are such that they promote reaction.

Several aggregate types were tested by Davis & Coull (1991) with some showing potential for slow expansion when the alkali content is at least 2.8kg per cubic meter of concrete. This included ortho-quartzite and tillite from quarries in the Western Cape and KwaZulu Natal, respectively. It was found that these aggregates can be regarded as non-reactive as the alkali content in most cement is too low. The highest occurrence of ASR in South Africa has been observed in various structures containing concrete with aggregates from the Malmesbury Group, which is the oldest rock formation in the South Western Cape and consists of alternating layers of greywacke, sandstone and slate. An irrigation dam containing aggregates from the Bokkeveld Group, also belonging to the Cape Supergroup, has been affected by ASR according to Oberholster (2009).

It appears that the reactive constituents in South African aggregates are most likely strained quartz as recognized by features such as deformation bands, deformation lamellae and extinction bands and microcrystalline quartz. Quartzitic sandstone from Matjiesfontein were examined and can be seen in Figure 2-12. Several quartz crystals show discolorations within the grains and is indicative of strained quartz, albeit only partial straining according to Van Wyk (2013), as not every quartz crystal within the sample were strained. Fresh tillite have been commonly used as aggregate to produce excellent concrete according to Brink (1983). Tillite used as aggregate for concrete in KwaZulu-Natal, however, has been identified as being potentially reactive, although it does not constitute a deleterious service record according to Oberholster (2009). The effects of ASR on structures, according to Poole (1992) commonly appears between 5 and 15 years after construction, with some cases reporting deterioration after as much as 25 to 40years.

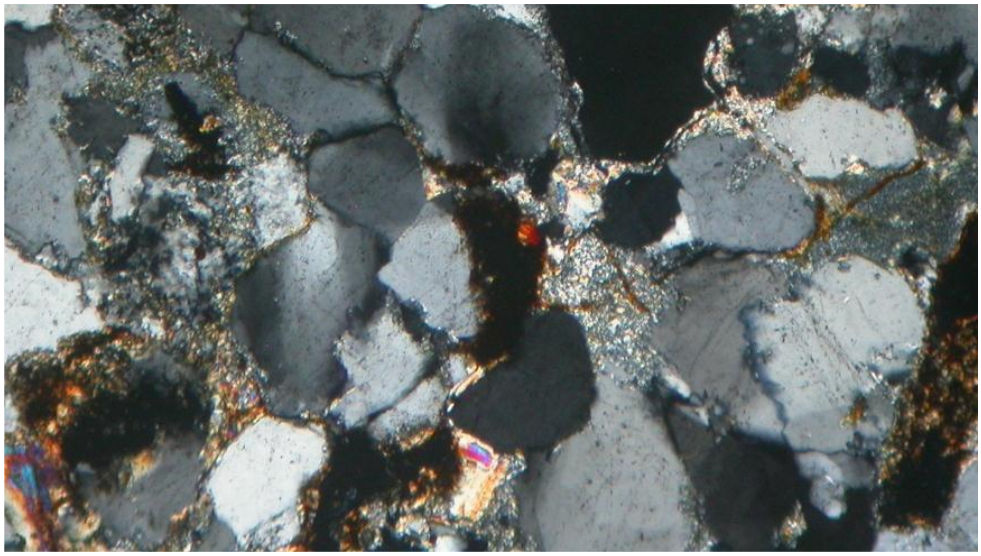

**Figure 2-12: Strained quartz in quartzitic sandstone by Van Wyk (2013)**

## 2.6 Flooding

The site is in a valley where significant runoff is expected during the rainy season. Three drainage channels run through the site. Flood levels are important to consider where structures are to be built, as flooding can act as an obvious destructive force to infrastructure. Peak floods will consequently be determined and analysed in HEC-RAS to produce flood plain delineations for two of the drainage channels on site. The hypothesis in this regard is that the site has sufficient drainge capacity, as it can be speculated that peak flows should be little, considering that the catchment areas for both channels are very small. However, other factors such as steep slopes, short watercourses and the impermeable nature of the site, promotes higher flow.

The three main catogories of methods for the determination of peak flow in rivers or streams are as follows:

- Statistical methods
- Deterministic methods
- Empirical methods

Floods can be determined using statistical methods that is based on historical data for various return periods and are subsequently only useful to catchments for which flow records exist as stated by Van Dijk *et al.* (2013). Statistical methods are recommended for determining flood peaks when long records are available, but no such records exist for the drainage channels under consideration as they are only minor drainage lines.

The deterministic methods used in South Africa are the following:

- The Rational method
- The Unit Hydrograph method
- The Standard Design Flood method
- The SCS-SA (Soil Conservation Service – Southern Africa) method

The Rational method is based on the law of conservation of mass and is recommended for catchments smaller than 15km$^2$, while the Unit Hydrograph method is based on regional analyses of historical data and is recommended for catchments 15km$^2$ to 5000km$^2$ according to Van Dijk *et al.* (2013). The Standard Design Flood method is based on calibrated discharge coefficients for return periods of 2 and 100 years. The calibrated discharge parameters are based upon historical data that were determined for 29 basins across South Africa. The SCS-SA method takes of most factors affecting run-off and it enables synthetic hydrographs to be estimated.

Empirical methods should be used for checking the results obtained by statistical and deterministic methods according to Van Dijk *et al.* (2013). They require a combination of experience, historical data and/or the results of the aforesaid methods. The methods are summarised in Table 2-6 and their recommendation based on catchment area.

**Table 2-6: Feasible flood calculation methods by Van Dijk *et al.* (2013)**

| Flood calculation method | Maximum area (km$^2$) |
|---|---|
| Statistical methods | Preferably larger areas |
| Rational method | < 15 |
| Unit Hydrograph method | 15 – 5 000 |
| Standard Design Flood method | No limitation |
| SCS-SA method | < 30 |
| Empirical methods | Preferably larger areas |

Flood plain mapping is generally a four step process that can be summarised as follows by Van Dijk & Van Vuuren (2013):

- Preparation of accurate topographic mapping of the river and adjacent lands;
- Calculation of the expected discharge for different return periods;
- Calculation of the expected water levels along the river for the calculated discharges using mathematical models that simulate the hydraulic characteristics of the river and;
- Plotting the flood lines to show inundated areas.

## 2.7 Foundations

Foundations are the lowest part of the structure with the primary purpose of transmitting all structural loads to the ground without causing shear failure or excessive settlement of any underlain material.

### 2.7.1 Type of foundations

Foundations are generally divided into two categories namely shallow and deep foundations. A depth-to-width ratio, referring to the depth to founding level and the smaller plan dimension of the foundation, is often used in differentiating between the two, although an absolute ratio does not exist. Das (2002) states for example that a for a depth-to-width ratio of less than four the foundation is shallow, whereas Day (2014) considers a depth-to-width ratio of less than two as being shallow. For a depth-to-width ratio larger than these the foundation should be considered deep. The selection of a foundation type surely depends on the applied loading, geometry of the structure and the geotechnical conditions. Terminology for the various foundation types often differ slightly in the literature, but for shallow foundations shown in Figure 2-13, the terms are generally universal.

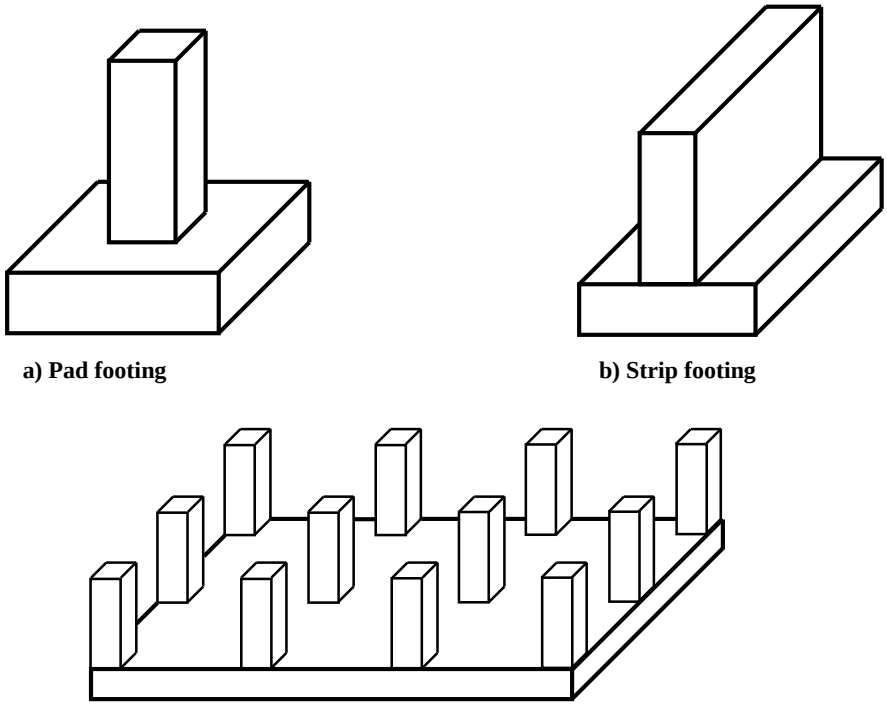

**a) Pad footing** **b) Strip footing**

**c) Raft**

**Figure 2-13: Shallow foundation types**

Spread footings are typically divided into pad and strip footings for supporting point and line loads respectively and can be stepped, tapered or combined. If bearing capacity is very low, the use of a raft foundation is sometimes required in which case the structure is supported by a single foundation as a whole. When shallow foundations become impractical, piles or other types of deep foundations are often required for sufficient stability of the structure. A pile cap is used when columns do not extend

directly into the ground. So from a practical perspective, spread footings and rafts are considered shallow, whereas piles and caissons are considered deep.

As mentioned, various factors influence the selection of a foundation type and this applies for radio-telescope structures as well. Design drawings obtained of the foundations for the KAT-7 telescope antennas showed that they are pad footings, whereas those for the MeerKAT telescope antennas according to Campbell (2013), was deep foundations for which each included eight steel-reinforced concrete piles, ranging in depth from 5m to 10m, and a square pile cap of 5.2m and thickness of 1.25m. The geotechnical site investigation by Fourie *et al*. (2007) found bedrock to be shallow and thus piling might be avoided for telescopes at the MSGO. Even though minimal excavation might be needed, there might be other factors to consider that will influence the depth of the foundation as mentioned by Craig (2004), such as the depth to which frost action is subjected (not typically a problem in South Africa), and the depth to which seasonal swelling and shrinkage of soil takes place.

### 2.7.2 Design of foundations

The aim of design is to provide a safe, serviceable, durable, economical and aesthetically pleasing structure, with the following three methods for design of concrete structures given by Robberts and Marshall (2010):

- The permissible stress method;
- The load factor method and;
- The limit states method.

In the permissible stress method, the ultimate strength of the material would be divided by a lump factor of safety to obtain design resistance within the elastic range according to Robberts and Marshall (2010), of which the applied load must then not exceed this permissible stress. The applied loads are increased in the load factor method with by a factor of safety to give design loads and should not exceed the ultimate strength of the material. The limit states method overcomes several of the shortcomings from the previous two in that partial factors of safety are applied to both material strengths and applied loads.

Poulos (2002) identifies some of the gaps in foundation design between research and practice and evaluates the traditional design methods that should be discarded, modified or retained. There is a general move in geotechnical engineering towards the limit states design method and two approaches exist:

- The load and resistance factor design approach and;
- The partial safety factor approach.

The load and resistance factor design approach, also referred to as the American approach, entails the reduction of the ultimate resistance by applying a strength reduction factor to it and the increase in applied loading by applying load factors to the load components. The partial safety factor approach, also referred to as the European approach, is the same as above except that design strength parameters are obtained by reducing the characteristic strength values of the soil with partial factors of safety. When considering design criteria, Robberts and Marshall (2010) states that foundation properties are frequently determined by the expected settlement rather than the safe bearing capacity of the founding material. This statement is assumed to be the case for foundations in soil. It was stated by Teng (1962) that the properties of bedrock fall into the problem of bearing capacity and permeability in common foundation practice. Settlement in rock does however also require special study in the case of special structures for which settlement needs to be small according to Bell (1980). The elastic modulus of a jointed rockmass can be determined by Goodman Jack tests, otherwise the correlation by Bieniawski (1978) can be used according to Day (1987). For bearing failure, the following three types exist in terms of Day (2014):

- General shear failure;
- Local shear failure and;
- Punching shear failure.

Table 2-7 is adapted from SABS 0161 (1980), which is intended to provide a presumed dry or saturated bearing capacity for different soil and rock types. For rocks, the dry or saturated condition does technically not apply and the table is therefore adjusted accordingly. The values are further representative of central and static loads on the foundation, and should be modified if loading is eccentric or inclined to the vertical (or both). It is further emphasised in that for shale in class 3, bedding planes can affect the stability of excavations and heaving might be a problem as a result of the clay content comprising the rock.

**Table 2-7: Presumed safe bearing capacity on the foundation (SABS 0161, 1980)**

| Class | Supporting rock description | Presumed bearing capacity (kPa) |
|---|---|---|
| 1 | Fresh rock, massively bedded, intact (igneous, metamorphic or sedimentary) and requiring blasting for excavation | 5 000 |
| 2 | Fresh rock, fractured or jointed, which can be excavated with difficulty by pneumatic picks, but normally requires light blasting | 1 000 |
| 3 | Shale, of hard rock consistency | 200 - 400 |
| 4 | Decomposed rock (to be assessed as soil) | - |

## 2.8 Summary

The literature review started with background information on radio telescopes in order to get a more in-depth understanding of how these structures are used in the sciences and why it is necessary for proper engineering investigations when designing, constructing and maintaining these structures. This was followed by a review on the geology of the area, as it relates directly to the engineering properties of rock and the geotechnical conditions on site that are to be investigated. The geology is to a lesser extent directly related to the engineering properties of soil, and the basic engineering properties of soil were subsequently reviewed separately as they are also investigated later on for a variety of different soils collected from site. A review on ASR potential considering the present geological formations was done as a basis for testing it experimentally on sandstone and tillite samples. The methodology for flood plain mapping was reviewed as it is performed in an attempt to identify the risk associated with flooding in the main study area. Finally, design methodologies were reviewed as a foundation design for a SKA-type radio telescope is undertaken as part of the study.

# Chapter 3

# Methodology for Site Characterization

## 3.1 Introduction

This chapter describes the methodology followed for site characterization, which is the term chosen to describe the collection of various types of data regarding the physical characteristics of the MSGO site. After the first site inspection, a GPS survey was conducted over the main study area and afterwards soil and rock samples were collected between the town and site. The methodology is then split into two sections as the site investigation and laboratory tests. The site investigation is divided into geotechnical and hydrological subsections. The geotechnical investigation is based on core drilling at three selected locations spaced over the study area as potential positions for radio telescope antennas. This entailed core logging, rock mass rating and petrographic analysis for detailed descriptions of the rock properties. These results are used as basis for material properties in the foundation design. The hydrological investigation is based on the survey data and flood calculation methods. This involved determining the basic catchment characteristics, estimating flood discharges and computing simple flood lines for the two drainage channels adjacent to the study area. The flood lines are plotted against the existing ground surface in the digital terrain model (DTM) created with the GPS data. The laboratory tests on collected soil and rock samples are treated separately. Soil samples were tested in accordance with the standard

test methods for untreated soils and gravels. This included grading, determination of Atterberg limits, compaction and California Bearing Ratio tests. Rock samples were tested for compressive strength, which included unconfined compressive strength and point load index tests. They were further tested for particle and relative densities, followed by alkali-silica reactivity and petrographic analysis. The basic breakdown is shown in Figure 3-1 and detailed descriptions for each method are discussed in the following sections.

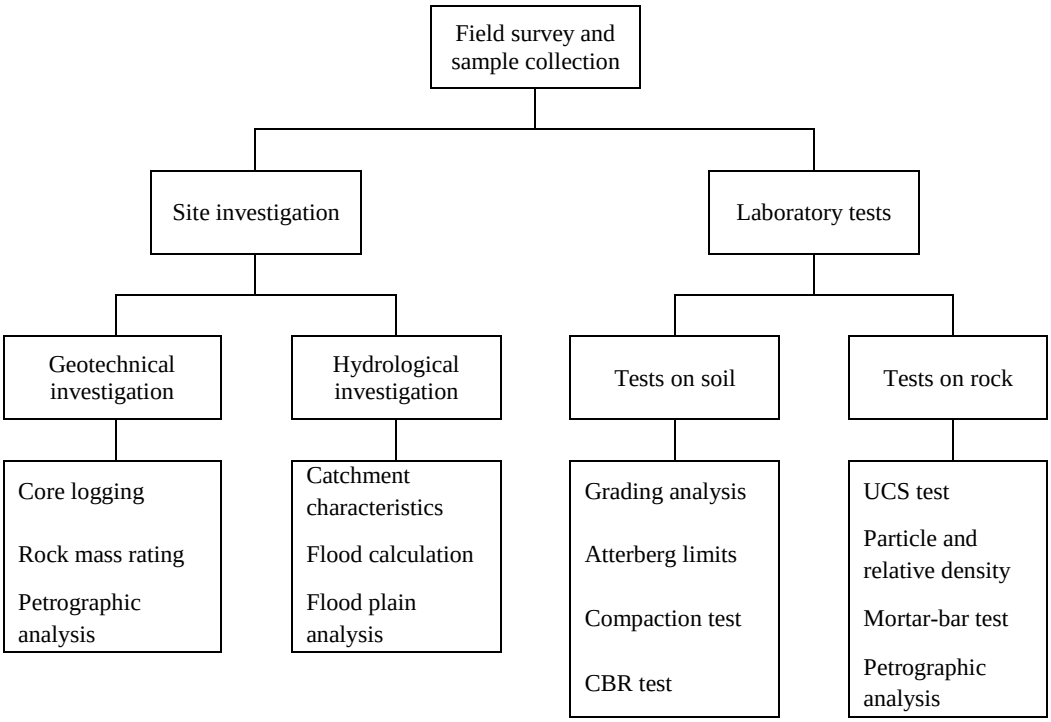


**Figure 3-1: Site characterization**

## 3.2 Field survey and sample collection

A detailed GPS survey of the area earmarked for radio telescope antennas was done with data points measured in a rough grid of approximately 4x4m using the TrimbleR4 GNSS system. This was deemed accurate enough for the purposes of the survey, which are mainly the following:

- Create a DTM of the site in Civil3D by joining the survey data with that of other surveys done on previous studies;
- Use the DTM in performing a hydraulic flood plain analysis in HEC-RAS on the drainage channels on either side of the study area in order to assess the drainage capacity of the site;
- Aid in future planning and execution of development on site and;
- Surveying the site to such precision allowed the researcher to familiarize himself with the environment and be able to decide on where it will be sensible for core drilling and sample collection.

A total of six various types of disturbed soil were sampled and collected from site for performing laboratory tests. Samples 1, 2 and 3 were selected as the most relevant and important. Quartzitic sandstone and tillite rocks were chosen in the field such that they were large enough so that intact cores could be obtained, yet small enough to be able to be collected, carried and transported to the laboratory. The sandstone samples were toppled rocks taken at the foot of the Witteberg mountain on site and the tillite samples were excavated material dumped next to the sports field in Matjiesfontein village for civil services. The shale sample (later logged as phyllite) originated from the first borehole as the in situ founding material for the radio telescope foundation design. Figure 3-2 shows the locations from which all samples were retrieved.

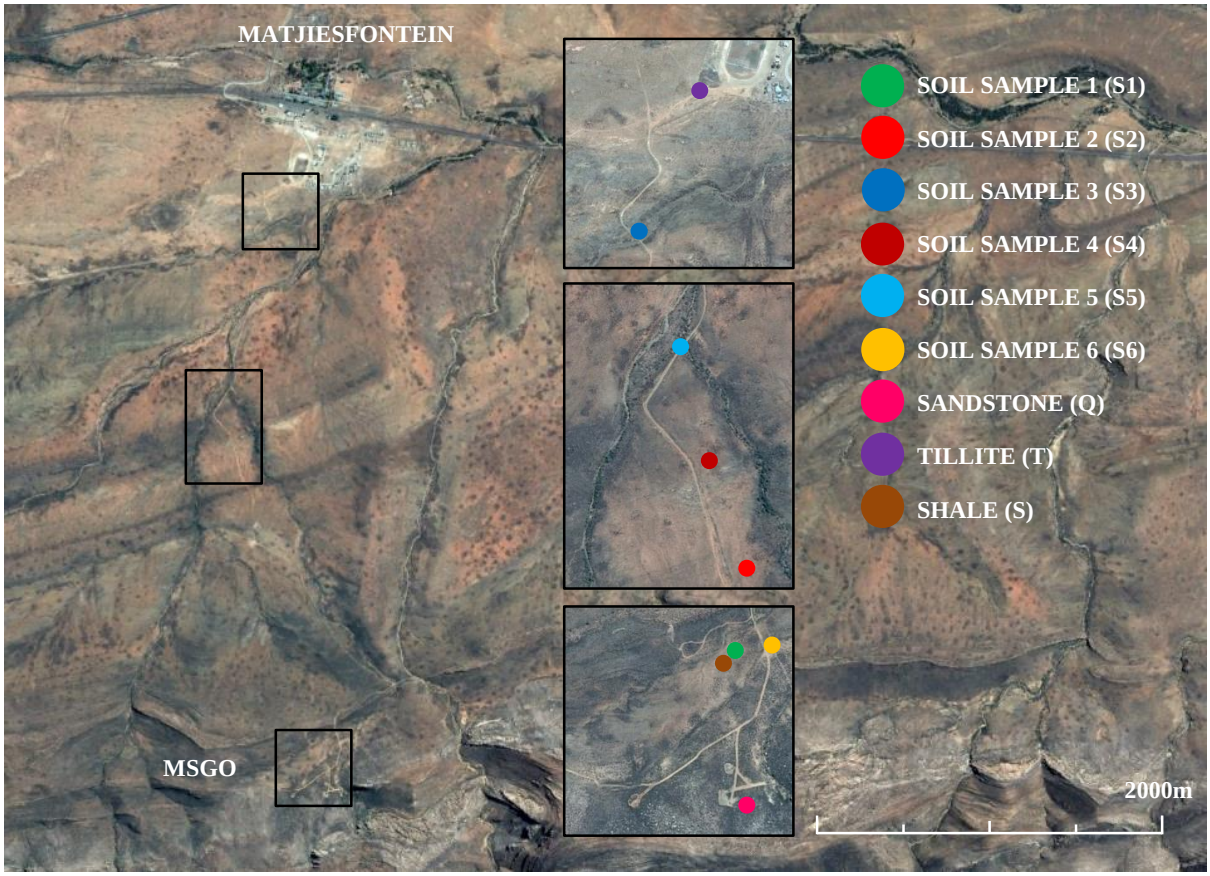


**Figure 3-2: Key plan showing locations of retrieved soil and rock samples**

## 3.3 Geotechnical investigation

The geotechnical investigation is based on core drilling at three selected locations spaced over the study area as potential positions for radio telescope antennas.

### 3.3.1 Core logging

The positions for drilling were chosen to be spread across the study area in order to gain a good representation of geotechnical information of the site. It was also ensured that the positions lie outside of the buffer zones of 10m allocated to the drainage channels (Ecosense Consulting Environmentalists, 2015a). Figure 3-3 shows the typical setup for the drilling. The core logging was performed in accordance with the guide for core logging by the Association of Engineering Geologists (1976), which was briefly discussed in Section 2.3.3 of the literature study. The core logging sheets are attached in Appendix A and contains the interpretation of the material from each borehole.

**Figure 3-3: Drilling in progress**

### 3.3.2 Rock mass rating

The Rock Mass Rating (RMR) system by Bieniawski (1989) is a classification system for rock that combines the most significant geological parameters of the rock mass. The following are the six parameters used to classify a rock mass in the RMR system:

- Unconfined compressive strength (UCS)
- Rock quality designation (RQD)
- Spacing of discontinuities
- Condition of discontinuities
- Groundwater conditions
- Orientation of discontinuities

The rating is used for the design and construction of excavations in rock, such as tunnels, mines, slopes and foundations. A rating is assigned to each of these parameters and the sum is then used to rate the rock in order to obtain a class number according to Table 3-1. The table shows an increase in class number results in a decrease in the quality of the rock mass. Each class is associated with a rock mass rating range and description. It further assigns each class to ranges for cohesion and angle of internal friction.

**Table 3-1: Rock mass classes and their meanings by Bieniawski (1989)**

| Class number | I | II | III | IV | V |
|---|---|---|---|---|---|
| Rock mass rating range | 81 - 100 | 61 - 80 | 41 - 60 | 21 - 40 | < 21 |
| Rock mass description | Very good | Good | Fair | Poor | Very poor |
| Cohesion of rock mass, $c$ (kPa) | > 400 | 300 - 400 | 200 - 300 | 100 - 200 | < 100 |
| Friction angle of rock mass, $\varphi$ (deg) | > 45 | 35 - 45 | 25 - 35 | 15 - 25 | < 15 |

### 3.3.3 Petrographic analysis

Petrography is a branch of petrology that focuses on the detailed description of rock. Analysis is performed using a petrographic microscope, which is the instrument most commonly used for studying rock mineralogy for classification. A diamond saw is used to cut a thin slice from the rock sample and pulverized until flat. The material is then mounted on a glass disk and grinded until the sample is about 30µm thick using progressively finer abrasive grit according to Van Tonder (2016). In Figure 3-4 a thin section is being examined under the petrographic microscope. The samples analyzed included rock from each borehole, sandstone, tillite, and the mortar-bars in which sandstone and tillite was used as aggregate. The results from the petrographic analysis are attached in Appendix C, which contains detailed descriptions and photomicrographs of the thin sections.

**Figure 3-4: The petrographic microscope**

## 3.4 Hydrological investigation

The hydrological investigation is based on the survey data and flood calculation methods and is essentially a check of the drainage capacity of the site.

### 3.4.1 Characteristics catchments

In using any method for flood determination, three basic catchment characteristics need to be known. This is the area of the catchment, the longest watercoarse and the average slope of the longest watercoarse in the catchment. The catchment area includes all surfaces which will have a contribution to the flood in question. The area can readily be obtained with software such as AutoCAD by tracing its watershed on a topographical map and prompting for the area. The longest watercourse for each channel was surveyed by GPS from downstream to upstream until they were no longer considered as defined.

Average slopes can be determined from the channel profiles using the so called 10/85 method, in which the difference in height at 10% and 85% of the longest watercoarse is taken over the distance between these points. The heights are calculated from the dataset by means of linear interpolation. The average slope $S$ is calculated as follows by Van Dijk *et al.* (2013):

$$S = \frac{H_{85L} - H_{10L}}{0.75L}$$

Where

$H_{0.85L}$ elevation height at 85% of the chainage distance along the longest watercourse (masl)

$H_{0.10L}$ elevation height at 10% of the chainage distance along the longest watercourse (masl)

$L$ length of longest watercoarse (m)

The length of the longest watercourses and other parameters necessary for calculating the average slopes with the 10/85 method are given in Table 3-2 below for each drainage channel.

**Table 3-2: Calculation of average slopes with the 10/85 method**

| Parameter | Northern channel | Southern channel |
|---|---|---|
| Length of longest watercourse, $L$ (m) | 817.929 | 462.561 |
| Chainage at 10% of watercourse length, $0.10L$ (m) | 81.793 | 46.256 |
| Chainage at 85% of watercourse length, $0.85L$ (m) | 695.240 | 393.177 |
| Elevation at 10% of watercourse length, $H_{0.10L}$ (masl) | 1 024.178 | 1 025.443 |
| Elevation at 85% of watercourse length, $H_{0.85L}$ (masl) | 1 060.375 | 1 046.161 |

### 3.4.2 Flood calculation

Floods are calculated using the catchment characteristics and rainfall data. The Rational and SDF methods were chosen as the most suitable and their calculations are explained in this section. The empirical methods were also used for comparison. The flood calculations for the selected methods are attached in Appendix B for both the northern and southern drainage channels.

For the Rational and SDF methods, the peak flow $Q_T$ with respect to return period $T$ is calculated as follows by Van Dijk *et al.* (2013):

$$Q_T = \frac{C_T I_T A}{3.6}$$

Where

| | |
|---|---|
| $C_T$ | run-off coefficient |
| $I_T$ | average rainfall intensity (mm/hour) |
| $A$ | effective catchment area (km$^2$) |
| 3.6 | conversion factor |

The run-off coefficient is determined differently for the two methods. For the Rational method, the run-off coefficient $C_T$ is generally calculated as follows

$$C_T = \alpha C_{1T} + \beta C_2 + \gamma C_3$$

Where

| | |
|---|---|
| $C_{1T}$ | adjusted contribution to run-off from rural areas |
| $C_2$ | contribution to run-off from urban areas |
| $C_3$ | contribution to run-off from lakes |
| $\alpha$ | proportion of catchment consisting of rural areas |
| $\beta$ | proportion of catchment consisting of urban areas |
| $\gamma$ | proportion of catchment consisting of lakes |

The site is rural only ($\alpha = 1$) and its adjusted contribution to run-off $C_{1T}$ is calculated as follows by Van Dijk *et al.* (2013):

$$C_{1T} = C_1 \times F_t$$

Where

| | |
|---|---|
| $C_1$ | contribution to run-off from rural areas |
| $F_t$ | adjustment factors for initial saturation for steep and impermeable catchments |

The contribution to run-off from rural areas $C_1$ is calculated as follows by Van Dijk *et al.* (2013):

$$C_1 = C_s + C_p + C_v$$

Where

$C_s$ contribution to run-off from surface slope

$C_p$ contribution to run-off from permeability

$C_v$ contribution to run-off from vegetation

For the SDF method, the run-off coefficient $C_T$ is calculated as follows by Van Dijk *et al.* (2013):

$$C_T = \frac{C_2}{100} + \left(\frac{Y_T}{2.33}\right)\left(\frac{C_{100}}{100} - \frac{C_2}{100}\right)$$

Where

$Y_T$ return period factors

$C_2$ calibration factor for 2-year return period (%)

$C_{100}$ calibration factor for 100-year return period (%)

The time of concentration is the time it takes for the entire catchment to contribute to the flood as it peaks on a hydrograph. The time of concentration $T_c$ is calculated as follows by Van Dijk *et al.* (2013):

$$T_c = \left(\frac{0.87L^2}{1000S}\right)^{0.385}$$

Where

$L$ length of longest watercourse (km)

$S$ average slope (m/m)

As the time of concentration is less than 6 hours, the modified Hershfield equation must be used to calculate the point rainfall $P_{t,T}$ as follows by Van Dijk *et al.* (2013):

$$P_{t,T} = 1.13(0.41 + 0.64\ln T)(0.27\ln(60T_c) - 0.11)(0.79M^{0.69}R^{0.20})$$

Where

$T$ return period (years)

$M$ Rainfall for 2-year return period (mm)

$R$ Days of thunder (days/year)

The average rainfall intensity is calculated as follows by Van Dijk *et al.* (2013):

$$I_T = \frac{P_{t,T}}{T_c} \times ARF$$

Where

$ARF$ area reduction factor taken as 100% for these small catchments

### 3.4.3 Flood plain analysis

HEC-RAS was used for the flood plain analysis, which is a computer program that models the hydraulics of water flow through natural rivers and other channels. The program is one-dimensional, meaning that there is no direct modeling of the hydraulic effect of cross section shape changes, bends, and other two- and three-dimensional aspects of flow. The basic computational procedure of HEC-RAS for steady flow is based on the solution of the one-dimensional energy equation. Energy losses are evaluated by friction and contraction or expansion. The surface created from the survey data was used to define an alignment for the channel centerlines and draw perpendicular cross sections in Civil3D. A Mannings n-value of 0.04 was chosen as appropriate and assigned to all the cross sections. A steady flow analysis was performed using the design floods for the 10, 20, 50, 100 and 200 year return periods and a critical depth was chosen for the reach boundary conditions. From this, water surface profiles were created and delineated against the existing ground surface.

## 3.5 Tests on soil

The standard test methods in TMH1 (1986) for untreated soils and gravels were performed on samples as shown in Table 3-3.

**Table 3-3: Summary of tests performed on local soil**

| Test | | Soil samples |
|---|---|---|
| Grading analysis | Sieve analysis | 1 - 6 |
| | Washing | 1 - 6 |
| | Hydrometer analysis | 1 - 4 |
| Atterberg limits | Liquid limit | 1 - 4 |
| | Plastic limit | 1 - 4 |
| | Linear shrinkage | 1 - 4 |
| Compaction test | | 1 - 3 |
| California Bearing Ratio test | | 1 - 3 |

The three main samples are shown in Figure 3-5 being sample 1 (left), sample 2 (middle) and sample 3 (right). These were chosen to perform compaction and CBR tests.

**Figure 3-5: Main soil samples**

### 3.5.1 Grading analysis

The grading analysis essentially consists of a sieve analysis, washing and hydrometer analysis. Each soil sample is passed through a riffler until a sample of required size, representative of the field sample, is obtained. It is then sieved through a series of the standard sieves, using a mechanical sieve shaker, having the following apertures: 63.0mm, 53.0mm, 37.5mm, 26.5mm, 19.0mm, 13.2mm, 4.75mm, 2.0mm and 0.425mm. After sieving, the material retained on each sieve is weighed and the mass recorded. The soil fines, material smaller than 0.425mm, are further used in the mechanical analysis and determination of Atterberg limits. Washing is done to determine the amount of material smaller than 0.075mm. An amount of 100g from the dried soil fines, obtained from the procedure above, is weighed out and thoroughly washed through the 0.075mm-sieve. The material retained after washing is put in the oven to dry at 110°C for 24 hours and the mass recorded.

The percentage $P$ passing the 0.075mm-sieve is calculated as follows (TMH, 1986):

$$P = \frac{S_f(A - B)}{A}$$

Where

$S_f$ percentage soil fines in the sample (%)

$A$ mass of fine material before washing (g)

$B$ mass of the dry material retained on the 0.075mm sieve after washing (g)

In addition to washing, a soil mortar analysis can be performed by expressing the coarse sand fraction (2.0mm – 0.425mm), fine sand fraction (0.425mm – 0.075mm) and fraction smaller than 0.075mm as percentages of the soil mortar.

The percentage coarse sand is expressed as follows (TMH, 1986):

$$\frac{S_m - S_f}{S_m} \times 100$$

The percentage fine sand is expressed as follows (TMH, 1986):

$$\frac{S_f - P}{S_m} \times 100$$

The percentage material smaller than 0.075mm is expressed as follows (TMH, 1986):

$$\frac{P}{S_m} \times 100$$

Where

$S_m$ percentage soil mortar in the sample (%)

The fine sand fraction is subdivided further by sieving the oven-dried material retained on the 0.075mm-sieve after washing through the 0.250mm and 0.150mm sieves. The material retained on each is weighed and the coarse fine sand (0.425mm – 0.250mm), medium fine sand (0.250mm – 0.150mm) and fine fine sand (0.150mm – 0.075mm) fractions expressed as percentages of the soil mortar.

The percentage coarse fine sand is expressed as follows (TMH, 1986):

$$\frac{W_1 \times S_f}{S_m}$$

The percentage medium fine sand is expressed as follows (TMH, 1986):

$$\frac{W_2 \times S_f}{S_m}$$

The percentage fine fine sand is expressed as follows (TMH, 1986):

$$\frac{W_3 \times S_f}{S_m}$$

Where

$W_1$ mass of fraction per 100g of fine material retained on the 0.250mm sieve (g)

$W_2$ mass of fraction per 100g of fine material retained on the 0.150mm sieve (g)

$W_3$ mass of fraction per 100g of fine material retained on the 0.075mm sieve (g)

The hydrometer analysis is a sedimentation process to determine the particle sizes distribution of the soil fraction smaller than 0.075mm. It uses a specially calibrated hydrometer and is based on Stokes' law, which is that the maximum grain diameter $d$ can be calculated as follows (TMH, 1986):

$$d = \sqrt{\frac{300nL}{980T(G - G_1)}}$$

Where

| | |
|---|---|
| $n$ | viscosity of the suspension in Pascal seconds (distilled water has a viscosity of 0.001005Pa.s at 20°C) |
| $L$ | distance in centimeter over which particles settle in a given time $T$ |
| $T$ | time in minutes it takes for particles to settle |
| $G$ | relative density of the soil particles |
| $G_1$ | relative density of the suspension (water has a relative density of 0.99823 at 20°C) |

An amount of 100g from the dried soil fines is again weighed and put in a canning jar adding about 400mℓ of distilled water and 5mℓ of each the sodium oxalate and sodium silicate solutions. The mixture is stirred well with a glass rod and left to stand overnight. After the mixture has been allowed to stand, it is dispersed tor 15minutes with a standard dispersing paddle. The paddle is washed clean with distilled water allowing the wash water to run into the container with the suspension and then poured into the Bouyoucos cylinder. The canning jar is rinsed with distilled water, making sure everything is transferred to the cylinder.

The cylinder is then filled with distilled water up to the 1205mℓ mark with the hydrometer inside. The hydrometer is removed and, using the palm of one hand to cover the opening, inverted a few times to make sure that the temperature is uniform throughout the mixture. It is then placed in the bath at which it is kept as close to 20°C as possible. Once the content in the cylinder is near 20°C, the cylinder is shaken again as before so that a homogenous suspension can be obtained and returned to the bath. The first reading ($C$) is taken an hour later after the hydrometer is inserted again and the temperature of the content also checked. The cylinder is shaken again and placed on a table with the hydrometer inserted about 20 seconds later to take the second reading ($F$) at 40 seconds. It is then repeated, but with the hydrometer inserted about 10 seconds later to take the final reading ($E$) at 18 seconds. The hydrometer readings are taken to the nearest 0.5 and the temperature readings to the nearest 0.1°C.

The percentage coarse sand $P_1$ in the soil mortar is calculated as follows (TMH, 1986):

$$P_1 = \frac{100(S_m - S_f)}{S_m}$$

The percentage fine sand $P_2$ in the soil mortar is calculated as follows (TMH, 1986):

$$P_2 = \frac{S_f(100 - F)}{S_m}$$

Where

$F$ hydrometer reading after 40 seconds

The percentage silt $P_3$ in the soil mortar is calculated as follows (TMH, 1986):

$$P_3 = \frac{S_f(F - C)}{S_m}$$

Where

$C$ hydrometer reading after 1 hour

The percentage clay $P_4$ in the soil mortar is calculated as follows (TMH, 1986):

$$P_4 = C \times \frac{S_f}{S_m}$$

The percentage silt and clay $P_5$ in the soil sample is calculated as follows (TMH, 1986):

$$P_5 = F \times \frac{S_f}{100}$$

The percentage of the soil sample passing the 0.075mm sieve $P_6$ is calculated as follows (TMH, 1986):

$$P_6 = E \times \frac{S_f}{100}$$

Where

$E$ hydrometer reading after 18 seconds

### 3.5.2 Atterberg limits

The Atterberg limits are determined for soil samples 1, 2, 3 and 4. An amount of 48g from the dried soil fines is weighed for determining the liquid limit, plastic limit and linear shrinkage. A small amount of distilled water is added and mixed using a soil spatula until a stiff consistency is achieved. About three quarters of the somewhat wet material is placed in the cup of the liquid limit device and pressed flat using the spatula. The material is then halved down the middle using the standard groove cutting tool and the sling is turned at a rate of two ticks of the cup dropping against its pedestal per second. The sling is kept turning until the base from both sides of the groove flows and touches one another over a distance of 1cm. The number of ticks to achieve this is recorded and 3g of material, weighed to the nearest 0.01g, is put in the oven to dry at 110°C for 24 hours. The procedure is repeated twice, with slightly more water added each time to increase the fluidity of the material. After removing the three

specimens from the oven, it is left to cool down while being protected against the ingress of hygroscopic moisture and weighed again. The three moisture contents are plotted against their respective number of ticks and connected with a trend line, from which the liquid limit is obtained as the moisture content corresponding to 25 ticks.

The moisture content $\omega$ as a percentage of the dry mass is calculated as follows (TMH, 1986):

$$\omega = \frac{a - b}{b - c} \times 100$$

Where

$a$ mass of the container and wet material (g)

$b$ mass of the container and dry material (g)

$c$ mass of the container (g)

For determining the plastic limit, approximately 3g from the wet material is taken to form an ellipsoid by hand. The specimen is rolled out in the palm until it is shaped into a little roll of about 3mm in diameter, as shown in Figure 3-6. It is then remoulded again to form an ellipsoid and rolled out in the palm. The procedure is repeated until the roll crumbles before it reaches a diameter of 3mm. Failure to reach this diameter is due to loss of plasticity and the specimen is weighed to the nearest 0.01g. The material is then dried in the oven at 110°C for 24 hours and the test is repeated for a second specimen.

**Figure 3-6: Rolling out of soil for determining plastic limit**

After removing the two specimens from the oven, it is left to cool down while being protected against the ingress of hygroscopic moisture. It is then weighed again and the moisture content determined as before. The average of the two moisture contents is taken as the plastic limit provided that they do not differ by more than 1.5%.

Immediately after completion of the third test in determining the liquid limit, the remaining material is used for determining the linear shrinkage. A small, clean and dry linear shrinkage mould is heated and the inside covered with a thin layer of molten wax. It is then cooled down by applying a wet cloth to the outside surface of the mould, which prevents the wax layer from cracking. The mould is then filled with the material and cut flush at the top with the spatula. The filled mould is then placed in the oven to dry at 110°C for 24 hours, after which it is removed and left to air dry.

The linear shrinkage $LS$ is calculated as follows (TMH, 1986):

$$LS = Shrinkage\ measured\ in\ mm \times f$$

Where

$f$ factor obtained from TMH depending on number of ticks $N$ corresponding to the moisture content of the final specimen in the liquid limit test

### 3.5.3 Compaction test

The maximum dry density and optimum moisture contents are determined for samples 1, 2 and 3 in the compaction test. They are air-dried and passed through a 19mm sieve, with aggregate retained on the sieve crushed to pass the sieve. Using a riffler, each sample is divided into five samples of 7kg each and into one of 21kg, with only the former used in the compaction test. A sample is then put into the mixer and while being mixed, an amount of water close to optimum is added. The wet material is mixed thoroughly so that the moisture can spread throughout the material. A small amount of soil is then removed for determining the actual moisture content. It is weighed and placed in the oven to dry at 110°C for 24 hours. Before compaction, the weight of the mould is recorded and then fixed to the base of the compaction machine. Filter paper is placed at the bottom to prevent the material from getting stuck to the base. The collar is fixed to the mould and compaction can begin, as shown in Figure 3-7.

**Figure 3-7: Soil under compaction**

The material is compacted in five layers by a 4.536kg free-falling rammer hitting the soil 55 times over a distance of 457.2mm. After the fifth layer has been compacted, the surface of the material should protrude about 15mm above the top of the mould. The mould is then removed from the base of the machine, fixed to a base plate on the ground and its collar carefully removed. The excess material is then removed using a straight edge tool so that the material is cut flush with the top of the mould, as shown in Figure 3-8 below.

**Figure 3-8: Finishing sample after compaction**

Loose stones are pressed in the sample with the flat surface of the straight edge and material scraped off are passed through a 4.75mm sieve and worked into the surface, filling all holes formed from stones. The sample can then be weighed and removed from the mould so that the next sample can be tested. The procedure is repeated for the other four samples, but with the amount of water added varying from the first amount such that at least two coordinates will be located on either side of the vertex on the moisture-density curve. When the dry densities for the five samples are plotted against their corresponding moisture contents, the points on either side of the vertex are connected with straight lines to cross each other at the top. Just below this crossing, they are connected with a smooth curve from which the maximum dry density and optimum moisture content can be obtained.

The moisture content $d$ as a percentage of the dry mass is calculated as follows (TMH, 1986):

$$d = \frac{a - b}{b - c} \times 100$$

Where

$a$ mass of the container and wet material (g)

$b$ mass of the container and dry material (g)

$c$ mass of the container (g)

The dry density $D$ (kg/m$^3$) is calculated as follows (TMH, 1986):

$$D = \frac{W}{d + 100} \times F$$

Where

$W$ mass of the material after compaction (g)

$F$ factor for the volume of the mould

The factor $F$ is calculated as follows (TMH, 1986):

$$F = \frac{100}{V} \times 1000$$

Where

$V$ volume of the mould (mℓ)

### 3.5.4 California Bearing Ratio test

The CBR was determined for samples 1, 2 and 3 in the CBR test. This value is reflective of the materials resistance to penetration and its use as road construction material. If material tested proves to be of the necessary quality, it could be used for patching which will improve the access conditions for delivery of the structural components of the radio telescope and construction equipment. It will also ease driving comfort so that the site is generally more accessible to staff and visitors.

The additional 21kg sample prepared in the compaction test is mixed thoroughly and two specimens are taken for determining the hygroscopic moisture content by being placed in the oven to dry at 110°C for 24 hours. This is done to be able to calculate the amount of water needed for optimum moisture content, at which compaction is performed.

The water $W$ needed to reach optimum moisture content is calculated as follows (TMH, 1986):

$$W = \frac{z(y - x)}{100 + x}$$

Where

$x$ hygroscopic moisture content (%)

$y$ optimum moisture content (%)

$z$ mass of the air-dried sample (g)

The remaining material is taken from storage and the calculated amount of water added. The wet material is mixed thoroughly in the mixer so that the moisture can spread throughout the material. A small amount of soil is then removed and placed in a container for confirming the moisture content. It is weighed and placed in the oven to dry at 110°C for 24 hours. The moisture content should not differ by more than 0.3% from the optimum moisture content determined earlier. Three samples are

compacted as before, but at different compaction efforts. The first sample is compacted just as in the compaction test. The second sample is compacted similarly, but the rammer hits the soil only 25 times per layer. The third sample is compacted in only three layers by a 2.495kg free-falling rammer hitting the soil 55 times per layer over a distance of 304.8mm. The surface of each sample is finished, as described previously, and turned upside down so that the bottom surface with the filter paper faces up. A perforated plate and a weight of 4.536kg are placed on top of each sample and then placed inside an open container. After the gauge is put on the sample and the initial reading recorded, the containers are filled with water. It is left to soak for four days, after which another reading is recorded. This is to determine swelling of the material as a percentage of the initial sample height of 127mm.

The swelling $S$ is calculated as follows (TMH, 1986):

$$S = \frac{k - L}{127} \times 100$$

Where

$k$ reading after the material has soaked for four days (mm)

$L$ reading before the material has soaked (mm)

The perforated plates and weights are removed and the water is carefully drained from each sample. It is placed in the press one at a time with a 5.56kg weight placed in the middle of the sample. The press is set to penetrate the sample at a rate of 1.27mm per minute. The test is continued until the press penetrates the sample to a depth of at least 9mm. All data is digitally recorded from which the load-penetration curves are plotted. The loads required to penetrate the sample 2.54mm, 5.08mm and 7.62mm are obtained. They are then calculated as a percentage of the standard CBR values given in Table 3-4.

**Table 3-4: Standard CBR values**

| Penetration depth (mm) | Californian standard load (kN) |
|---|---|
| 2.54 | 13.344 |
| 5.08 | 20.016 |
| 7.62 | 25.354 |

The load-penetration curves often start concave upwards, which should be corrected by extending the straight line portion of the graph downwards to cut the horizontal axis, which is taken as the new zero reading. The CBR at 2.54mm penetration is used to evaluate the quality of material and plotted on logarithmic scale against dry density on natural scale for the three compactive efforts. The dry densities are expressed as percentages of the maximum dry density. The three points are connected with a trend line from which the design CBR can easily be obtained at the desired density.

## 3.6 Tests on rock

The sandstone and tillite samples were directly collected from the field, while the phyllite sample was obtained from core drilling. The tests performed on the rock samples are shown in Table 3-5 and were mainly focused on sandstone and tillite. Only one sample from borehole 1 conformed to the requirements for UCS as set out in the next section. A petrographic analysis was performed on all rocks and mortar-bars as discussed earlier.

**Table 3-5: Summary of tests performed on local rock**

| Test | Rock samples |
|---|---|
| UCS and point load index tests | Q, T, S |
| Particle and relative density test | Q, T |
| Mortar-bar test | Q, T |

### 3.6.1 Unconfined compressive strength and point load index tests

Six core specimens were obtained from both sandstone and tillite. These were drilled from a number of sandstone and tillite samples collected from site. The core specimens measured 45mm in diameter, which meant their lengths had to be cut to 90mm, as the general standard for length to diameter ratio of rock and concrete cylinders are 2. All six of the sandstone specimens were subsequently tested for UCS as shown in Figure 3-9 (a). The phyllite specimen also conformed to the requirement and were tested for UCS. None of the tillite specimens conformed this requirement, as they broke more easily. Point load tests were performed instead, as the length to diameter ratio in the diametrical point load test needs to be at least 1.5. The six tillite specimens were tested in this manner with the point load aparatus shown in Figure 3-9 (b). The point load index obtained can be used in Figure 3-10 to estimate a UCS value. diameter of core sample in the case of the diametrical test. The unconfined compression strength $\sigma$ is calculated as follows:

$$\sigma = \frac{F}{A}$$

Where

$F$ load recorded at failure (N)

$A$ cross-sectional area of core sample ($mm^2$)

The area $A$ is calculated as follows:

$$A = \frac{\pi d^2}{4}$$

Where

$d$ diameter of core sample (mm)

**a) UCS test** **b) Point load index test**

**Figure 3-9: Compression tests on sandstone and tillite**

The point load index $I_S$ is calculated as follows from Byrne & Berry (2008):

$$I_S = \frac{P}{d^2}$$

Where

$P$ point load recorded at failure (N)

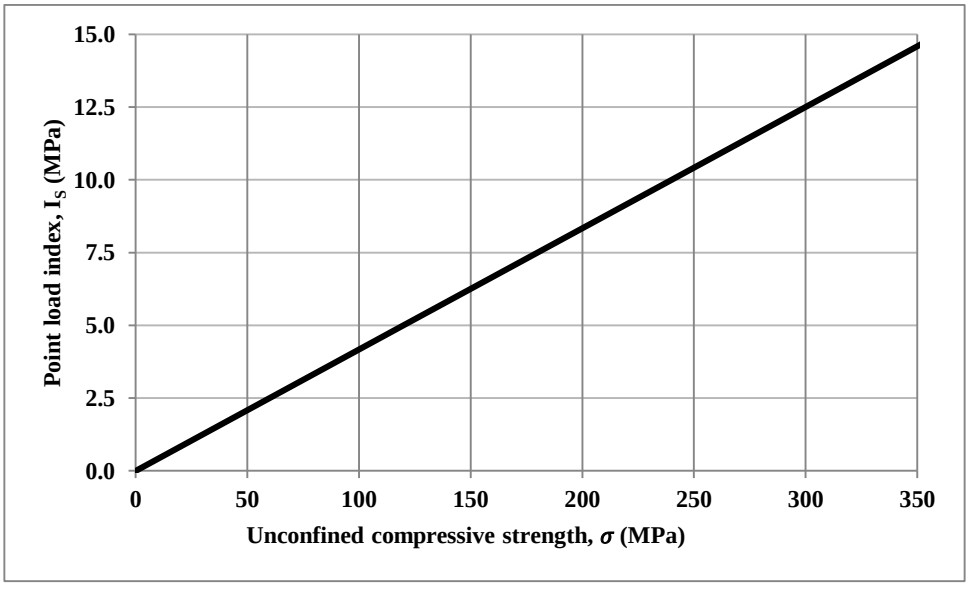


**Figure 3-10: Point load index correlation with UCS from Byrne & Berry (2008)**

### 3.6.2 Particle and relative densities

The particle and relative densities of sandstone and tillite are determined using SANS 5844. The relative density of aggregate needs to be known for the mortar-bar test. The ratio of dry materials for the test mortar must be 1 part cement to 2.25 parts of graded aggregate by mass for aggregate with a relative density equal to or greater than 2.45. The aggregate proportion $p$ for a relative density less than 2.45 can be calculated as follows (ASTM, 2007):

$$p = 2.25 \times \frac{RD}{2.65}$$

Where

$RD$ relative density of aggregate to water

The particle and relative densities were obtained using the pycnometer shown in Figure 3-11. For both sandstone and tillite, aggregate retained on the 2.36mm-sieve as prepared for the mortar-bar test, was used. This fraction was used as it was available in abundance after crushing and sieving. Using this fraction also made the test easier, allowing trapped air to escape easier. The aggregate was soaked in water for 24 hours in order to have the pores filled. After soaking, a fan was used to dry the surface of the aggregate until a saturated surface-dried state have been reached. The pycnometer was filled to a third with this aggregate and weighed. It was then filled with water with a suction device used to rid entrapped air, and weighed again.

**Figure 3-11: Pycnometer**

The weights of the pycnometer alone and the pycnometer filled only with water were also recorded. All the aggregate was removed from the pycnometer and placed in the oven at 110°C for 24 hours, after which it was weighed again.

The particle density $\delta_{ps}$ on a saturated surface-dried basis is calculated as follows (SANS, 2006):

$$\delta_{ps} = \frac{m_a}{m_a - (m_c - m_d)} \times \delta_w$$

Where

$m_a$ mass of saturated surface-dry aggregate (g)

$m_c$ mass of pycnometer, aggregate and water (g)

$m_d$ mass of pycnometer filled with water (g)

$\delta_w$ density of water (kg/m$^3$)

The particle density $\delta_{po}$ on an oven-dried basis is calculated as follows (SANS, 2006):

$$\delta_{po} = \frac{m_b}{m_a - (m_c - m_d)} \times \delta_w$$

Where

$m_b$ mass of oven-dried aggregate (g)

The apparent relative density is calculated as follows (SANS, 2006):

$$RD = \frac{m_b}{m_b - (m_c - m_d)}$$

### 3.6.3 Mortar-bar test

The test for potential alkali-silica reaction was performed using the ASTM C 1260-7 method. The rocks used in the test were broken up using a jack-hammer so they would fit into the crusher. The crushed aggregate of sandstone (left) and tillite (right) are shown in Figure 3-12.

**Figure 3-12: Crushed sandstone and tillite**

The crushed aggregate were subsequently graded according to the requirements in Table 3-6. After the aggregate has been separated into the various sieve sizes, each size was washed to remove adhering dust and fine particles. It was then left to dry in the oven at 110°C for 24 hours. The dry sizes were then weighed out according to proportioning requirements in Table 3-6. The total mass of aggregate used for thee mortar-bar samples is specified in the test procedure as 990g and the mass of cement as 440g. Thus for six samples of each aggregate type, this becomes 1 980g and 880g respectively.

**Table 3-6: Proportioning of aggregate according to grading requirements**

| Sieve size | | Proportioning of aggregate | |
|---|---|---|---|
| **Passing (mm)** | **Retained (mm)** | **Mass (%)** | **Mass (g)** |
| 4.75 | 2.36 | 10 | 198 |
| 2.36 | 1.18 | 25 | 495 |
| 1.18 | 0.60 | 25 | 495 |
| 0.60 | 0.30 | 25 | 495 |
| 0.30 | 0.15 | 15 | 297 |

Figure 3-13 shows the graded portions for sandstone and tillite (the container on the bottom right is the cement portion). Each portion was stored in a clean plastic bag and sealed untill further use. Four identical moulds were built with three compartments each and their specifications can be found on the drawing attached in Appendix F. A water cement ratio of 0.47 by mass is further specified, equating to 413.6g of water needed in the mixture. As the ingredients were poured into the mixer and allowed to blend, the interior surfaces of the moulds were covered with a release agent. They were then filled with the mortar mixture in two approximately equal layers, each being compacted with a tamper. After moulds have been further compacted on the vibrator table, excessive mortar was scraped flush with the top of the moulds using a trowel. The metal gauge studs were gently put in place using the spacer that comes with the gauge. The mortar-bars were then stored in the moist room for 24 hours. Once carefully removed from the moulds, initial readings were recorded to the nearest 0.002mm. The six mortar-bars of each aggregate type were placed in labelled containers and submerged in water. The containers were made from a type of perspex resistant to sodium hydroxide at high temperature. These were then placed in the left compartment of the tank which contained water already heated to 80°C, for 24 hours.

The containers were removed from the tank one at a time. Each mortar-bar was removed, measured and placed on a towel. The reading for each bar had to be recorded within 10 to 20 seconds after removal from its container. This is called the zero reading and is necessary to accommodate for thermal expansion. After all mortar-bars were measured, they were returned to their container, this time submerged in 1N NaOH (each litre of solution contains 40.0g of NaOH) at 80°C and returned to the tank.

**a) Sandstone**

**b) Tillite**

**Figure 3-13: Graded aggregate**

The NaOH solution was prepared by Alaud (2015) and tested at the Department of Process Engineering. The test method states that the time between removal and return of the mortar-bars to the tank must not exceed 10 minutes. Four subsequent readings were taken every seven days with the procedure being identical to that as described above. Each comparator reading is multiplied by the gauge factor of 0.81 and the gauge division of 0.002 to convert to a linear distance in millimetres. The method states that length change of less than 0.1% at 16 days after casting is usually indicative of innocuous behaviour, while more than 0.2% is indicative of potentially deleterious expansion.

The change in length $L$ at any age is calculated as follows (ASTM, 2007):

$$L = \frac{L_x - L_i}{G} \times 100$$

Where

$L_x$ comparator reading of specimen at *x* age minus comparator reading of reference bar at *x* age (mm)

$L_i$ initial comparator reading of specimen minus comparator reading of reference bar at the same time (mm)

$G$ nominal gauge length of 200mm

# Chapter 4

# Results

## 4.1 Introduction

This chapter reports and interprets the results obtained following the methodology described in the previous chapter. The first section is about the processed survey data showing the digital terrain model of the main study area and the two profiles for the drainage channels. The following two sections are on reporting and interpreting the findings of the site investigation, which includes the geotechnical and hydrological investigations. The results of the geotechnical investigation include the core logging, rock mass rating of borehole 1 and important petrographic results. The results of the hydrological investigation include the determined catchment parameters, flood calculations and the resultant flood line analysis. The laboratory results, which include findings on the tests performed on local soil and rock samples. The results on soil include grading, Atterberg limits, compaction and California Bearing Ratio on selected samples. The results of the rock sample analysis include unconfined compressive strength and diametrical point load tests on the sandstone and tillite. One sample from borehole 1 in the geotechnical investigation was also tested for UCS as a requirement for the rock mass rating and indicator for other parameters in the design. It further reports the findings of the densities obtained, followed by the results of the mortar-bar test. The section thereafter is dedicated to the classification of soil with respect to soil type and material quality. The final section is on the evaluation of soil and rock for engineering purposes, such as the three river sands for fine aggregate in concrete, backfill material for trenches and patching material for maintenance of the access road. The section ends with the evaluation of rock as coarse aggregate.

## 4.2 Digital terrain model and channel profiles

The digital terrain model of the site was created in AutoCAD Civil3D using the combined survey data. An aerial photo was then draped over the surface in AutoCAD Infraworks and the resulting model is shown in Figure 4-1. The model is bounded by the access road from the bottom right to the top left. The northern channel can be seen on the right with the southern channel on the left. The model was used in the flood line delineation of these drainage channels.


**Figure 4-1: Digital terrain model of the main study area**

The channel profiles were also obtained from the survey data and are shown below in Figure 4-2 as elevation in meter above sea level against chainage. The chainage starts at zero where the channels intercept the access road, which are the points at which the floods were determined. The profiles are used to calculate the average slopes to be used in the flood calculations.

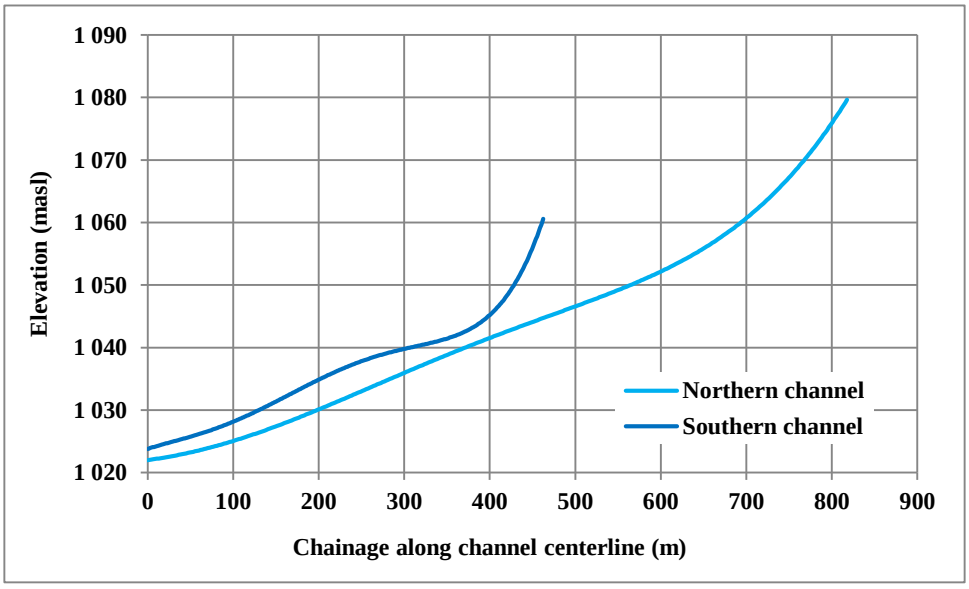


**Figure 4-2: Channel profiles**

## 4.3 Geotechnical results

This section reports and interprets the results on the geotechnical investigation. The borehole locations are shown in Figure 4-7 in the next section. The core boxes, filled with recovered cores from these boreholes, were photographed and are shown in Figure 4-3. The logging order is from top left to bottom right and the core logging sheets are attached in Appendix A. It contains the geotechnical information regarding the recovery and general description of the rock according to the core logging guide by the Association of Engineering Geologists (1976).

**Figure 4-3: Core logs from borehole 1 (top), borehole 2 (middle) and borehole 3 (bottom)**

The drilling method unfortunately resulted in numerous driller breaks and, in addition to natural fractures, made the recovery data very difficult to log. Discussions with Fouché (2016) led to the decision to treat the log of each borehole as a single drill run. Borehole 1 yielded the best general core recovery and was the only one from which a standard sample could be prepared for the unconfined compressive strength test, which verified the rock hardness (very hard rock) assessed during the core logging. With the geological map indicating Kweekvlei shale and considering the presence of micacious minerals indicating metamorphism, the rock is described as a slate or phyllite. The material from borehole 2 proved difficult to log, as it was highly fractured without any intact core pieces. A noteworthy observation is that the first ±300mm of core looks the same as the core from borehole 1, while the rest of the material appears to be similar to that of borehole 3, having the same type of flow banding. The dark grey and dark green gray bands of mudstone and siltstone from borehole 3, respectively, were mostly resistant to being scraped with a knife and were therefore considered as medium hard. The rock grades down into core with more siltstone than mudstone lenses with depth. The general description of each borehole log is visually represented in Figure 4-4 and includes descriptions of the upper soil according to the standard system by Jennings *et al.* (1973).

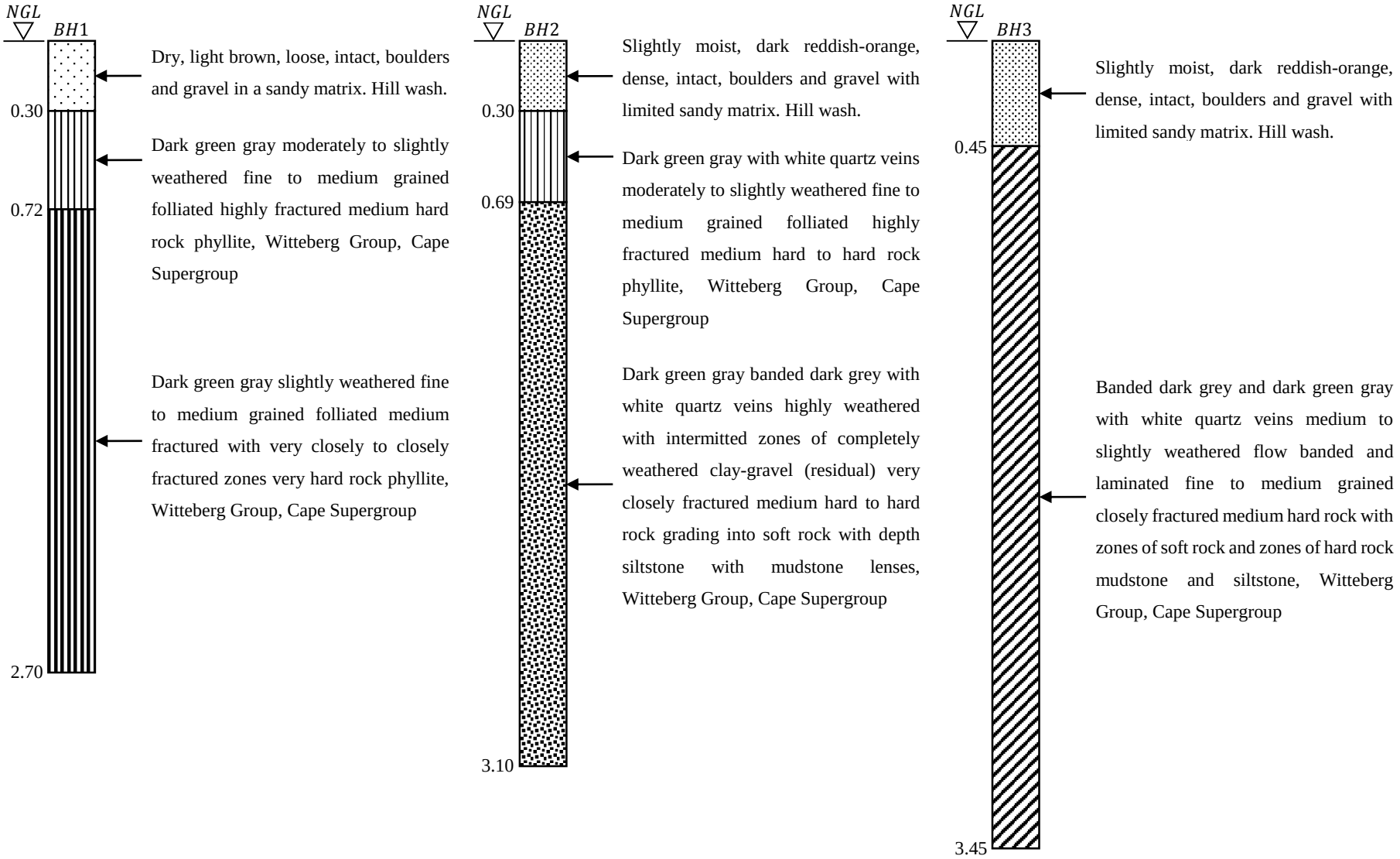


**Figure 4-4: Borehole logs**

**Table 4-1: Overall rock mass rating of borehole 1**

| Parameter | | Range of parameter values and their corresponding ratings | | | | | | |
|---|---|---|---|---|---|---|---|---|
| 1 | Unconfined compressive strength (MPa) | < 1 | 1 - 5 | 5 - 25 | 25 - 50 | 50 - 100 | 100 - 250 | > 250 |
| | Rating | 0 | 1 | 2 | 4 | **7** | 12 | 15 |
| 2 | Rock quality designation (%) | 0 - 25 | | | 25 - 50 | 50 - 75 | 75 - 90 | 90 - 100 |
| | Rating | 3 | | | **8** | 13 | 17 | 20 |
| 3 | Spacing of discontinuities (mm) | < 60 | | | 60 - 200 | 200 - 600 | 600 - 2 000 | > 2 000 |
| | Rating | 5 | | | **8** | 10 | 15 | 20 |
| 4 | Discontinuity length (m) | > 20 | | | 10 - 20 | 3 - 10 | 1 - 3 | < 1 |
| | Rating | **0** | | | 1 | 2 | 4 | 6 |
| | Discontinuity separation (mm) | > 5 | | | 1 - 5 | 0.1 - 1 | < 0.1 | None |
| | Rating | 0 | | | 1 | **4** | 5 | 6 |
| | Roughness of discontinuities | Slickensided | | | Smooth | Slightly rough | Rough | Very rough |
| | Rating | 0 | | | 1 | **3** | 5 | 6 |
| | Discontinuity infill (mm) | Soft fill > 5 | | | Soft fill < 5 | Hard fill > 5 | Hard fill < 5 | None |
| | Rating | 0 | | | 2 | 2 | **4** | 6 |
| | Weathering of discontinuities | Completely weathered | | | Highly weathered | Medium weathered | Slightly weathered | Unweathered |
| | Rating | 0 | | | 1 | 3 | 5 | **6** |
| 5 | Groundwater (general conditions) | Flowing | | | Dripping | Wet | Damp | Completely dry |
| | Rating | 0 | | | 4 | 7 | **10** | 15 |
| 6 | Strike and dip orientations | Very unfavourable | | | Unfavourable | Fair | Favourable | Very favourable |
| | Rating adjustment | -25 | | | -15 | -7 | **-2** | **0** |

The RMR on the rock from borehole 1 was performed as founding material. The format of the rating table was modified to ensure that irrelevant information is being discarded and is shown in Table 4-1. As a personal modification, the columns have been mirrored to have the ratings in increasing order from left to right. The subvertical discontinuity orientations were considered to be favourable in the rating adjustment, as it results in higher in-situ stability of the rock mass according to Croukamp (2014). A rock mass rating of 48, which describes the rock mass as fair rock in Table 3-1, was obtained. This rating is considered to be somewhat conservative for a number of reasons. The rock quality designation is fairly low (35%) as a result of assuming most fractures as natural, even though several were induced by the driller. The discontinuity length or persistence is also not known from borehole data and zero was therefore assigned as its rating. For these reasons, instead of adding more conservative assumptions by simply selecting the lower boundary values in class III as shear strength parameters, linear interpolation is used to find intermediate parameters. By assigning the lower rating of 41 to 200kPa and the upper rating of 60 to 300kPa, cohesion of 234kPa is obtained. The same approach for 25° and 35°, respectively, results in an angle of friction of 29°. These parameters will be divided by partial material factors in the foundation design. The sample prepared for UCS was weighed and measured in order to determine the unit weight of the founding material, an important parameter in the weight density term of the bearing capacity equation in foundation design. The mass was recorded as 3.6kg and the volume calculated as 0.00137$m^3$, resulting in a density of 2 623.59$kg/m^3$ and unit weight of 25.737$kN/m^3$.

## 4.4 Hydrological results

This section reports and interprets the results on the hydrological investigation. Both catchments are shown in Figure 4-5 with the areas shaded light blue and dark blue representing the surfaces contributing to the northern and southern channels, respectively.

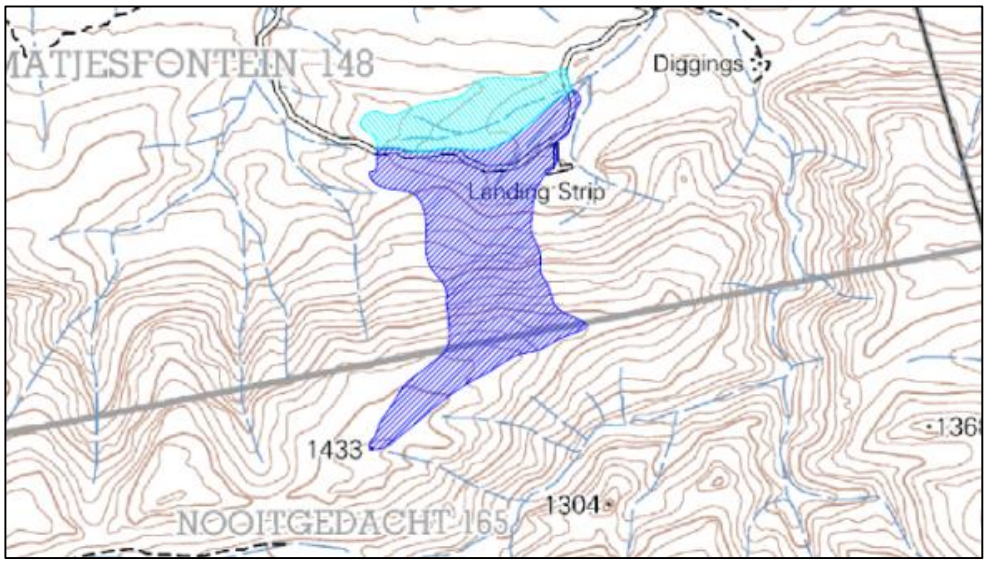


**Figure 4-5: Extract from topographical map showing catchments (NTS)**

The areas were obtained in AutoCAD and the length and average slopes of the channels were calculated from the GPS data after they were surveyed. A summary of the basic catchment characteristics for both catchments is contained in Table 4-2 below. These parameters are unique for each catchment and form the basis for flood calculation.

**Table 4-2: Summary of catchment characteristics**

| Parameter | Northern channel | Southern channel |
|---|---|---|
| Area, $A$ ($m^2$) | 143 417.954 | 478 405.588 |
| Longest watercourse, $L$ (m) | 817.929 | 462.561 |
| Average slope, $S$ (m/m) | 0.059 | 0.060 |

The MSGO is equipped with a weather station on site, but staff at HartRAO have stated that data recorded thus far is unreliable. The station is also relatively new with the record length only covering a few years, adding to the unreliability. Fortunately, the South African Weather Bureau has rainfall data listed from a weather station in town, of which the design rainfall depths are summarized in Table 4-3 (a) and is deemed representative for the Rational method. For the SDF method, the design rainfall data used depends upon the relevant SDF basin in which the catchments are located. The site is located in SDF basin 19 and its representative weather station is based in Letjiesbos. The design rainfall depths are given in Table 4-3 (b). The mean annual precipitation (MAP) for the two stations are incidentally both 165mm. The important value in these tables is the 2-year return period daily rainfall needed in the modified Hershfield equation for time of concentrations less than 6 hours.

**Table 4-3: Design rainfall depths**

**a) Matjiesfontein**

| Duration (days) | Return period, $T$ (years) | | | | | | |
|---|---|---|---|---|---|---|---|
| | **2** | **5** | **10** | **20** | **50** | **100** | **200** |
| **1** | 25 | 37 | 46 | 55 | 68 | 80 | 92 |
| **2** | 30 | 44 | 54 | 64 | 78 | 90 | 103 |
| **3** | 33 | 48 | 59 | 71 | 87 | 101 | 116 |
| **7** | 37 | 53 | 65 | 76 | 93 | 107 | 121 |

**b) Letjiesbos**

| Duration (days) | Return period, $T$ (years) | | | | | | |
|---|---|---|---|---|---|---|---|
| | **2** | **5** | **10** | **20** | **50** | **100** | **200** |
| **1** | 34 | 55 | 72 | 92 | 124 | 152 | 185 |
| **2** | 38 | 64 | 87 | 112 | 153 | 190 | 233 |
| **3** | 40 | 68 | 93 | 121 | 166 | 206 | 254 |
| **7** | 45 | 79 | 110 | 145 | 202 | 254 | 315 |

The flood calculation sheets for each drainage channel are attached in Appendix B. It contains calculations using the Rational, Standard Design Flood and empirical methods. The peak floods from the Standard Design Flood method were chosen as representative for both channels and are presented in Table 4-5 as the design floods in cubic meters per second.

**Table 4-4: Design floods**

| Drainage channel | Return period, *T* (years) | | | | | | |
|---|---|---|---|---|---|---|---|
| | **2** | **5** | **10** | **20** | **50** | **100** | **200** |
| **Northern** | 0.2 | 0.6 | 1.0 | 1.4 | 2.0 | 2.5 | 3.1 |
| **Southern** | 0.7 | 2.4 | 3.8 | 5.5 | 8.0 | 10.1 | 12.3 |

Figure 4-6 shows idealised hydrographs for the 20 year and 200 year floods for each channel with rising limbs equal to the time of concentration and falling limbs equal to twice this duration. A very conservative approach was followed in HEC-RAS to delineate these floods by assuming steady flow conditions. Floods in natural channels are typically characterized by unsteady non-uniform flow according to Chadwick *et al.* (2004), but are the most complex to analyze.

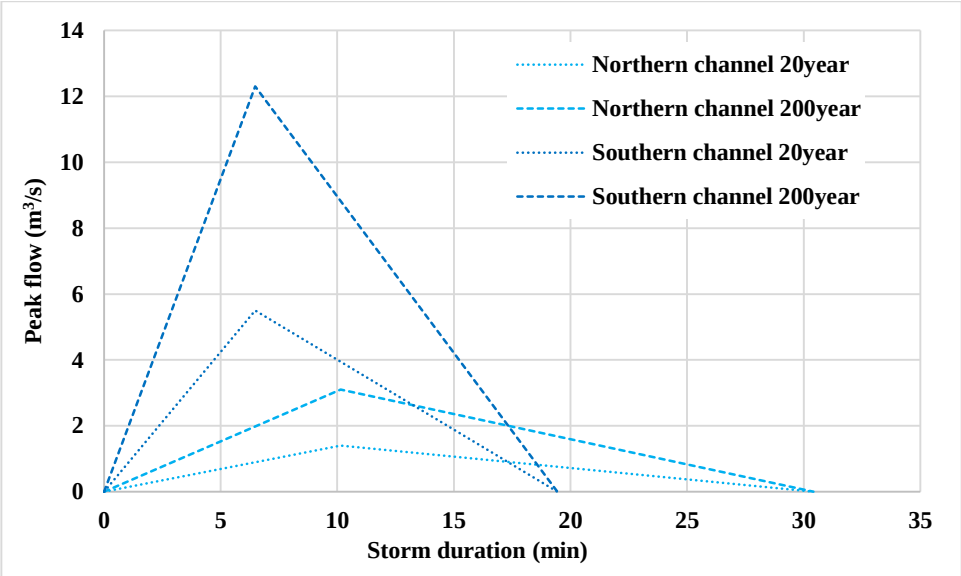


**Figure 4-6: Simplified hydrographs**

The resulting conservative flood lines are shown in Figure 4-7. The dramatic widening in delineation seen in both channels is due to the flat topography where they become temporarily ill-defined and water is spread outwards. When considering the borehole locations as potential positions for radio telescope antennas, it is clear that the hypothesis of flooding not posing any threat to structures located in the main study area is validated. Although the analysis is not necessarily a realistic estimation, it serves to emphasize the favourable drainage capacity of the site and a more exact analysis is therefore not justified.

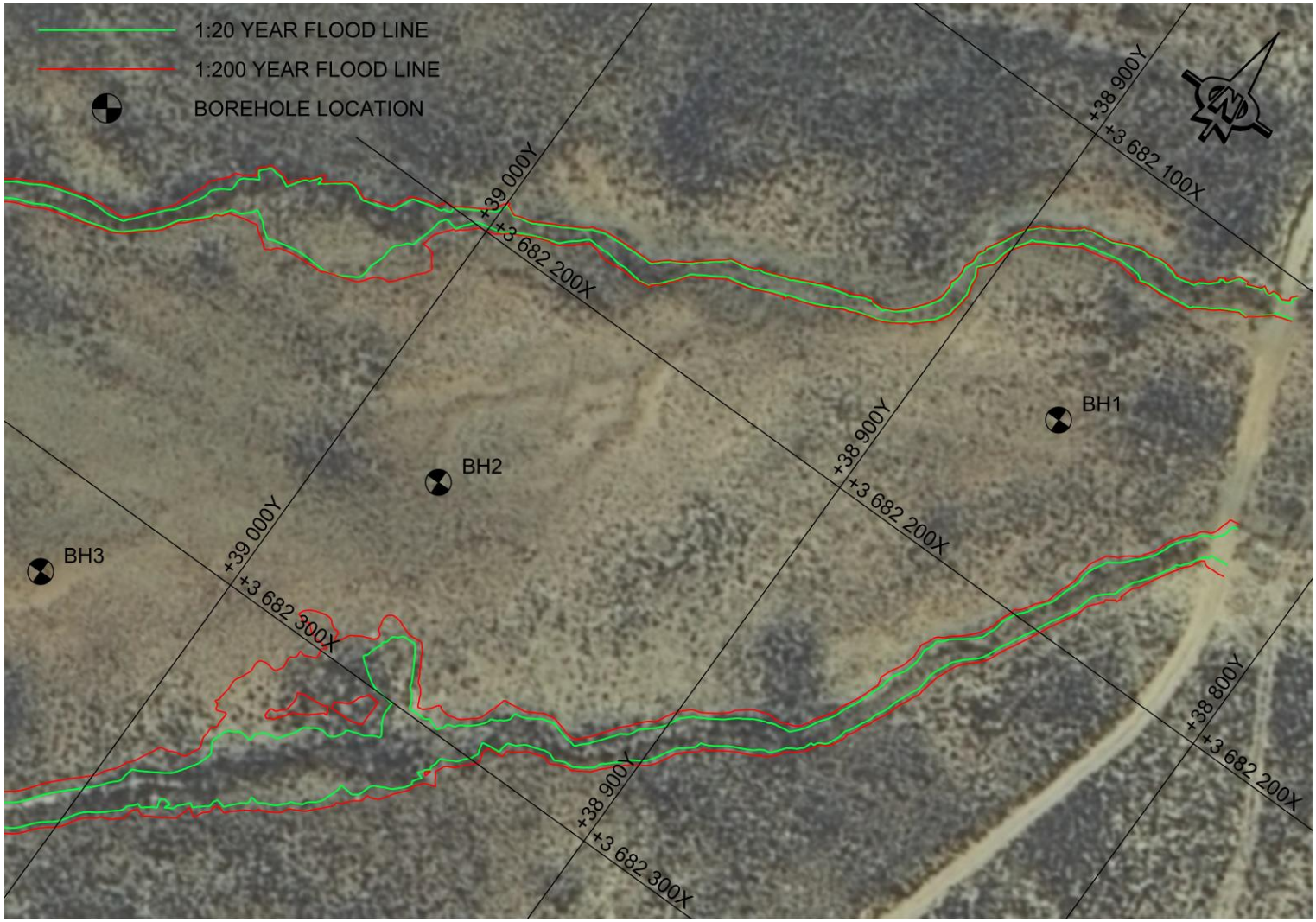


**Figure 4-7: Flood lines and borehole locations (scale 1:1500)**

## 4.5 Results on soil

This section reports and interprets the findings of the laboratory tests performed on local soil after six disturbed soil samples were recovered, prepared and tested.

### 4.5.1 Grading analysis

The grading analysis included sieving, washing and hydrometer analyses. The grading curves for the six soil samples are shown in Figure 4-8 and the material passing the 0.075mm-sieve after washing are shown in Table 4-5. The detailed tables showing the grading results for each sample is given in Appendix D.

**Table 4-5: Percentage material passing the 0.075mm-sieve**

| Parameter description | Sample | | | | | |
|---|---|---|---|---|---|---|
| | 1 | 2 | 3 | 4 | 5 | 6 |
| Mass soil fines before wash, $A$ (g) | 100.0 | 100.0 | 100.0 | 100.0 | 100.0 | 100.0 |
| Mass soil fines after wash, $B$(g) | 72.1 | 91.7 | 94.2 | 27.4 | 75.9 | 88.3 |
| Percentage soil fines in the sample, $S_f$ (%) | 68.3 | 69.0 | 10.1 | 82.5 | 16.3 | 62.8 |
| Percentage passing 0.075mm-sieve, $P$ (%) | 19.1 | 5.7 | 0.6 | 59.9 | 3.9 | 7.4 |

The results of the soil mortar analysis are shown in Table 4-6 below and the results of the hydrometer analysis are given in Table 4-7. The results seem to be reasonably sensible when comparing the different soil types, considering the amount of soil fines determined above. It is however stated in TMH1 that the method does not ensure absolute results.

**Table 4-6: Results of soil mortar analysis**

| Parameter description | Sample | | | | | |
|---|---|---|---|---|---|---|
| | 1 | 2 | 3 | 4 | 5 | 6 |
| Percentage soil mortar in the sample, $S_m$ (%) | 76.7 | 89.1 | 59.5 | 97.1 | 73.2 | 96.4 |
| Percentage coarse sand (%) | 10.9 | 22.6 | 83.0 | 15.1 | 77.7 | 34.8 |
| Percentage fine sand (%) | 64.2 | 71.0 | 16.0 | 23.3 | 16.9 | 57.5 |
| Percentage material smaller 0.075mm (%) | 24.8 | 6.4 | 1.0 | 61.6 | 5.4 | 7.6 |
| Mass retained on the 0.250mm-sieve, $W_1$ (g) | 17.4 | 40.3 | 65.9 | 5.0 | 33.5 | 28.4 |
| Mass retained on the 0.150mm-sieve, $W_2$ (g) | 27.9 | 30.8 | 21.2 | 16.9 | 36.2 | 52.4 |
| Mass retained on the 0.075mm-sieve, $W_3$ (g) | 26.8 | 20.6 | 7.1 | 5.5 | 6.2 | 7.6 |
| Percentage coarse fine sand (%) | 15.5 | 31.2 | 11.2 | 4.3 | 7.5 | 18.5 |
| Percentage medium fine sand (%) | 24.8 | 23.8 | 3.6 | 14.4 | 8.1 | 34.1 |
| Percentage fine fine sand (%) | 23.9 | 16.0 | 1.2 | 4.7 | 1.4 | 4.9 |

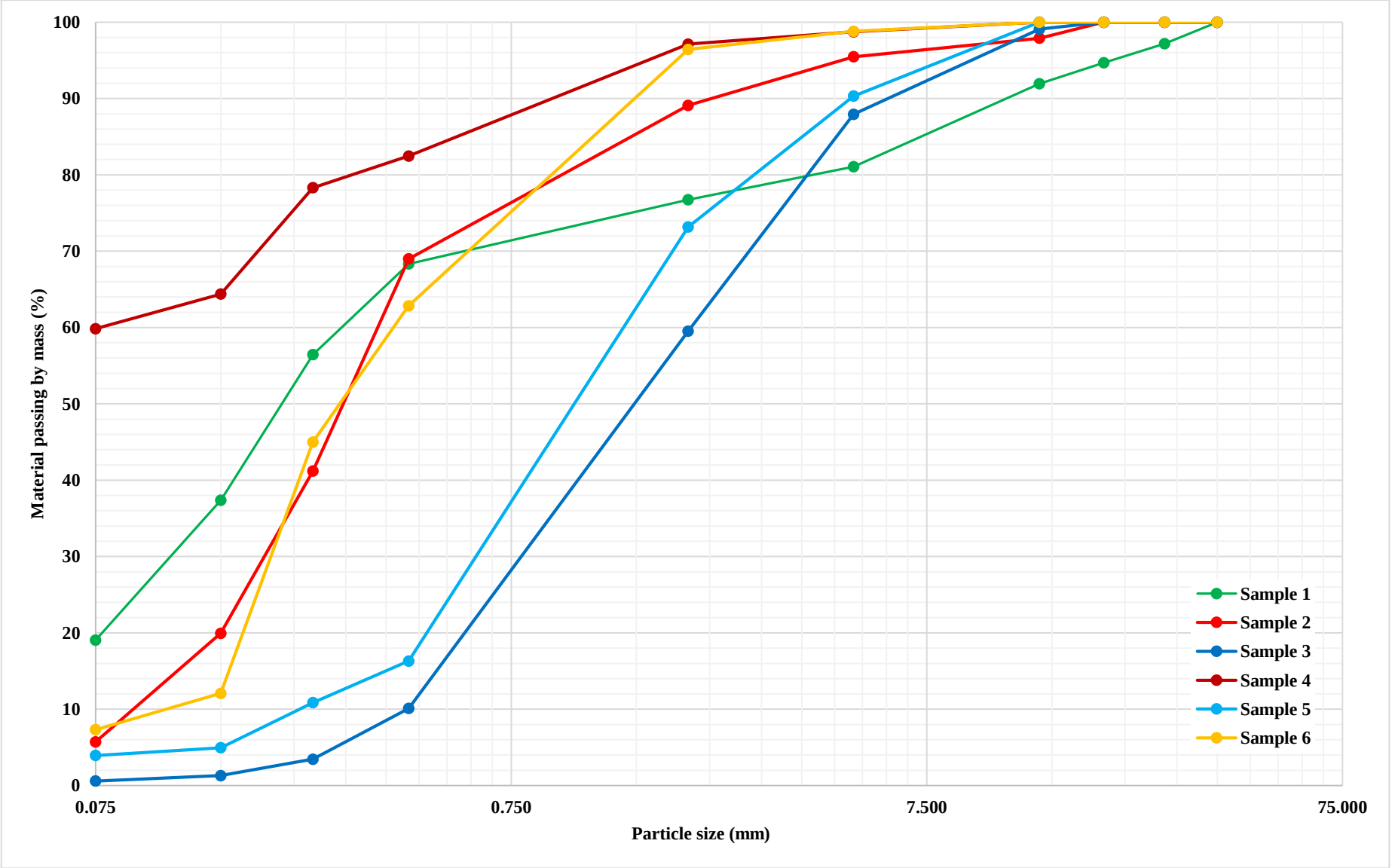


**Figure 4-8: Grading curves**

**Table 4-7: Results of hydrometer analysis**

| Parameter description | Sample | | | |
|---|---|---|---|---|
| | 1 | 2 | 3 | 4 |
| Percentage coarse sand in the soil mortar, $P_1$ (%) | 10.9 | 22.6 | 83.0 | 15.1 |
| Percentage fine sand in the soil mortar, $P_2$ (%) | 71.7 | 60.0 | 13.1 | 47.6 |
| Percentage silt in the soil mortar, $P_3$ (%) | 3.5 | 2.6 | 0.6 | 22.9 |
| Percentage clay in the soil mortar, $P_4$ (%) | 13.9 | 14.9 | 3.3 | 14.4 |
| Percentage silt and clay in the sample, $P_5$ (%) | 13.3 | 15.5 | 2.3 | 36.2 |
| Percentage material passing the 0.075mm-sieve, $P_6$ (%) | 14.0 | 15.9 | 2.4 | 48.6 |

### 4.5.2 Atterberg limits

The Atterberg limits are the liquid and plastic limits, the plasticity index and the linear shrinkage. For the liquid limit, three specimens from each soil sample were tested at varying moisture contents, which were determined and are given with their corresponding number of ticks in Appendix D. These points are plotted in Figure 4-9 and connected with a trend line. The liquid limit is taken as the moisture content corresponding to 25 ticks of the cup against the pedestal of the liquid limit device.

For the plastic limit two specimens from each soil sample were repeatedly rolled out into the palm of the hand until they started to crumble. The moisture contents were calculated and are also given in Appendix D. The plastic limit is then taken as the average moisture content of the two. Table 4-8 gives a summary of the Atterberg limits for each sample with the liquid and plastic limits and the numerical difference between these values which is the plasticity index. Note that a plastic limit for sample 3 could not be determined and is thus termed non-plastic (NP), which equates to a plasticity index of zero.

**Table 4-8: Plasticity index**

| Parameter description | Sample | | | |
|---|---|---|---|---|
| | 1 | 2 | 3 | 4 |
| Liquid limit, *LL* (%) | 17 | 21 | 18 | 39 |
| Plastic limit, *PL* (%) | 14 | 14 | NP | 19 |
| Plasticity index, *PI* (%) | 3 | 7 | 0 | 20 |

The linear shrinkage values are summarized in Table 4-9. After being removed from the oven for determining the linear shrinkage, some of the samples had to be pressed back into the moulds before the shrinkage could be measured. The Atterberg limits are used to assess soil for a variety of applications in civil engineering.

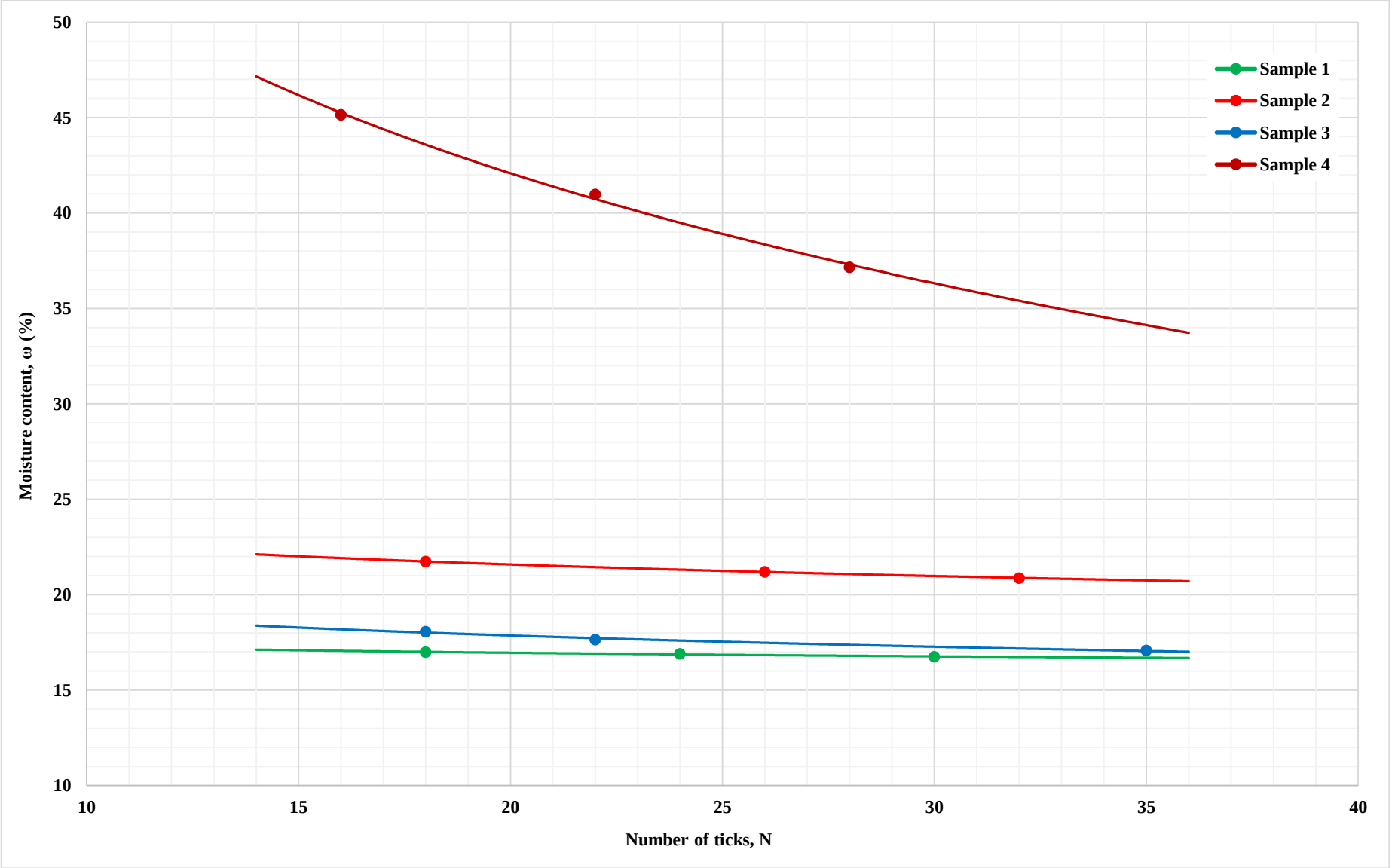


**Figure 4-9: Flow curves**

**Table 4-9: Linear shrinkage**

| Parameter description | Sample | | | |
|---|---|---|---|---|
| | 1 | 2 | 3 | 4 |
| Shrinkage measured (mm) | 2.5 | 6.0 | 0.0 | 12.0 |
| Factor from TMH1, $f$ | 0.62 | 0.62 | 0.62 | 0.61 |
| Linear shrinkage, $LS$ (%) | 1.6 | 3.4 | 0.0 | 7.3 |

### 4.5.3 Compaction results

The compaction results are shown in Figure 4-10 for the three main soil samples in the form of moisture-density curves. The five points of each sample were plotted and the conventional manner for determining the optimum moisture content and maximum dry density was followed. This is to plot the points and connect the points on either side of the turning point by straight lines, assuming the optimum moisture content where the two lines intercept one another. The two lines is then connected with a smooth curve from which the maximum dry density ca be obtained. The optimum moisture contents and their corresponding maximum dry densities are given in Table 4-10.

**Table 4-10: Maximum dry densities and optimum moisture contents**

| Parameter description | Sample | | |
|---|---|---|---|
| | 1 | 2 | 3 |
| Optimum moisture content, $\omega_{opt}$ (%) | 7.0 | 9.1 | 6.0 |
| Maximum dry density, $\rho_{d,max}$ (kg/m$^3$) | 2 042 | 2 045 | 2 000 |

The optimum moisture content give an indication of the water required for backfilling on site where services are to be installed in trenches underground, such as the existing pipeline and power/fibre optic cables for instruments like the radio telescopes and the satellite/lunar laser ranger. The optimum moisture content is further a requirement for the California bearing ratio test, as performed on soil sample 3 with the results given in the next section.

### 4.5.4 California bearing ratio results

The California bearing ratios were determined for the three main soil samples. Firstly, the hygroscopic moisture content was determined for the material. The procedure dictates that two specimens be taken for this calculation from each sample. With the hygroscopic moisture content known, the amount of water needed to reach the optimum moisture content of each sample were calculated. After the addition and mixing of the required water to the material, a specimen of each sample was taken to verify that the optimum moisture contents have indeed been achieved. All these calculations are given in Appendix D.

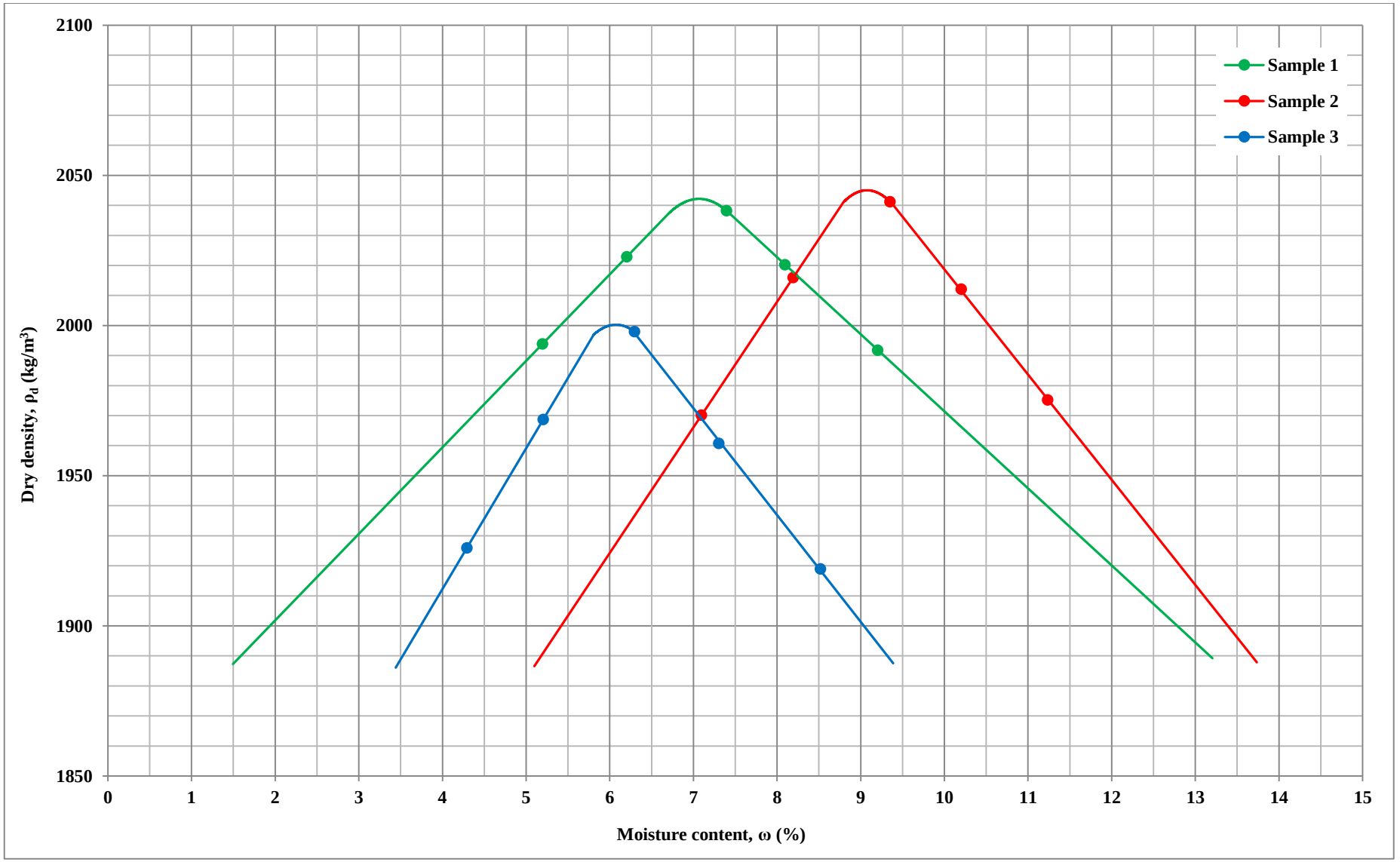


**Figure 4-10: Moisture-density curves**

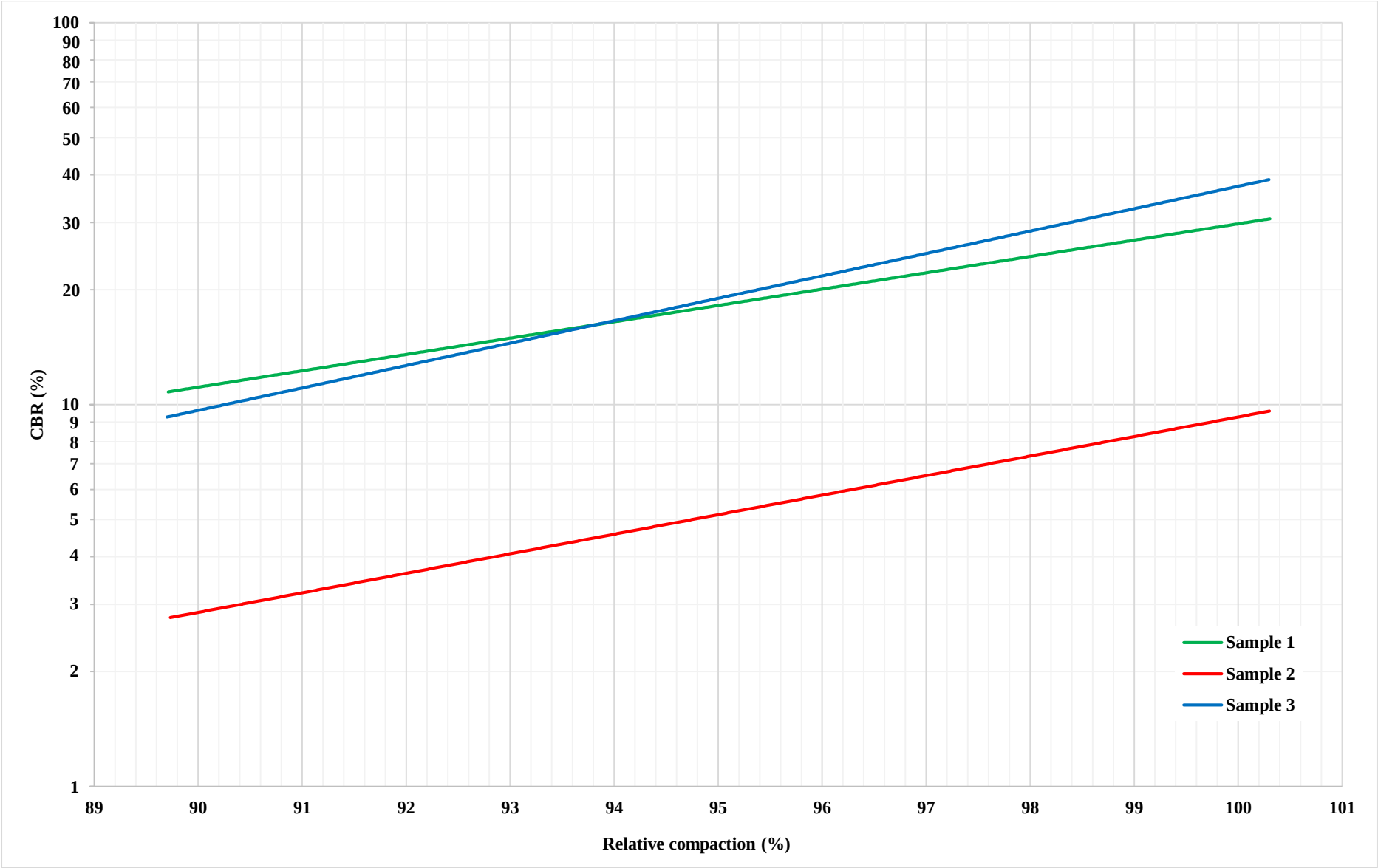


**Figure 4-11: CBR-density curves**

The material was then compacted at the three varying compaction efforts. The results for the swelling of the three specimens are also given in Appendix D and it can be seen that virtually no swelling was observed after four days of soaking. The specimens were drained and taken to the press where they were subjected to penetration depths of up to 9mm, as shown by the bearing ratio curves in Appendix D. It can be seen that the higher the compaction effort, the higher the load is needed to penetrate the material. The CBR values associated with a penetration depth of 2.54mm are used to describe the quality of material. These can be obtained from the CBR curves and are given in Table 4-11 for each specimen.

**Table 4-11: Load required to penetrate 2.54mm (kN)**

| Sample | MOD | NRB | STD |
|---|---|---|---|
| **1** | 4.25 | 2.30 | 1.60 |
| **2** | 1.40 | 0.60 | 0.40 |
| **3** | 5.00 | 2.38 | 1.40 |

The Californian standard loads are 13.344kN, 20.016kN and 25.354kN for penetration depths of 2.54mm, 5.08mm and 7.62mm respectively. The loads from Table 4-11 are taken as percentages of the Californian standard loads to obtain the Californian bearing ratio values shown in Table 4-12.

**Table 4-12: California bearing ratios (%)**

| Sample | MOD | NRB | STD |
|---|---|---|---|
| **1** | 31.85 | 17.24 | 11.99 |
| **2** | 10.49 | 4.50 | 3.00 |
| **3** | 37.47 | 17.84 | 10.49 |

These CBR values are then plotted against their respective dry densities, calculated as percentages of the maximum dry density for each sample. The three points of each sample are then connected with a trend line from which the design CBR at the required percentage of maximum dry density can be obtained. The three CBR-density curves are given in Figure 4-11.

## 4.6 Results on rock

This section reports and interprets the findings of the laboratory tests performed on local rock after several rock samples were recovered, prepared and tested.

### 4.6.1 Unconfined compressive strength results

The average unconfined compressive strengths of sandstone and tillite, were calculated as 74.5MPa and 70.9MPa respectively. The calculations of the six individual samples each for sandstone and tillite are given in Appendix D. All the sandstone samples had a length-to-diameter ratio of 2.1 and the tillite samples were all greater than 1.5. The UCS result of the core sample obtained from borehole 1 was 83.1MPa.

### 4.6.2 Particle and relative density test results

The results of the particle and relative densities for sandstone and tillite are given in Table 4-13. The relative density for both sandstone and tillite are greater than 2.45, which dictates that the test mortar for the mortar-bar test must be 1 part cement to 2.25 parts of graded aggregate by mass.

**Table 4-13: Particle and relative densities**

| Description | Sandstone | Tillite |
|---|---|---|
| Particle density on a saturated surface-dried basis, $\delta_{ps}$ (kg/m$^3$) | 2 633.1 | 2 662.3 |
| Particle density on an oven-dried basis, $\delta_{po}$ (kg/m$^3$) | 2 626.0 | 2 638.9 |
| Relative density, $RD$ | 2.64 | 2.70 |

### 4.6.3 Mortar-bar test results

The results of the mortar-bar test suggest that no significant expansion due to alkali-silica reactivity were present for any of the aggregate types. The rapid increase in Figure 4-12 between the initial and zero readings are due to thermal expansion, as the specimens were first introduced to water at 80°C before being moved to the sodium hydroxide solution, also heated to 80°C. Only a slight expansion was recorded for both the sandstone and tillite specimens after 14 days in the solution, which can be regarded as negligible and thus innocuous expansion. It should be noted that according to Oberholster (2009) the reactivity of aggregates from the same geological formation and even from the same quarry can differ widely. Nevertheless, the results are positive and the results of the petrography are given in Appendix C. In the sandstone some straining was observed in quartz grains with less than 20% of all grains showing undulose extinction of average 11.2$^o$ according to the Dolar-Mantuani (1975) method which falls within the limits for rocks indicating a low ASR potential. The undulose extinction is generally not a good indicator of ASR according to Oberholster (2016). The raw readings for both aggregates are given in Appendix D.

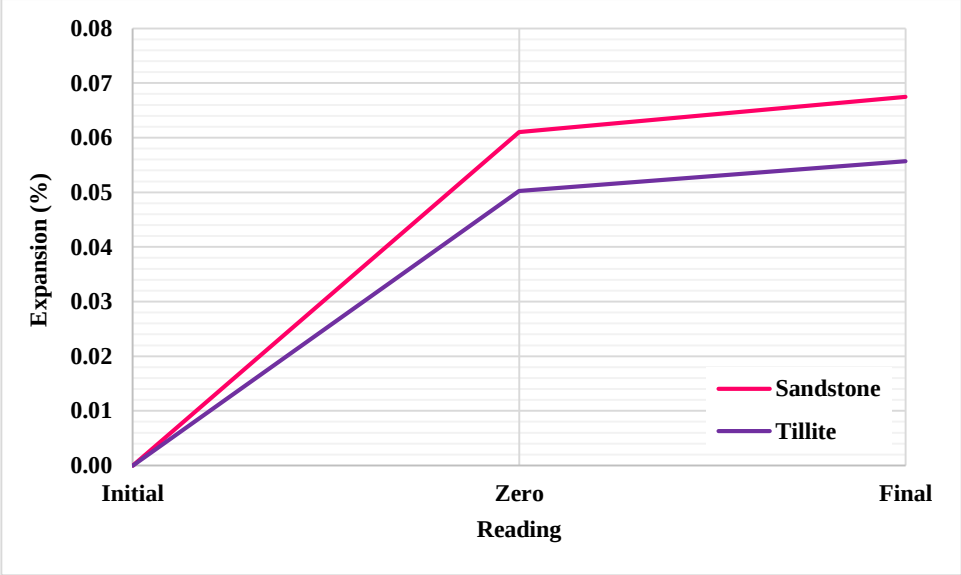


**Figure 4-12: Average expansion during mortar-bar test**

## 4.7 Soil classification

The soils are classified in terms of soil type and material quality in this section using the results previously obtained.

### 4.7.1 Soil type

The soil type of the six soil samples can readily be classified using the Unified Soil Classification System and are summarized in Table 4-14 below.

**Table 4-14: Soil type classification**

| Sample | Symbol | Soil type |
|---|---|---|
| 1 | SM | Silty sand |
| 2 | SP | Poorly graded sand |
| 3 | SW | Well-graded sand |
| 4 | CL | Sandy clay |
| 5 | SW | Well-graded sand |
| 6 | SP | Poorly graded sand |

For the classification of coarse grained soils, the percentage of gravel and sand are determined from the sieve analysis and are classified as GW, GP, SW or SP for soils with less than 5% fines or as GM, GC, SM or SC for soils with more than 12% fines. Soils with fines between 5% and 12% are considered borderline cases that require dual symbols. The system uses the plasticity chart in Figure 4-13 for the classification of fine grained soils, but also for gravels and sands with appreciable amounts of fines.

**Table 4-15: The Unified Soil Classification System from Byrne & Berry (2008)**

| Major Divisions | | | Group Symbol | Typical Names | | Laboratory Classification Criteria | |
|---|---|---|---|---|---|---|---|
| Coarse Grained Soils (more than 50% greater than 0.075mm) | Gravels (more than 50% of coarse fraction greater than 4.5mm) | Clean Gravels | GW | Well-graded gravels, gravel-sand mixtures | | $1 < \frac{{D_{30}}^2}{D_{10} \times D_{60}} < 3$ and $\frac{D_{30}}{D_{10}} > 4$ | |
| | | | GP | Poorly graded gravels, gravel-sand mixtures | | Not meeting both the above gradation requirements for GW | |
| | | Gravels with fines | GM | $\frac{d}{u}$ | Silty gravels, gravel-sand-silt mixtures | Atterberg limits below A-line or PI less than 4 | Above A-line with PI between 4 and 7 are borderline cases requiring use of dual symbols |
| | | | GC | Clayey gravels, gravel-sand-clay mixtures | | Atterberg limits below A-line with PI greater than 7 | |
| | Sands (more than 50% of coarse fraction smaller than 2.0mm) | Clean Sands | SW | Well-graded sands, gravelly sands | | $1 < \frac{{D_{30}}^2}{D_{10} \times D_{60}} < 3$ and $\frac{D_{60}}{D_{10}} > 4$ | |
| | | | SP | Poorly graded sands, gravelly sands | | Not meeting both the above gradation requirements for SW | |
| | | Sands with fines | SM | $\frac{d}{u}$ | Silty sands, sand-silt mixtures | Atterberg limits below A-line or PI less than 4 | Limits plotting in hatched zone with PI between 4 and 7 are borderline cases requiring use of dual symbols |
| | | | SC | Clayey sands, sand-clay mixtures | | Atterberg limits below A-line with PI greater than 7 | |
| Fine Grained Soils (more than 50% of material smaller than 0.075mm) | Silts and clays (LL less than 50%) | | ML | Inorganic silts and very fine sands, rock flour, silty or clayey fine sands | | See Figure 4-13 | |
| | | | CL | Inorganic clays of low medium plasticity, gravelly, sandy, silty or lean clays | | | |
| | | | OL | Organic silts and organic silty clays of low plasticity | | | |
| | Silts and clays (LL greater than 50%) | | MH | Inorganic silts,micaceous or diatomaceous line sandy or silty soils | | | |
| | | | CH | Inorganic clays of high plasticity, fat clays | | | |
| | | | OH | Organic clays of medium to high plasticity, organic silts | | | |
| | Highly Organic Soils | | Pt | Peat and other highly organic soils | | | |

The Unified Soil Classification System is given in Table 4-15. Sample 1 is classified as a silty sand, since it has a significant amount of fines with a PI of less than four. Samples 2 and 6 are classified as poorly graded sands, while samples 3 and 5 conformed to the grading requirements for well-graded sand. Sample 4 plotted closest to a sandy clay on the plasticity chart. Despite the fact that only six samples were classified, it is believed that they are good indicators of the variety of soil at the MSGO.

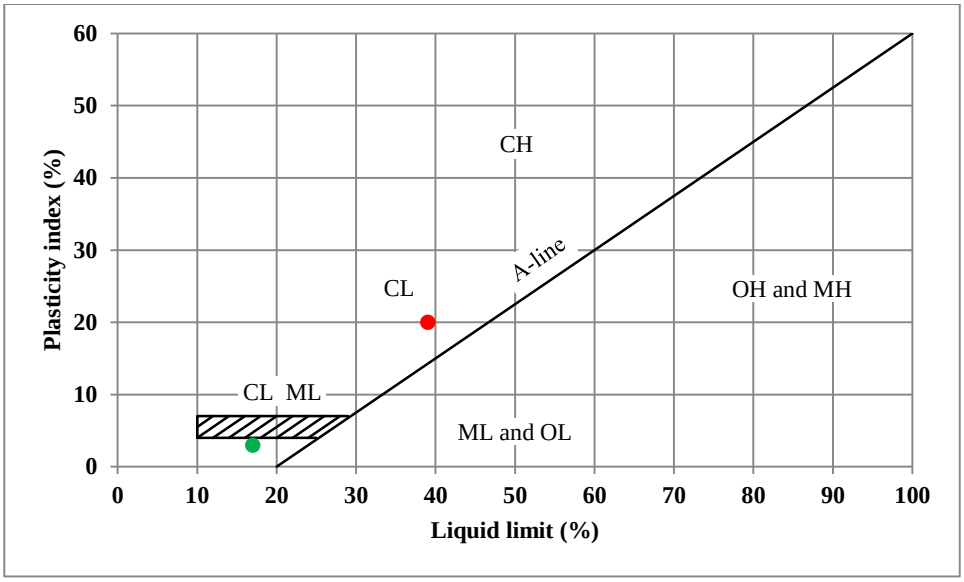


**Figure 4-13: The plasticity chart**

### 4.7.2 Material quality

The material quality of the three main soil samples can readily be classified using TRH14 for road construction material. Table 4-16 gives the parameters needed in the classification for each sample and then gives the actual classification. Sample 1 proved to be of the best quality and is classified as G7 material, while sample 2 is classified as G10 material as it had very low CBR values and is subsequently considered as poor material. Sample 3 was also considered as good material, albeit being classified as G8 material when its CBR at 93% MOD AASHTO density is only 0.5% short of the 15% necessary to conform to the requirement for G7 material quality.

**Table 4-16: Material quality classification**

| Parameter description | Sample | | |
|---|---|---|---|
| | 1 | 2 | 3 |
| Liquid limit, *LL* (%) | 17 | 21 | 18 |
| Plasticity index, *PI* (%) | 3 | 7 | 0 |
| Grading modulus, $G_M$ | 1.4 | 1.4 | 2.3 |
| CBR @ 93% MOD AASHTO (%) | 15.0 | 4.0 | 14.5 |
| CBR @ 95% MOD AASHTO (%) | 18.0 | 5.1 | 19.0 |
| CBR @ 98% MOD AASHTO (%) | 24.5 | 7.4 | 28.5 |
| Swell @ 100% MOD AASHTO (%) | 0.01 | 0.03 | 0.00 |
| Classification | G7 | G10 | G8 |

## 4.8 Evaluation of soil and rock

In this section some of the results are used to evaluate the materials for certain engineering performances, but can be used in any other applications as well.

### 4.8.1 Concrete aggregate

The three river sand samples can be evaluated as fine aggregate for concrete by grading the material passing the 4.75mm-sieve according to the series of sieves indicated in Figure 4-14. If any material is desired to be used, it can be obtained by screening the material in the same manner on site. The detailed tables showing the grading results for each sand are given in Appendix D.

The histogram in Figure 4-14 shows the percentage of material on each sieve for the three river sands from which the dominant fractions can be identified. The fineness modulus, which is a measure of the average fineness or coarseness of an aggregate according to Addis (1998), can also be calculated from the grading results. This is done by dividing the sum of cumulative percentages retained on all sieves down to 0.15mm by 100. The two similar sands of samples 3 and 5 both have fineness moduli to that of a coarse sand being 3.3 and 3.2, respectively. Sand from sample 6 have a fineness modulus of 1.7, which is that of a fine sand. If coarse (sample 3) and fine (sample 6) sands are blended to a 50:50 ratio, then theoretically a medium sand can be obtained with a fineness modulus of 2.5. As the coarse and fine sands transgress the respective coarse and fine limits (Addis, 1998), the blended sand shows a suitable grading in Figure 4-15. This is not necessarily recommended as source material and preparation might be costlier than to simply use imported material.

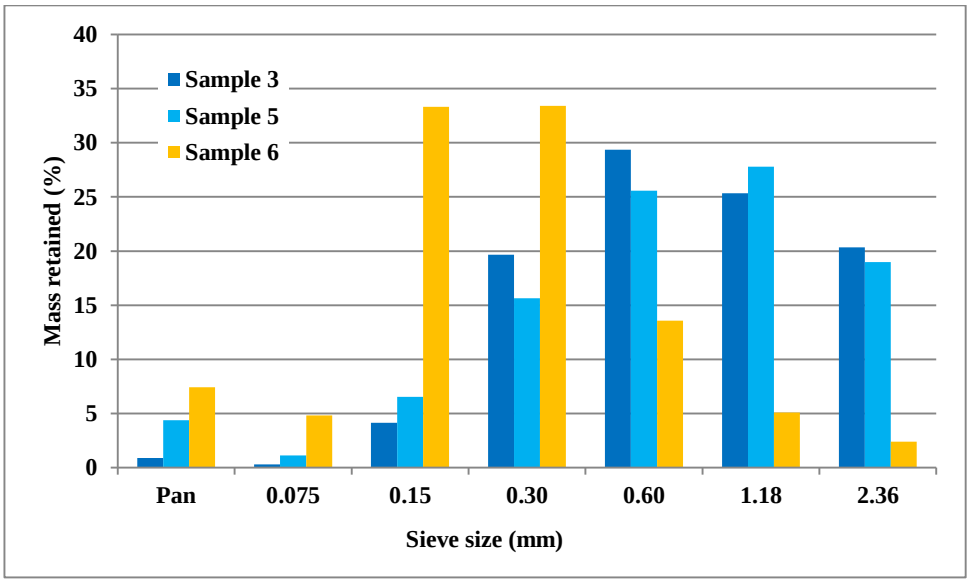


**Figure 4-14: Histogram of river sands**

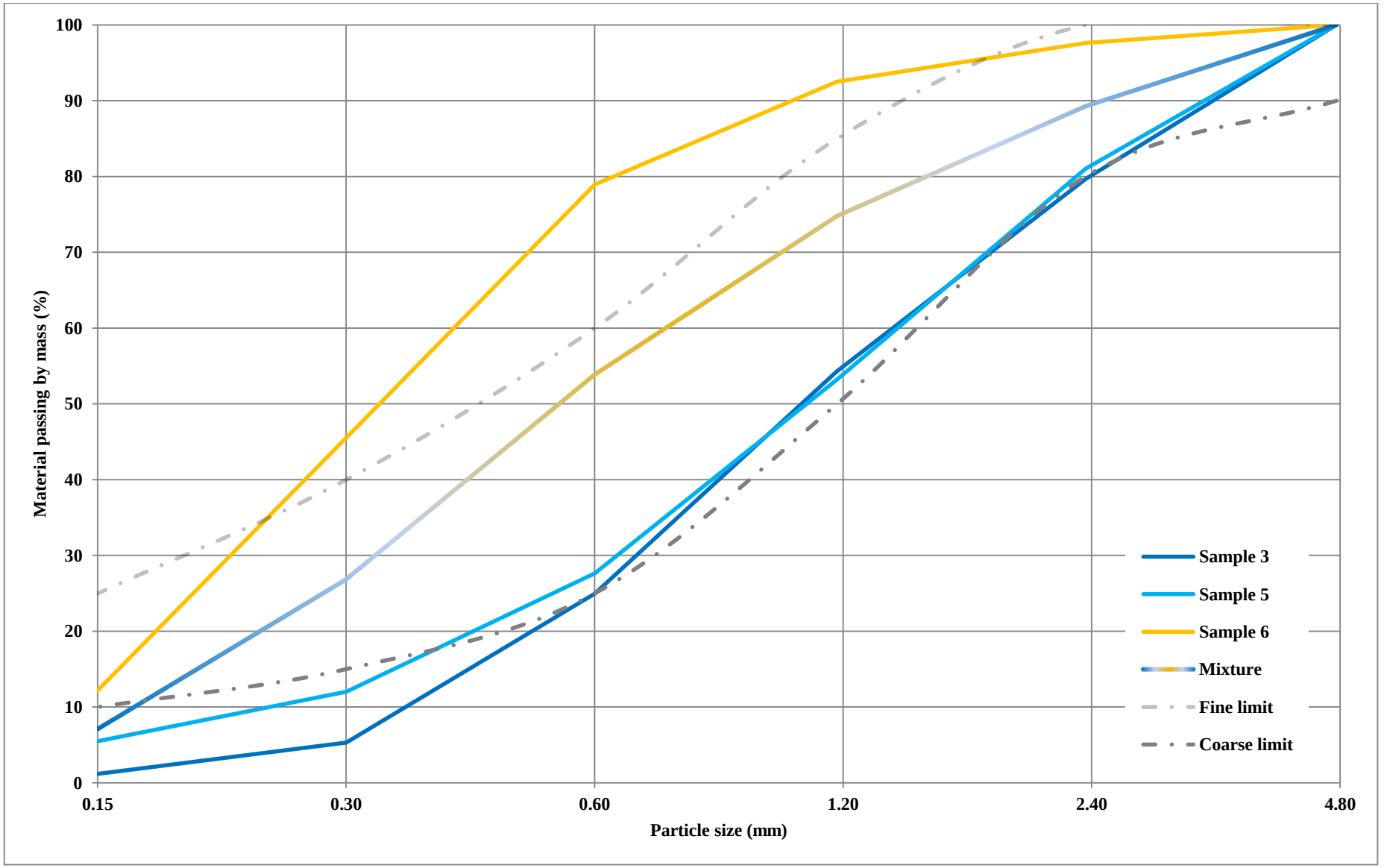


**Figure 4-15: Evaluation of soil as fine aggregate**

The most apparent application of the results on the sandstone and tillite are their use as coarse aggregate in concrete. The concrete mix design in Table 4-17 with a target strength of 40MPa using local sandstone can be used, as the unconfined compressive strengths were found to be much greater than 40MPa. The mortar-bar test suggested no ASR, which was confirmed by the petrographic results. Although the mortar-bar test also suggested no ASR when tillite was used, the petrographic results indicated a risk for ASR. If boulders on site can be crushed and screened for aggregate without having to open a quarry, it can lead to economical savings without negative environmental impacts that will render the MSGO site aesthetically displeasing.

**Table 4-17: Concrete mix design by Van Wyk (2013)**

| w/c = 0.55 | On 1000ℓ | | | | | | On 10ℓ |
|---|---|---|---|---|---|---|---|
| | Mass (kg) | | RD | | Mass (kg) | | Mass (kg) |
| Water | 180 | ÷ | 1.00 | = | 180 | | 1.80 |
| CEM II/B-M (L-S) 42.5N | 327 | ÷ | 3.14 | = | 104 | 648 | 3.27 |
| Stone (Sandstone) | 950 | ÷ | 2.61 | = | 364 | | 9.50 |
| Sand (Malmesbury) | 922 | ÷ | 2.62 | = | 352 | 352 | 9.22 |

## 4.8.2 Fill material

The material can be evaluated to be used as backfill and selected fill in trenching for the placement of services, which may hold certain requirements. Sections through trenches for flexible water pipes (SABS, 1983) and power cable ducts (SABS, 1981) with typical details and minimum vertical dimensions are shown in Figure 4-16.

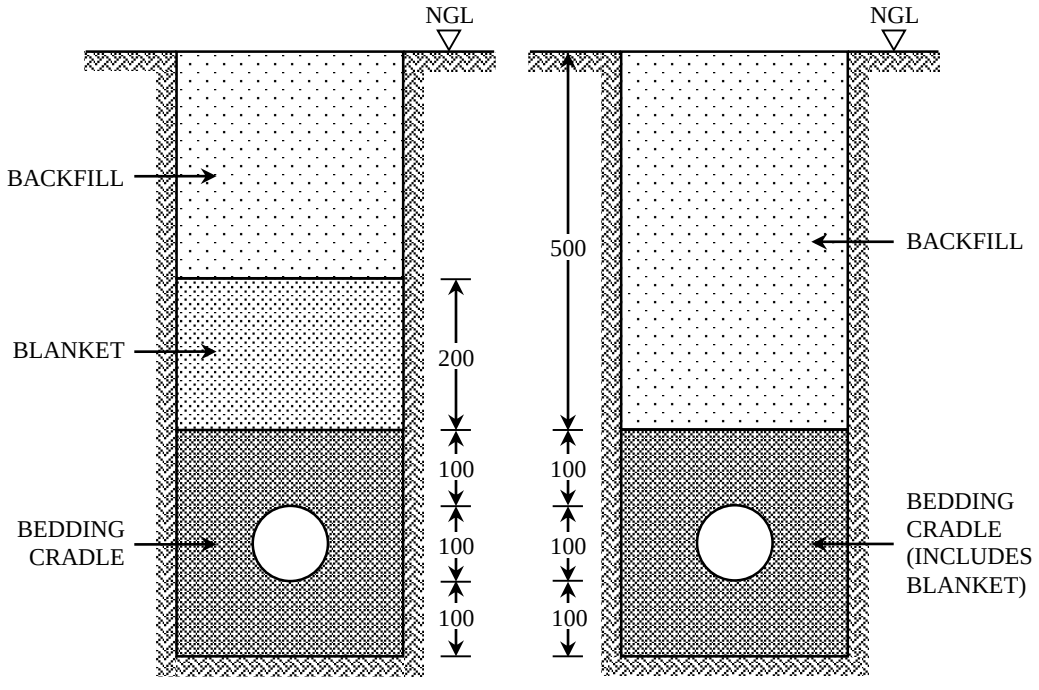


**(a) Flexible pipes** **(b) Power cable ducts**

**Figure 4-16: Typical trench details**

None of the material conforms to the requirements for the bedding cradle in trenches for flexible pipes, which must be a selected granular material that is singularly graded, meaning that at least 90% by mass is retained on a single sieve of specified diameter. The requirements for the bedding cradle in trenches for power cable ducts, however, is less stringent and must be a selected soil of a granular nature such that the material:

- Has a PI < 6;
- Is free from vegetation and;
- Is free from lumps and stones larger than 15mm.

Material may be used as selected fill for the blanket layer in trenches for flexible pipes if the material:

- Has a PI < 6;
- Is free from vegetation and;
- Is free from lumps and stones larger than 30mm.

For areas not subject to traffic, excavated material may be used as backfill in both trenches if the material:

- Contains little organic material;
- Excludes stones of which the average dimension exceeds 150mm;
- Is compacted to at least 90% mod AASHTO density or the same density as the surrounding area.

The areas subject to traffic load, as is the case at the site entrance, excavated material may be used as backfill in both trenches if the material:

- Has a PI < 12 and;
- CBR of 15% at 93% mod AASHTO for cohesive soils and at 98% mod AASHTO for non-cohesive soils.

### 4.8.3 Patching material

The three main soil samples are evaluated for patching in Table 4-18. The oversize index is the percentage of material retained on the 37.5mm sieve. The shrinkage product is the product of the linear shrinkage and the percentage of soil mortar in the sample. The grading coefficient is the product of the fraction passing the 4.75mm sieve and the difference between the fractions passing the 26.5mm and 2.0mm sieves. The CBR requirement of 15 at 95% density can readily be obtained from the CBR curves given earlier.

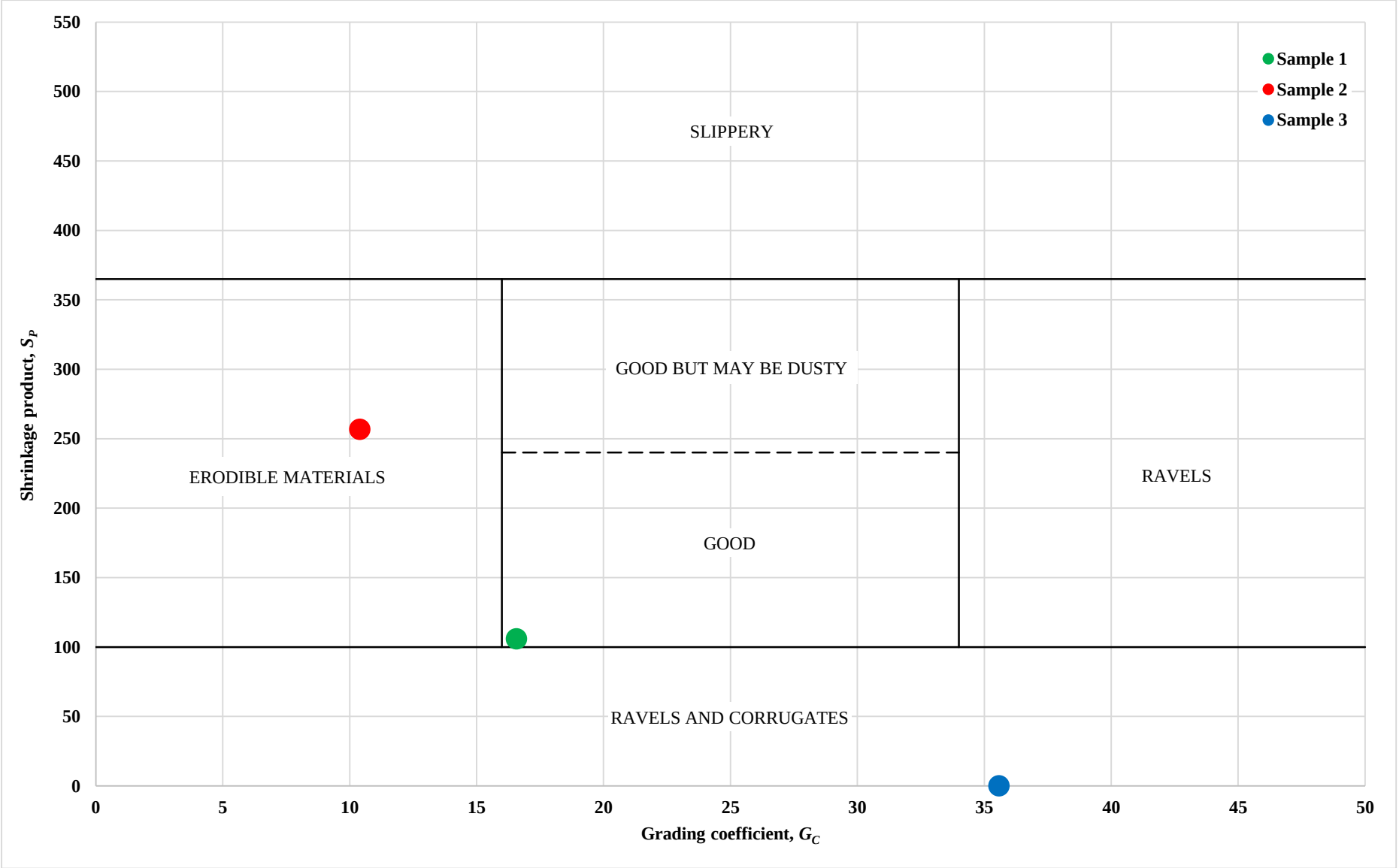


**Figure 4-17: Evaluation of soil as patching material**

**Table 4-18: Evaluation of soil as patching material**

| Parameter description | TRH20 | Sample | | |
|---|---|---|---|---|
| | | **1** | **2** | **3** |
| Maximum particle size (mm) | 37.5 | 28.0 | 14.0 | 14.0 |
| Oversize index, $I_O$ (%) | 5 | 0 | 0 | 0 |
| Shrinkage product, $S_P$ | 100 - 240 | 106 | 257 | 0 |
| Grading coefficient, $G_C$ | 16 - 34 | 17 | 10 | 36 |
| CBR @ 95% MOD AASHO (%) | 15 | 18 | 5 | 19 |

Figure 4-17 shows the performance of the material based on the shrinkage product and grading coefficient. Material from sample 1 only just falls in the desirable zone and also conforms to the other requirements and should therefore perform well in general. Material from sample 2 falls in a zone that generally perform satisfactorily, but are particularly prone to erosion by water. It also does not conform to the CBR requirement and should be avoided. Due to the non-plastic nature of material of sample 3, it falls in the zone highly susceptible to ravelling (the formation of loose material) and corrugations. Material in this zone lacks cohesion and regular maintenance will be necessary if it is used.

# Chapter 5

# Foundation Design

## 5.1 Introduction

The design of stable foundations is an important aspect in the successful operation of sensitive instruments such as radio telescopes, as any unaccounted movement will affect the precision of the instrument. The structures need to withstand heavy loading over its design lifetime which includes permanent loads such as self-weight and variable loads like wind, seismic and other imposed loads. During the time of this study, no specific radio telescope model has been earmarked for the MSGO site, although interest have been shown by foreign institutions for collaboration. At the onset of this study, informal discussions between stakeholders of the MSGO and the Minister of Science and Technology at the time pointed to a possibility of SKA-type radio telescope antennas being allocated to the observatory in a collaborative effort between the MSGO and SKA. For this reason and the intent to base the design on actual loading requirements, SKA South Africa was approached for this information and the loads for a MeerKAT antenna were received. Figure 5-1 shows a single antenna, which is one in an array of sixty-four antennas near Carnarvon in the Northern Cape. The method in which the loads are specified is incomplete however, as it does not provide a breakdown of the load combinations, but only the resultant loads, a problem encountered frequently in practice (Day, 2016). The chapter starts by setting out the design methodology, after which the nominal loads and characteristic material properties used in the design are discussed. The design criteria are then considered with a breakdown of the design calculations for the various limit states. The chapter ends with final remarks on the design.

**Figure 5-1: MeerKAT radio telescope antenna**

## 5.2 Design methodology

The design methodology adopted is the limit state method using EN 1997-1 as basis for design. Partial load factors were taken from SANS 10160-1 and partial material factors from EN 1997-1. The Vestas foundation design guidelines, developed for the design of wind turbine foundations, were also consulted as the basic geometry of the problem is similar to that of a typical wind turbine structure. A circular foundation was chosen for design, which can be argued to be more economical than a square foundation when it comes to these types of structures, as reinforced concrete in the corners may be redundant. This notion is based on the dish being able to be turned 360°, which implies that bending moments and horizontal forces can effectively act about and in the direction of any axis, respectively, so that the main axes will not be fixed.

The following design criteria were considered as relevant that must be checked at the appropriate limit state:

- Overall stability
- Sliding resistance
- Bearing resistance
- Settlement

Overall stability or sliding resistance are believed to be the governing design consideration in determining the foundation size, due to the nature of the dish-shaped structure having to withstand large moments resulting from wind in survival conditions. Founding on rock emphasizes this viewpoint, as bearing resistance and settlement are both unlikely to be critical, but have to be evaluated formally. The spreadsheets containing the design calculations are attached in Appendix E.

## 5.3 Nominal loads and characteristic material properties

This section gives the nominal loads acting on the foundation and the characteristic material parameters that must be able to resist the induced loads under ultimate and serviceability conditions. These are thus unfactored values, meaning partial factors for loads and materials have to be applied in the limit state design method.

### 5.3.1 Nominal loads

The following loads are considered to act on the foundation:

- Normal force at the tower base ($F_Z$);
- Shear force at the tower base ($F_R$);
- Torsional moment at the tower base ($M_Z$);
- Bending moment at the tower base ($M_R$);
- Self-weight of the foundation and;
- Buoyancy.

The dead load of the tower includes the weight of the dish, its support structure and any other permanent equipment attached. These loads are transferred from the structure to the foundation via a bolted connection with the point of application taken at the centre of the foundation. The nominal loads for a SKA-type radio telescope antenna are given in Table 5-1.

**Table 5-1: Nominal loads**

| Load conditions | $F_Z$ (kN) | $F_R$ (kN) | $M_Z$ (kNm) | $M_R$ (kNm) |
|---|---|---|---|---|
| Survival conditions (ULS) | 603 | 158 | 126 | 1 398 |
| Normal operating conditions (SLS) | 474 | 20 | 30 | 440 |

The ultimate limit state loads provided have essentially been interpreted as nominal or characteristic values of the loads with the application of partial load factors to obtain design values. As no breakdown has been provided about the make-up of the moment, i.e. wind load or eccentricity of the dish, it has conservatively been taken as an imposed action and factored accordingly. The serviceability limit state loads are taken as the maximum loads when the equipment is in operation and have been used as they are, without any factors. They are not serviceability loads derived from the same characteristic values as used in the ULS checks as is normally the case according to Day (2016). For the calculation of self-weight of the foundation, the unit weight of concrete is 24.525kN/m$^3$ when using a density of 2 500kg/m$^3$ for 2% reinforcement as per the Southern African Steel Construction Handbook (2013). For calculations involving buoyancy, the unit weight of water is taken as 9.81kN/m$^3$. The coordinate system in which all of these loads are applied is illustrated in Figure 5-2.

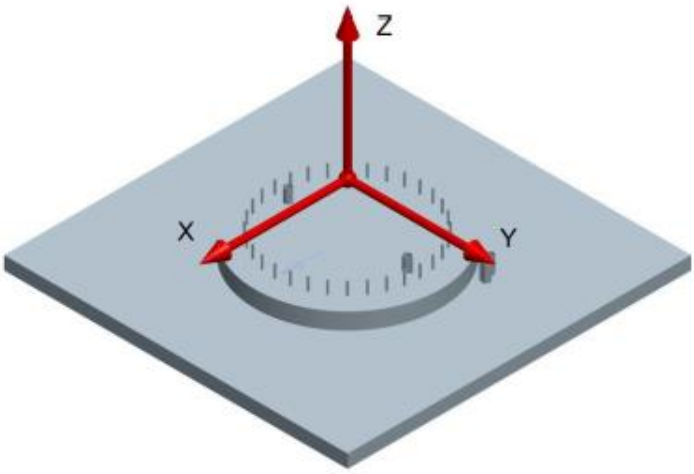


**Figure 5-2: Coordinate system**

### 5.3.2 Characteristic material properties

The characteristic material properties were either directly obtained from the results or were derived from literature using the results as reference. Table 5-2 gives a summary of the characteristic material properties used in the design. The cohesion and friction angle were obtained from the rock mass rating system. It is important to note that the Mohr failure envelope of intact rock is not linear, but slightly concave downwards. This has been shown by Hoek and Brown (1980) for various rock types and may be considered for more specific shear parameters under certain stress states. For this design however, the parameters obtained with Bieniawski (1989) are considered conservative and satisfactory.

**Table 5-2: Characteristic material properties**

| | |
|---|---|
| Cohesion, $c$ (kPa) | 234 |
| Angle of internal friction, $\phi$ (degrees) | 29 |
| Elastic modulus, $E$ (GPa) | 10 |
| Poisson's ratio, $\nu$ | 0.05 |
| Bulk unit weight of overburden, $\gamma$ (kN/m$^3$) | 18 |
| Saturated unit weight of overburden, $\gamma_{sat}$ (kN/m$^3$) | 21 |
| Unit weight of founding material, $\gamma$ (kN/m$^3$) | 26 |

The elastic modulus was obtained from correlation between UCS and elastic modulus in A Guide to Geotechnical Engineering in Southern Africa (2008). The so called design line was chosen assuming some degree of conservatism. The Poisson's ratio, in the absence of sufficient information, are obtained from Gercek (2006) and taken conservatively as the lower bound in the typical range for Poisson's ratio for shale. The bulk and saturated unit weight values chosen for the overburden material are typical values for dense and well-graded sand (Unit Weight of Soil, 2012), although the soil cover at borehole 1 was classified as silty sand. This is deemed an acceptable assumption and, since the material after the

initial 300mm below NGL becomes denser and quickly transitions into rock, the values can be regarded as conservative when used in the surcharge term in the bearing resistance calculations. The unit weight of the founding rock was calculated from the sample prepared for UCS, and is used for both the bulk and saturated unit weight values in the weight density term in the calculations for bearing resistance.

## 5.4 Design criteria

The design considerations as mentioned previously are evaluated and discussed in this section. The partial factors are shown in the design calculations with the resulting design loads and material strengths. The final criteria checks are shown in tabular form at the end of each design consideration.

### 5.4.1 Overall stability

Overall stability or overturning is a general design consideration and is classified as an ultimate limit state at the equilibrium limit state with appropriate partial load factors. It is assumed that the foundation will rotate about a tangent to the edge of the foundation, i.e. about point $O$ in Figure 5-3, also showing the applied loads. Safety against overturning is satisfied when (EN 1997, 2004):

$$M_{dst} \leq M_{stb}$$

Where

$M_{dst}$ destabilizing moment about point $O$ caused by unfavourable actions (kNm)

$M_{stb}$ stabilizing moment about point $O$ caused by favourable actions (kNm)

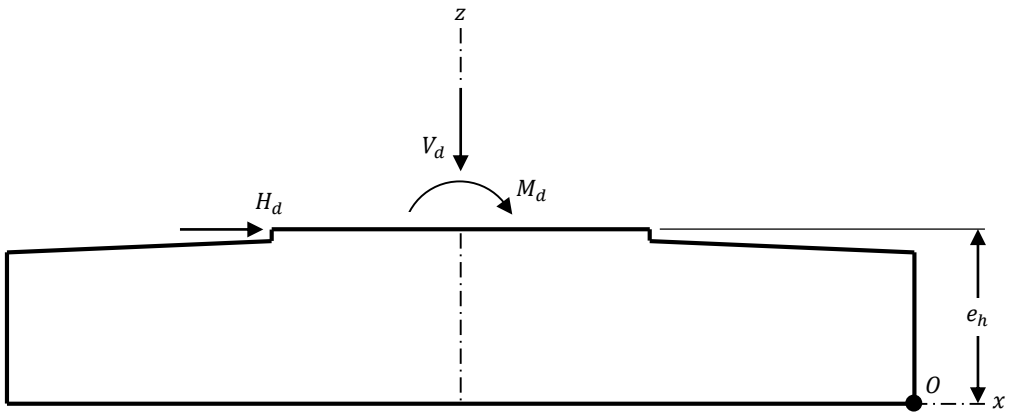


**Figure 5-3: Overall stability of foundation**

The stabilising design moments include:

- Dead load of the tower;
- Dead load of the foundation and;
- Buoyancy applied as a negative value, all of which act over an eccentricity $R$ about point $O$.

The destabilising design moments include:

- Bending moment at the base of the tower;
- Shear force at the base of the tower which acts over an eccentricity $e_h$ about point $O$.

The stabilising design moment $M_{stb}$ is calculated as follows:

$$M_{stb} = (\gamma_G F_Z + \gamma_G W - \gamma_G F_B)R$$

Where

| | |
|---|---|
| $\gamma_G$ | partial load factor for favourable actions (varies) |
| $W$ | self-weight of foundation, $\gamma_c V$ (kN) |
| $\gamma_c$ | unit weight of reinforced concrete (kN/m$^3$) |
| $V$ | total volume of foundation (m$^3$) |
| $F_B$ | buoyancy force, $\gamma_w V_w$ (kN) |
| $\gamma_w$ | unit weight of water (kN/m$^3$) |
| $V_w$ | volume of foundation under water table (m$^3$) |

The destabilising design moment $M_{dst}$ is calculated as follows:

$$M_{dst} = \gamma_G M_R + \gamma_G F_R e_h$$

Where

| | |
|---|---|
| $\gamma_G$ | partial load factor for unfavourable actions (varies) |
| $e_h$ | eccentricity of horizontal shear force to point $O$ |

The final check for overturning is performed as moment equilibrium is considered about point $O$ and the resulting factor of safety is shown in Table 5-3 below.

**Table 5-3: Factor of safety against overturning**

| | |
|---|---|
| Stabilizing moments, $M_{stb}$ (kNm) | 2 341 |
| Destabilizing moments, $M_{dst}$ (kNm) | 2 044 |
| $M_{stb}/M_{dst} \geq 1$ | 1.145 |

### 5.4.2 Sliding resistance

Failure against sliding needs to be checked at the ultimate limit state when loading is not normal to the foundation base, i.e. when a horizontal force is present. Active and passive earth pressure shall not be included. This is because active pressure will be present against the entire circumference of the foundation due to backfill and will thus be in equilibrium, while passive pressure implies that a certain amount of movement is allowed. Figure 5-3 can also be considered as a free body diagram for sliding by considering forces and ignoring moments. Safety against sliding is satisfied when (EN 1997, 2004):

$$H_d \leq R_d$$

Where

$H_d$ design horizontal force (kN)

$R_d$ design shearing resistance (kN)

Since the torsional moment cannot be directly applied in the design calculations, the Vestas Foundation Design Guideline proposes a formula for an equivalent shear to take account of the interaction between the resultant shear force and torsional moment.

The equivalent shear $F_R{}'$ is calculated as follows (Vestas, 2011):

$$F_R{}' = 2\frac{M_Z}{L'} + \sqrt{F_R{}^2 + (2\frac{M_Z}{L'})^2}$$

Where

$L'$ effective length of the compressed area assuming plastic soil distribution (m)

This force is then taken as the design horizontal force $H_d$ that acts to destabilize the foundation. The design shearing resistance is calculated as follows (EN 1997, 2004):

$$R_d = V_d \tan \phi_d$$

Where

$V_d$ design vertical force (kN)

The final check for sliding is performed as force equilibrium is considered in the horizontal direction and the resulting factor of safety is shown in Table 5-4 below.

**Table 5-4: Factor of safety against sliding**

| | |
|---|---|
| Stabilizing force, $R_d$ (kN) | 377 |
| Destabilizing force, $H_d$ (kN) | 346 |
| $R_d/H_d \geq 1$ | 1.092 |

### 5.4.3 Bearing resistance

Bearing capacity is calculated at the ultimate limit state and a plastic distribution of the soil pressure is assumed. Safety against bearing failure is satisfied when (EN 1997, 2004):

$$V_d \leq R_d$$

Where

$V_d$ design vertical force (kN)

$R_d$ design bearing resistance (kN)

The effective compressed area $A'$, for a circular foundation, is calculated as follows (Vestas, 2011):

$$A' = 2\left(R^2\, cos^{-1}\left(\frac{e}{R}\right) - e\sqrt{R^2 - e^2}\right)$$

Where

$R$ radius of the foundation (m)

$e$ eccentricity from center of foundation (m)

The eccentricity $e$ is calculated as follows:

$$e = \frac{M_d}{V_d}$$

Where

$M_d$ design moment (kNm)

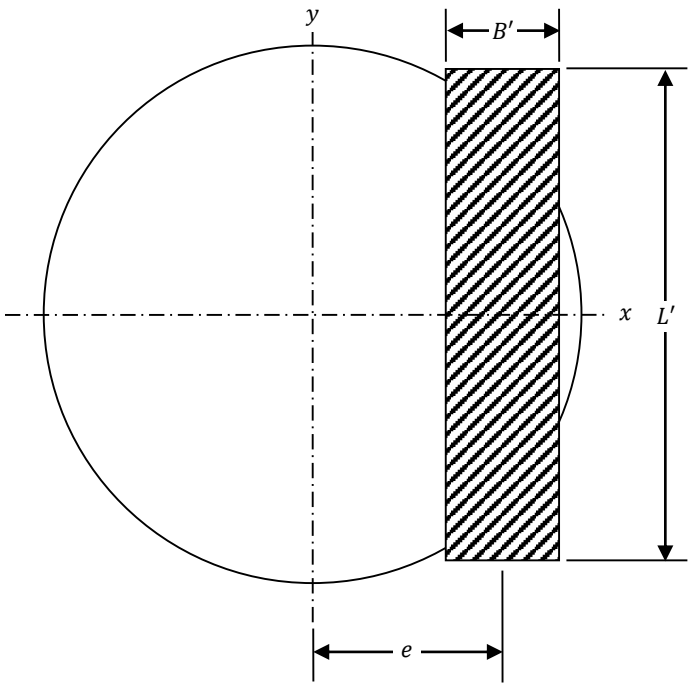


**Figure 5-4: Compressed area assuming plastic distribution**

The elliptical main dimensions, width $B_e$ and length $L_e$ respectively, are calculated as follows (Vestas, 2011):

$$B_e = 2(R - e)$$

$$L_e = 2R\sqrt{1 - \left(1 - \frac{B_e}{2R}\right)^2}$$

The effective dimensions, width $B'$ and length $L'$ respectively, are then calculated as follows (Vestas, 2011):

$$L' = \sqrt{A'\frac{L_e}{B_e}}$$

$$B' = L'\frac{B_e}{L_e}$$

The effective compressed area, comprised of the effective dimensions, is arranged such that it is symmetrical around the resultant vertical force, as shown in Figure 5-4. The equations that were used for the bearing capacity, shape and inclination factors were obtained from EN 1997-1 and are summarized in Table 5-5. The bearing capacity, in general form, is calculated as follows (EN 1997, 2004):

$$\frac{R_d}{A'} = cN_c s_c i_c + qN_q s_q i_q + \frac{1}{2}\overline{\gamma}B'N_\gamma s_\gamma i_\gamma$$

Where

- $N$ bearing capacity factors with subscripts for cohesion $c$, surcharge $q$ and weight density $\gamma$
- $s$ shape factors with subscripts for cohesion $c$, surcharge $q$ and weight density $\gamma$
- $i$ inclination factors with subscripts for cohesion $c$, surcharge $q$ and weight density $\gamma$

**Table 5-5: Equations for bearing capacity, shape and inclination factors**

| **Bearing capacity terms, $x$** | **Bearing capacity factors, $N_x$** | **Shape factors, $s_x$** | **Inclination factors, $i_x$** |
|---|---|---|---|
| Cohesion ($c$) | $(N_q - 1)\cot\phi$ | $\frac{s_q N_q - 1}{N_q - 1}$ | $i_q - \frac{1 - i_q}{N_c \tan\phi}$ |
| Surcharge ($q$) | $e^{\pi\tan\phi}\tan^2\left(45° + \frac{\phi}{2}\right)$ | $1 + \left(\frac{B'}{L'}\right)\sin\phi$ | $\left(1 - \frac{H_d}{V_d + cA'\cot\phi}\right)^m$ |
| Weight density ($\gamma$) | $2(N_q - 1)\tan\phi$ | $1 - 0.3\left(\frac{B'}{L'}\right)$ | $\left(1 - \frac{H_d}{V_d + cA'\cot\phi}\right)^{m+1}$ |

The exponent $m$ in the expressions of inclination factors for surcharge and weight is calculated as follows (EN 1997, 2004):

$$m = \frac{2 + \left(\frac{B'}{L'}\right)}{1 + \left(\frac{B'}{L'}\right)}$$

The cohesion term can readily be obtained from its factors and the rock mass cohesion estimated from Bieniawski (1989). For the surcharge and weight density terms, the location of the water table has a significant effect as illustrated in Figure 5-5. The water table has no effect when its depth is greater than the foundation width below founding level and the following cases are thus considered by Smith (1974):

- The depth to water table is less than the foundation width below founding level;
- The depth to water table is above founding level but below natural ground level and;
- The water table is above natural ground level.

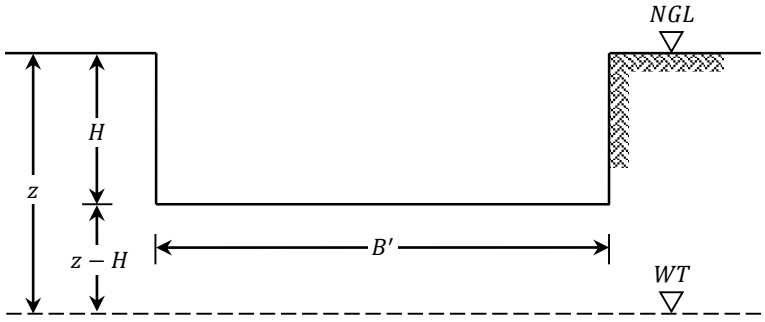


**a) Depth to water table less than effective width $B'$ below founding level**

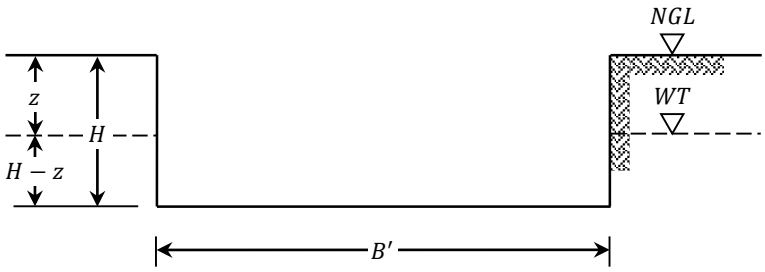


**b) Depth to water table above founding level but below natural ground level**

**Figure 5-5: Location of water table**

For the case shown in Figure 5-5 (a), the following apply respectively for surcharge and weight density in the baring capacity equation from Smith (1974):

$$q = \gamma H$$

$$\overline{\gamma} = \gamma' + \frac{(z - H)}{B'}(\gamma - \gamma')$$

For the case shown in Figure 5-5 (b), the following apply respectively for surcharge and weight density in the baring capacity equation from Smith (1974):

$$q = \gamma z + \gamma'(H - z)$$

$$\overline{\gamma} = \gamma'$$

The last case in which the water table is above natural ground level is not considered further as it was shown that flooding is highly improbable. The borehole proved to be empty after a follow-up visit to see if groundwater was at all present. The final check for bearing is shown in Table 5-6.

**Table 5-6: Factor of safety against bearing failure**

| | |
|---|---|
| Design bearing resistance, $R_d$ (kN/m$^2$) | 11 374 |
| Design vertical force, $V_d$ (kN) | 972 |
| $R_d/V_d \geq 1$ | 12 |

### 5.4.4 Settlement

Settlement is calculated at the serviceability limit state and an elastic distribution of the soil pressure is assumed, and the predicted settlement is limited to an acceptable magnitude. The soil pressure $q$ at any point below the foundation is calculated as follows:

$$q = \frac{V_d}{A} \pm \frac{M_d y}{I}$$

Where

$A$ area ($\pi R^2$) of foundation in contact with the ground (m$^2$)

$I$ moment of inertia ($\frac{\pi}{4}R^4$) of the foundation about the axis of bending (m$^4$)

$y$ perpendicular distance from the neutral axis to any point where stress is being calculated (m)

The maximum and minimum pressure will occur at $y = R$ and $y = -R$ respectively, so that

$$\frac{y}{I} = R\left(\frac{4}{\pi R^4}\right) = \frac{4}{\pi R^3}$$

Substituting the above into the original equation, the maximum $q_{max}$ and minimum $q_{min}$ soil pressures are calculated as follows

$$q_{max} = \frac{V_d}{A} + \frac{4M_d}{\pi R^3}$$

$$q_{min} = \frac{V_d}{A} - \frac{4M_d}{\pi R^3}$$

Here $q_{max}$ must not exceed a maximum allowable pressure, while $q_{min}$ will influence the size of the foundation. Under normal operating conditions, the foundation should be in full contact with the ground, that is to say that compressive stress must be present everywhere below foundation. To ensure that there are no gapping between the foundation and the supporting ground, the minimum pressure must be positive, i.e. $q_{min} \geq 0$

$$\frac{V_d}{A} - \frac{4M_d}{\pi R^3} \geq 0$$

Simplifying the above yields

$$\frac{M_d}{V_d} \leq \frac{R}{4}$$

The moment $M_d$ can be replaced by $V_d$ acting at an eccentricity $e$, so that $M_d = V_d e$ and substitution into the above yields

$$e \leq \frac{R}{4}$$

Thus, all pressures below the foundation will be compressive as long as the eccentricity does not exceed the limit above. For the above condition the foundation will be in full contact with the soil under normal operating conditions. If the condition is false the foundation will lose some contact with the soil and gapping, as illustrated in Figure 5-6, will occur. The minimum and maximum pressures obtained were 74kPa and 17kPa, respectively. The maximum pressure is less than the presumed safe bearing capacity given for shale of hard rock consistency in SABS 0161 (1980), which is specified as between 200 – 400kPa. Furthermore, the minimum pressure is greater than zero and indeed means that the foundation shall remain in full contact with the ground.

The shear modulus $G$ of the founding material is calculated as follows (Vestas, 2011):

$$G = \frac{E}{2(1+\nu)}$$

Where

| | |
|---|---|
| $E$ | Young's modulus of the founding material (MPa) |
| $\nu$ | Poisson's ratio of the founding material |

The vertical $k_z$ and rotational $k_\theta$ stiffness of the foundation are calculated as follows (Vestas, 2011):

$$k_z = \frac{4GR}{1-\nu}$$

$$k_\theta = \frac{8GR^3}{3(1-\nu)}$$

The vertical displacement $\delta$ and rotation $\theta$ of the foundation are calculated as follows (Vestas, 2011):

$$\delta = \frac{V_d}{k_z}$$

$$\theta = \frac{M_d}{k_\theta}$$

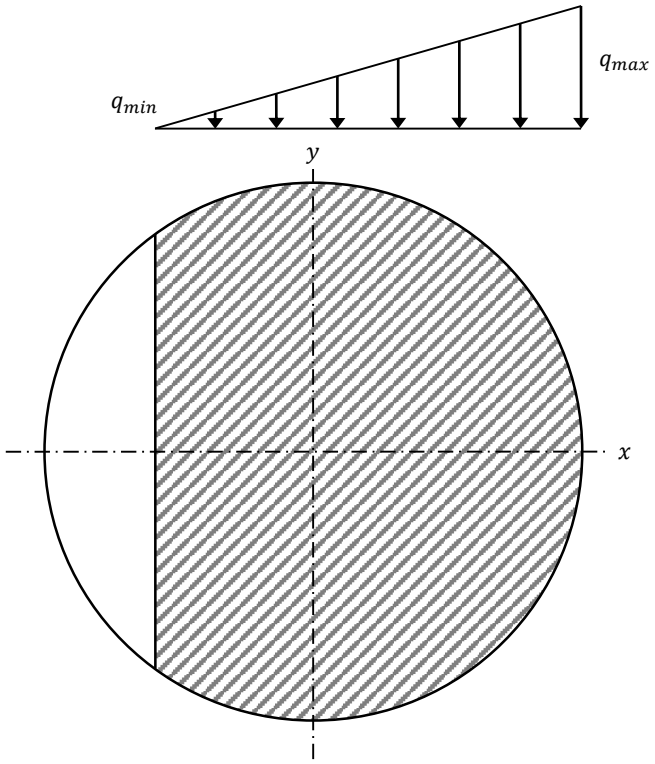


**b) Gapping**

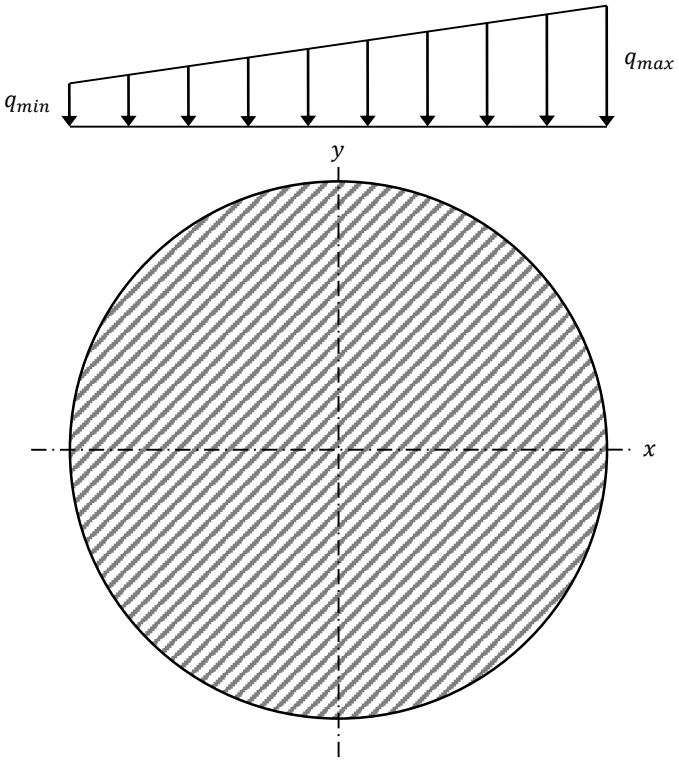


**b) No gapping**

**Figure 5-6: Compressed area assuming elastic distribution**

The final displacement and rotation under normal operating conditions are given in Table 5-7. The rotation falls well below the required limit of 2 arcseconds given by Bester (2016). This can be accredited to the high Young's modulus obtained from correlation with the UCS of the rock.

**Table 5-7: Vertical and rotational stiffness**

| | |
|---|---|
| Vertical stiffness, $k_z$ ($10^4$ kN/mm) | 5.514 |
| Rotational stiffness, $k_\theta$ ($10^8$ kNm/rad) | 2.780 |
| Vertical displacement, $\delta$ (mm) | 0.020 |
| Rotation, $\theta$ (arcseconds) | 0.343 |

## 5.5 Final remarks

The designed foundation has a diameter of 5.5m, which is governed by sliding at the ultimate limit state. The height of 1.0m was chosen as a fixed parameter and equals the approximate depth to bedrock. The assumption to neglect passive earth pressure is probably what makes sliding the governing criterion as appose to overall stability, which has a factor of safety against overturning also close to unity. A large reserve was present in the factor of safety against bearing failure, as was expected for the hard rock foundation. It was however noted in the design spreadsheet that the factor of safety of 12 was reduced by 50% when the diameter was reduced by 0.25m and conversely, increased by 50% when the diameter was increased by 0.25m. Settlement is of no concern due to the high foundation stiffness. The dimensions are summarized in Table 5-8 and a design drawing is attached in Appendix F showing the foundation size and other details.

**Table 5-8: Foundation dimensions**

| | |
|---|---|
| Diameter of foundation, $D$ (m) | 5.5 |
| Height of foundation, $H$ (m) | 1.0 |
| Diameter of pedestal, $d$ (m) | 2.5 |
| Height of pedestal, $h$ (mm) | 75 |
| Top of concrete crossfall, $s$ (%) | 2 |

For the structural design, a method for determining load concentration factors based on beam stiffness theory is given in Vestas (2011). The LCF can then be used to calculate the required radial and concentric reinforcement at the ultimate limit state. The reinforcement should be tied into the pedestal cage to ensure adequate load transfer. In terms of construction, once excavation to the design founding level is made, a layer of screed should be cast directly over the exposed surface to tie into the rock mass. This will protect the exposed founding material, which might be prone to slaking and will in addition make for a level construction surface. Backfilling around the foundation working area would be required to conform to an acceptable density.

# Chapter 6

# Closure

## 6.1 Introduction

This is the closing chapter of the thesis and concludes with a number of key outcomes followed by recommendations on the selection of local materials, on the emplacement of radio telescope antennas in the main study area and on future research in general. Additional photographs taken over the course of the research project, that was not included in the main report, are attached in Appendix G.

## 6.2 Conclusions

The site inspection set the basis for the research and followed by a GPS survey of the main study area and sample collection of various soil and rock types for testing. The survey data was used to create a digital terrain model of the site that turned out to be a good visual representation of the actual topography. In this phase of the research project, various materials were also selected for testing to ultimately be evaluated for engineering application.

The geotechnical investigation followed by selecting three locations on site for core drilling that can be regarded as potential positions for radio telescope antennas. The three borehole logs varied in terms of rock type and other core logging information. Borehole 1 had the best core recovery and its logging was subsequently performed with greater certainty. The rock was rated with the RMR system by Bieniawski (1989), in which a rating of 48 was calculated that described the founding material as fair

rock. This was a conservative means for obtaining shear strength parameters for the foundation design, as much higher values can be obtained when considering other methods. This was considered satisfactory as the problem of estimating rock mass quality is a complex one and the parameters, albeit conservative, still resulted in high bearing capacity. Samples from all three boreholes were studied petrographically. The digital terrain model was used in the hydrological investigation to delineate conservatively estimated flood lines for 20-year and 200-year floods, as calculated with the SDF method. It was shown that runoff for the two drainage channels adjacent to the main study area are simply too little to pose problems for structures located in this area. Due to the fact that these drainage channels are the most upper reaches and essentially originate on site, low peak flows could perhaps have been considered as obvious by any practicing engineer. The study however was viewed more as an academic exercise and in the process illustrate the efficient drainage capacity based on conservative assumptions.

The local soil and rock samples collected were tested in the laboratory to identify some of their engineering properties and potential for use as construction material. Six soil samples were collected from site that varied widely in soil type. From the three main samples, sample 1 was classified as a silty sand and overall as the best material. The advantage of using sample 1 material is that spoil resulting from excavation for structures on the main study area can be utilized elsewhere on site. It can be directly used as backfill in trenches for the laying of services in areas subject to traffic loading. Sample 2 material on the other hand was classified as poor and can only be used as backfill if the fill is not subject to traffic loading. Sample 3 material was also of very good quality and can easily be removed and hauled to site without causing aesthetically displeasing effects to the environment. Removal of sediment from the river bed can be an environmental violation, but could also improve the flow conditions if done correctly. This material was classified as a well-graded sand, although the soil lacks fine material which is believed to be the reason for the lower than expected maximum dry density, compared to samples 1 and 2. It subsequently also showed smaller CBR values than sample 1 at lower densities. Sample 4 had a relatively high PI and does not meet the plasticity requirement for backfill in trenches.

The UCS results proved the hardness of loose sandstone and tillite boulders taken from the site and from the town respectively. These rocks were also tested for ASR potential and the results of the mortar-bar test suggested that they are not reactive to ASR. This was somewhat of a surprising result for the test in which sandstone was used as fine aggregate, since strained quartz were detected in quartzitic sandstone by Van Wyk (2013). Recall that the name sandstone is used within the context of this study to mean quartzitic sandstone. It was however stated earlier that the ASR potential of rocks may vary significantly on the same site. Although some straining was observed in quartz grains with variable percentage of grains showing an undulose extinction (caused by the deformation of the crystal structures in minerals) this is not a good indication of ASR (Oberholster, 2016).

The first official MeerKAT foundation of the SKA consisted of 78m$^3$ of concrete according to Campbell (2013), just over three times more than the 25m$^3$ of concrete in the foundation designed for the MSGO. This was a deep foundation where the structure is supported by a pile cap of 1.25m thickness with five piles of depths ranging to as far as 10m. The more economic design in this thesis can be attributed to the more favourable founding conditions at the MSGO site. A visual impact assessment that was done on the MSGO site concluded that the radio telescopes will have a low visual impact (Ecosense Consulting Environmentalists, 2015b). Although some of the local residents, guests staying in the first floor hotel rooms and users of transport corridors might be visually aware of the radio telescopes, the distance provides acceptable shielding and the Witteberg an effective backdrop.

The main conclusion can be drawn back to the problem statement that sought to evaluate the suitability of the site for the emplacement of radio telescope antennas and their services. Based on the results from the site characterization, as well as from general observation, the MSGO site is indeed considered suitable and this study supports the emplacement of radio telescope antennas for conducting VLBI studies.

## 6.3 Recommendations

Recommendations for the selection of local materials, based only on those tested in this research project, are summarized as follows:

- If excavations in the main study area are done, sample 1 material is recommended to be used for spot regravelling of the access road for filling of the erosion gullies, such as those in Figure 6-1. This will not necessarily be a permanent solution, but may ease driving comfort on site. The material may also be used as the selected fill blanket and backfill in trenches, although stones greater than 30mm may be present.
- Sample 2 material did not perform well, but may be used as backfill in trenches not subject to traffic.
- Sample 3 material is also recommended to be used for spot regravelling as it also performed very well, especially under higher densities. The material may also be used as the selected fill blanket and backfill in trenches subject to traffic loading.
- Sample 4 material may only be used as backfill in trenches not subject to traffic.
- Sample 5 material is similarly graded than Sample 3, but has slightly more fines and should perform well.
- Sample 6 material was classified as a poorly graded sand and is therefore not expected to perform well.

- If rock is to be sourced on site, quartzitic sandstone is favoured above tillite to be used as coarse aggregate in the concrete mix design. Tillite weathers faster and should only be used if it can be regarded as fresh rock.

**Figure 6-1: Access road showing erosion**

Recommendations for the emplacement of radio telescope antennas in the main study area, when final positions are allocated, are summarized as follows:

- An appropriate number of positions per foundation should be selected for core drilling to verify the consistency of the subsurface profile.
- A better method for drilling should be used, which will be more expensive but will give more interpretable results in terms logging, especially in determining parameters such as RQD.
- A greater depth of drilling should be achieved in order to verify the favourability of the subsurface conditions;
- A gravity spread footing will be sufficient if hard rock is present everywhere below the foundation at a level below NGL that remains practical to construct.
- Positions should comply with the environmental requirements such as the buffer zones allocated to drainage channels and the proper disposal of waste material during and after construction.
- It is important to ensure that the radio-telescope structures are adequately earthed to avoid damage in the event of a lightning strike.

Recommendations for future research are summarized as follows:

- Repeating the mortar-bar test on larger sample groups, as it was mentioned before that not all rock of the same formation or even the same site will necessarily ASR.

- The Standard Test Method for Determination of Length Change of Concrete Due to Alkali-Silica Reaction (ASTM C1293) can also be used. It should be noted however that this test takes up to a year to perform and time management will therefore be of the utmost importance.
- A cost-benefit analysis can be performed on the use of local materials versus imported materials. If the financial status quo of the project remains limited, the use of more local material for development can possibly minimize expenditures in reducing the procurement of foreign materials.
- A study on the optimal routing of services can be done for the supply to and distribution of power on site, keeping in mind the variability of material.

# Bibliography

Addis, B. 1998. *Fundamentals of concrete*. Midrand: Cement and Concrete Institute.

Alaud, S. 2015. Personal interview. 1 November, Stellenbosch.

American Society for Testing and Materials International. 2002. *Standard Test Method for Unconfined Compressive Strength of Intact Rock Core Specimens*. West Conshohocken: ASTM International.

American Society for Testing and Materials International. 2007. *Standard Test Method for Potential Alkali Reactivity of Aggregates (Mortar-Bar Method)*. West Conshohocken: ASTM International.

American Society for Testing and Materials International. 2008. *Standard Test Method for Determination of Length Change of Concrete Due to Alkali-Silica Reaction*. West Conshohocken: ASTM International.

American Society for Testing and Materials International. 2011. *Standard Practice for Use of Apparatus for the Determination of Length Change of Hardened Cement Paste, Mortar, and Concrete.* West Conshohocken: ASTM International.

Association of Engineering Geologists. 1976. *A Guide to Core Logging for Rock Engineering.* Proceedings of the Symposium on Exploration for Rock Engineering. Johannesburg: Core Logging Committee of the South African Section of the Association of Engineering Geologists.

Bell, F.G. 1980. *Engineering Geology and Geotechnics.* London: Butterworth & Co (Publishers) Limited.

Bester, H. 2016. Struktuurlaste, E-mail to C.J.T. Janse van Rensburg [Online], 26 Jul. Available E-mail: hendrik@ska.ac.za.

Bieniawski, Z.T. 1978. *Determining rock mass deformability: Experience from case histories*, in Rock Mechanics and Mining Sciences, 15, pp.37-247.

Bieniawski, Z.T. 1989. *Engineering rock mass classifications.* New York: Wiley.

Botha, R. 2014. Personal interview. 7 April, Matjiesfontein.

Brink, A.B.A. 1979. *Engineering Geology of Southern Africa*. Volume 1. Pretoria: Building Publications.

Brink, A.B.A. 1981. *Engineering Geology of Southern Africa.* Volume 2. Pretoria: Building Publications.

Brink, A.B.A. 1983. *Engineering Geology of Southern Africa.* Volume 3. Pretoria: Building Publications.

Byrne, G. & Berry, A.D. 2008. *A Guide to Practical Geotechnical Engineering in Southern Africa.* Fourth edition. South Africa: Franki.

Campbell, K. 2013. First MeerKAT radio telescope antenna foundation laid. *Engineering News*, 15 August.

Chadwick, A., Morfett, J. & Borthwick, M. 2004. *Hydraulics in Civil and Environmental Engineering.* Fourth edition. London: Spon Press.

Clark, B.G. 2003. A Review of the History of VLBI, in *Radio Astronomy at the Fringe.* Charlottesville: Astronomical society of the pacific.

Combrinck, L., Fourie, C.J.S., Croukamp, L. & Saunders, I. 2007. Report on preliminary geotechnical and tropospheric site investigation for a proposed space geodetic observatory near Matjiesfontein in the Great Karoo. *South African Journal of Geology*, 110, September: 225-234.

Craig, R.F. 2004. *Craig's Soil Mechanics.* Seventh edition. London: Taylor & Francis.

Croukamp, L. 2014. Personal interview. 8 August, Matjiesfontein.

*Damaging Earthquakes.* 2012. [Online]. Available: http://www.geoscience.org.za/index.php?option=com_content&view=article&id=1617 [2014, September 5].

Das, B.M. 2002. *Principles of Geotechnical Engineering.* Fifth edition. Pacific Grove: Bill Stenquist.

Davis, D.E. & Coull, W.A. 1991. *Alkali-aggregate reaction: Choosing the right aggregate and cement for concrete.* Second edition. Sandton: Hippo Quarries.

Day, P.W. 1987. Prediction of Settlement. Unpublished class notes. Witwatersrand: South African Institution of Civil Engineers, Geotechnical division.

Day, P.W. 2014. Advanced Foundation Design. Unpublished class notes. Stellenbosch: Stellenbosch University.

Day, P.W. 2016. Personal interview. 19 September, Sandton.

Dolar-Mantuani, L. 1975. *Petrographic Aspects of Siliceous Alkali Reactive Aggregates*, Proceedings, Symposium on Alkali-Aggregate Reaction, Reykjavik, Iceland, pp. 87-100.

Ecosense Consulting Environmentalists. 2015a. *Vegetation Screening and Freshwater Ecological Assessment as Part of the Environmental Assessment and Authorisation Process for the Proposed Matjiesfontein Geodesy Station, Western Cape Province.* Johannesburg: Scientific Aquatic Services.

Ecosense Consulting Environmentalists. 2015b. *Visual Impact Assessment for Proposed Geodetic Observatory, Matjiesfontein.* Somerset West: Karen Hansen.

*Encyclopaedia Britannica*. 2016. [Online]. Available: https://global.britannica.com/science/radio-telescope [2016, November 20].

European Committee for Standardization. 2004. *Eurocode 7: Geotechnical design – Part 1: General Rules.* Brussels: European Committee for Standardization.

Fouché, N. 2016. Personal interview. 26 July, Stellenbosch.

*Fundamentals of Soil Compaction.* 2016. [Online]. Available: http://www.intelligentcompaction.com [2016, October 10].

Gercek, H. 2006. Poisson's ratio values for rocks. *International Journal of Rock Mechanics & Mining Sciences*, 44: 1–13.

Harvey, J.C. 1982. *Geology for Geotechnical Engineers.* Cambridge: Cambridge University Press.

Hoek, E. & Brown, E.T. 1980. *Underground Excavations in Rock.* London: The Institution of Mining and Metallurgy.

*Historical Earthquakes.* 2012. [Online]. Available: http://www.geoscience.org. [2014, September 2].

Jennings, J.E., Brink, A.B.A. & Williams, A.A.B. 1973. Revised guide to soil profiling for civil engineering purposes in Southern Africa. *South African Institution of Civil Engineers*, 15: 3-12.

Johnson, M.R., Anhaeusser, C.R. & Thomas, R.J. 2006. *The geology of South Africa.* Johannesburg: Geological Society of South Africa and Council for Geoscience.

Kloos, M. 2014. Access Road Solutions, Space Geodesy Site, Matjiesfontein. Unpublished bachelor's project. Stellenbosch: Stellenbosch University.

Oberholster, B. 2009. Alkali-silica reaction, in Owens, G. (ed.). *Fulton's Concrete Technology*. Ninth edition. Midrand: Cement and Concrete Institute.

Oberholster, B. 2016. Telephonic interview. 6 October.

Pellant, C. 2000. *Rocks and minerals.* Revised edition. London: Dorling Kindersley Limited.

Petrachenko, W., Behrend, D., Hase, H., Ma, C., Niell, A., Schuh, H. & Whitney, A. 2013. *The VLBI2010 Global Observing System (VGOS)*. Vienna: EGU General Assembly.

Poole, A.B. 1992. Introduction to alkali-aggregate reaction in concrete, in Swamy, R.N. (ed.). *The Alkali-Silica Reaction in Concrete.* New York: Van Nostrand Reinhold.

Poulos, H.G. 2002. Foundation Design – the research-practice gap. The Second Jennings Memorial Lecture. Sydney: The University of Sydney.

Robberts, J.M. & Marshall, V. 2010. *Analysis and design of concrete structures.* Pretoria: University of Pretoria.

Schuh, H. & Behrend, D. 2012. VLBI: A fascinating technique for geodesy and astrometry. *Journal of Geodynamics* [Electronic], 61. Available: http://www.sciencedirect.com.

Smith, G.N. 1974. *Elements of Soil Mechanics for Civil and Mining Engineers.* Third edition. London: Crosby Lockwood Staples.

*Soil Compaction.* 2016. [Online]. Available: http://www.globalsecurity.org [2016, October 10].

*Soil Compaction Handbook.* 2016. [Online]. Available: http://www.multiquip.com [2016, October 10].

South African Bureau of Standards. 1981. *Cable ducts.* Pretoria: South African Bureau of Standards.

South African Bureau of Standards. 1983. *Bedding (pipes).* Pretoria: South African Bureau of Standards.

South African Bureau of Standards. 1989. *Earthworks (pipe trenches).* Pretoria: South African Bureau of Standards.

South African National Standards. 2006. *Particle and relative densities of aggregates.* Pretoria: South African National Standards.

South African National Standards 10160. 2011. *Basis of structural design and actions for buildings and industrial structures – Part 1: Basis of structural design.* Pretoria: SABS Standards Division.

South African National Standards 10160. 2011. *Basis of structural design and actions for buildings and industrial structures – Part 5: Basis for geotechnical design and actions.* Pretoria: SABS Standards Division.

*Statistics South Africa.* 2011. [Online]. Available: http://www.statssa.gov.za [2016, October 26].

Tarbuck, E., Lutgens, F. & Tasa, D. 2011. *Earth: An Introduction to Physical Geology.* Tenth edition. New Jersey: Pearson.

Technical Methods for Highways. 1986. *Standard Methods of Testing Road Construction Materials.* Pretoria: Department of Transport.

Technical Recommendations for Highways. 1985. *Guidelines for Road Construction Materials.* Pretoria: Department of Transport.

Technical Recommendations for Highways. 1990. *The Structural Design, Construction and Maintenance of Unpaved Roads.* Pretoria: Department of Transport.

Teng, W.C. 1962. *Foundation Design.* New York: Prentice Hall.

*The Hartebeesthoek Radio Astronomy Observatory.* [S.a.] [Online]. Available: http://www.hartrao.ac.za [2014, May 2].

*The Square Kilometre Array South Africa.* [S.a.] [Online]. Available: http://www.ska.ac.za [2014, May 2].

*Unit Weight of Soil.* [2012] [Online]. Available: http://www.geotechnicalinfo.com [2016, October 30].

Van Dijk, M., Van Vuuren, S.J. & Smithers, J.C. 2013. Flood calculations, in Kruger, E. (ed.). *SANRAL Drainage Manual*. Sixth edition. Pretoria: The South African National Roads Agency SOC Ltd.

Van Dijk, M., Van Vuuren. 2013. Modelling of free surface flow and flood line calculations, in Kruger, E. (ed.). *SANRAL Drainage Manual*. Sixth edition. Pretoria: The South African National Roads Agency SOC Ltd.

Van Tonder, D. 2016. Personal interview. 19 September, Potchefstroom.

Van Wyk, P.R. 2013. Rock mechanics for construction of the gravimeter vault at the Matjiesfontein Space Geodesy and Earth Observation Observatory. Unpublished master's thesis. Stellenbosch: Stellenbosch University.

Wyllie, D.C. & Mah, C.W. 2004. *Rock Slope Engineering.* Fourth edition. London: Taylor & Francis.

# Appendix A

# Subsurface Data

| Borehole # (coordinates) | Depth (m) | Method | Core recovered (%) | Rock quality designation (%) | Fracture frequency | Colour, weathering, fabric and discontinuity surface spacing, hardness, rock name, stratigraphic horizon. Interpretive remarks |
|---|---|---|---|---|---|---|
| Borehole 1 (33°15'52.26"S; 20°34'58.26"E) | 0.30 | Digging | N/A | N/A | - | Dry, light brown, loose, intact, boulders and gravel in a sandy matrix. Hill wash |
| | 0.50 | Drilling | 89 | 35 | > 20 | Dark green gray moderately to slightly weathered fine to medium grained folliated highly fractured medium hard rock phyllite, Witteberg Group, Cape Supergroup |
| | 0.72 | | | | | |
| | 1.00 | | | | 9 | Dark green gray slightly weathered fine to medium grained folliated medium fractured with very closely to closely fractured zones very hard rock phyllite, Witteberg Group, Cape Supergroup<br><br>NOTES ON FRACURES:<br>1) Partially filled with clayey infill and stained orange-brown in places<br>2) Slightly rough fracture surfaces<br>3) Subvertical and subhorizontal orientations |
| | 1.27 | | | | | |
| | 1.43 | | | | > 20 | |
| | 1.50 | | | | 5 | |
| | 2.00 | | | | | |
| | 2.05 | | | | > 20 | |
| | 2.50 | | | | | |
| | 2.70 | | | | | |
| | 3.00 | | | | | |

| Borehole # (coordinates) | Depth (m) | Method | Core recovered (%) | Rock quality designation (%) | Fracture frequency | Colour, weathering, fabric and discontinuity surface spacing, hardness, rock name, stratigraphic horizon. Interpretive remarks |
|---|---|---|---|---|---|---|
| Borehole 2 (33°15'55.20"S; 20°34'54.18"E) | 0.30 | Digging | N/A | N/A | - | Slightly moist, dark reddish-orange, dense, intact, boulders and gravel with limited sandy matrix. Hill wash |
| | 0.50 | Drilling | 64 | 0 | > 20 | Dark green gray with white quartz veins moderately to slightly weathered fine to medium grained folliated highly fractured medium hard to hard rock phyllite, Witteberg Group, Cape Supergroup |
| | 0.69 | | | | | |
| | 1.00 | | | | | Dark green gray banded dark grey with white quartz veins highly weathered with intermitted zones of completely weathered clay-gravel (residual) very closely fractured medium hard to hard rock grading into soft rock with depth siltstone with mudstone lenses, Witteberg Group, Cape Supergroup |
| | 1.50 | | | | | |
| | 2.00 | | | | | |
| | 2.50 | | | | | |
| | 3.00 | | | | | |
| | | | | | | |
| | 3.10 | | | | | |

| Borehole # (coordinates) | Depth (m) | Method | Core recovered (%) | Rock quality designation (%) | Fracture frequency | Colour, weathering, fabric and discontinuity surface spacing, hardness, rock name, stratigraphic horizon. Interpretive remarks |
|---|---|---|---|---|---|---|
| Borehole 3 (33°15'57.36"S; 20°34'51.90"E) | 0.45 | Digging | N/A | N/A | - | Slightly moist, dark reddish-orange, dense, intact, boulders and gravel with limited sandy matrix. Hill wash |
| | 0.50 | Drilling | 97 | 15 | > 20 | Banded dark grey and dark green gray with white quartz veins medium to slightly weathered flow banded and laminated fine to medium grained closely fractured medium hard rock with zones of soft rock and zones of hard rock mudstone and siltstone, Witteberg Group, Cape Supergroup |
| | 1.00 | | | | | |
| | 1.50 | | | | | |
| | 2.00 | | | | | |
| | 2.50 | | | | | |
| | 3.00 | | | | | |
| | 3.45 | | | | | NOTES ON FRACURES:<br>1) Partially filled with clayey infill<br>2) Slightly rough to rough fracture surfaces<br>3) Two sets of subhorizontal and approximately 45° orientations |

# Appendix B

# Hydraulic Data

# Rational method for northern channel

| **Physical characteristics** | | | | | | | |
|---|---|---|---|---|---|---|---|
| Size of catchment, $A$ (km$^2$) | | | 0.143 | Weather station name | | Matjiesfontein | |
| Length of longest watercourse, $L$ (km) | | | 0.818 | Weather station number | | 0045134 W | |
| Average slope, $S$ (m/m) | | | 0.059 | Weather station coordinates | | 33°13'S; 20°35'E | |
| Time of concentration, $T_c$ (hours) | | | 0.169 | Mean annual precipitation, $MAP$ (mm) | | | 165 |
| Percentage dolomite area, $D$ (%) | | | 0 | Rainfall for 2-year return period, $M$ (mm) | | | 25 |
| Proportion consisting of rural areas, $\alpha$ | | | 1 | Days of thunder, $R$ (days/year) | | | 16 |
| Proportion consisting of urban areas, $\beta$ | | | 0 | | | | |
| Proportion consisting of lakes, $\gamma$ | | | 0 | | | | |
| **Rural** | | | | **Urban** | | | |
| **Surface slope** | % | Factor | $C_s$ | **Description** | % | Factor | $C_2$ |
| Vleis and pans (<3%) | 0 | 0.01 | 0.000 | **Lawns** | | | |
| Flat areas (3 to 10%) | 10 | 0.06 | 0.006 | Sandy and flat (<2%) | 0 | 0.10 | 0.000 |
| Hilly areas (10 to 30%) | 40 | 0.12 | 0.048 | Sandy and steep (>7%) | 0 | 0.20 | 0.000 |
| Steep areas (>30%) | 50 | 0.22 | 0.110 | Heavy soil and flat (<2%) | 0 | 0.17 | 0.000 |
| **Total** | 100 | | 0.164 | Heavy soil and steep (>7%) | 0 | 0.35 | 0.000 |
| **Permeability** | % | Factor | $C_p$ | **Residential areas** | | | |
| Very permeable | 0 | 0.03 | 0.000 | Houses | 0 | 0.50 | 0.000 |
| Permeable | 15 | 0.06 | 0.009 | Flats | 0 | 0.70 | 0.000 |
| Semi-permeable | 35 | 0.12 | 0.042 | **Industrial areas** | | | |
| Impermeable | 50 | 0.21 | 0.105 | Light industry | 0 | 0.80 | 0.000 |
| **Total** | 100 | | 0.156 | Heavy industry | 0 | 0.90 | 0.000 |
| **Vegetation** | % | Factor | $C_v$ | **Business areas** | | | |
| Thick bush and plantations | 20 | 0.03 | 0.006 | City center | 0 | 0.95 | 0.000 |
| Light bush and farmlands | 45 | 0.07 | 0.032 | Suburban | 0 | 0.70 | 0.000 |
| Grasslands | 25 | 0.17 | 0.043 | Streets | 0 | 0.95 | 0.000 |
| No vegetation | 10 | 0.26 | 0.026 | Maximum flood | 0 | 1.00 | 0.000 |
| **Total** | 100 | | 0.106 | **Total** | 0 | | 0.000 |

| **Run-off coefficient** | | | | | | |
|---|---|---|---|---|---|---|
| **Return period, $T$ (years)** | **2** | **5** | **10** | **20** | **50** | **100** |
| Rural run-off coefficient, $C_1$ | 0.426 | 0.426 | 0.426 | 0.426 | 0.426 | 0.426 |
| Adjustment factor for initial saturation, $F_t$ | 0.75 | 0.8 | 0.85 | 0.9 | 0.95 | 1 |
| Adjusted run-off coefficient, $C_{1T}$ | 0.320 | 0.341 | 0.362 | 0.383 | 0.405 | 0.426 |
| Run-off coefficient, $C_T$ | 0.320 | 0.341 | 0.362 | 0.383 | 0.405 | 0.426 |
| **Rainfall** | | | | | | |
| **Return period, $T$ (years)** | **2** | **5** | **10** | **20** | **50** | **100** |
| Precipitation depth, $P_{t,T}$ (mm) | 6.30 | 10.63 | 13.91 | 17.18 | 21.51 | 24.79 |
| Point intensity, $P_{iT}$ (mm) | 25.21 | 42.53 | 55.63 | 68.73 | 86.04 | 99.14 |
| Area reduction factor, $ARF$ (%) | 100 | 100 | 100 | 100 | 100 | 100 |
| Average rainfall intensity, $I_T$ (mm/hour) | 25.21 | 42.53 | 55.63 | 68.73 | 86.04 | 99.14 |
| **Peak flow** | | | | | | |
| **Return period, $T$ (years)** | **2** | **5** | **10** | **20** | **50** | **100** |
| Peak flow, $Q_T$ (m$^3$/s) | 0.3 | 0.6 | 0.8 | 1.0 | 1.4 | 1.7 |

# Standard design flood method for northern channel

| **Physical characteristics** | | | | | | | |
|---|---|---|---|---|---|---|---|
| Size of catchment, $A$ (km$^2$) | 0.143 | Weather station name | Letjiesbos | | | | |
| Length of longest watercourse, $L$ (km) | 0.818 | Weather station number | 0069483 W | | | | |
| Average slope, $S$ (m/m) | 0.059 | Weather station coordinates | 32°33'S; 22°17'E | | | | |
| Time of concentration, $T_c$ (hours) | 0.169 | Mean annual precipitation, $MAP$ (mm) | 165 | | | | |
| SDF drainage basin (#) | 19 | Rainfall for 2-year return period, $M$ (mm) | 34 | | | | |
| Calibration factor for $T_2$, $C_2$ (%) | 10 | Days of thunder, $R$ (days/year) | 16 | | | | |
| Calibration factor for $T_{100}$, $C_{100}$ (%) | 35 | | | | | | |
| **Run-off coefficient** | | | | | | | |
| **Return period, $T$ (years)** | **2** | **5** | **10** | **20** | **50** | **100** | **200** |
| Return period factors, $Y_T$ | 0 | 0.84 | 1.28 | 1.64 | 2.05 | 2.33 | 2.58 |
| Run-off coefficient, $C_T$ | 0.100 | 0.190 | 0.237 | 0.276 | 0.320 | 0.350 | 0.377 |
| **Rainfall** | | | | | | | |
| **Return period, $T$ (years)** | **2** | **5** | **10** | **20** | **50** | **100** | **200** |
| Precipitation depth, $P_{t,T}$ (mm) | 7.791 | 13.144 | 17.193 | 21.242 | 26.594 | 30.643 | 34.692 |
| Area reduction factor, $ARF$ (%) | 100 | 100 | 100 | 100 | 100 | 100 | 100 |
| Average rainfall, $P_{AvgT}$ (mm) | 7.791 | 13.144 | 17.193 | 21.242 | 26.594 | 30.643 | 34.692 |
| Average intensity, $I_T$ (mm/hour) | 46.121 | 77.805 | 101.774 | 125.742 | 157.427 | 181.395 | 205.364 |
| **Peak flow** | | | | | | | |
| **Return period, $T$ (years)** | **2** | **5** | **10** | **20** | **50** | **100** | **200** |
| Peak flow, $Q_T$ (m$^3$/s) | 0.2 | 0.6 | 1.0 | 1.4 | 2.0 | 2.5 | 3.1 |

# Empirical methods for northern channel

| **Physical characteristics** | | | | | |
|---|---|---|---|---|---|
| Size of catchment, $A$ (km$^2$) | 0.143 | Veld type | 5 | | |
| Length of longest watercourse, $L$ (km) | 0.818 | Kovacs region | K4 | | |
| Average slope, $S$ (m/m) | 0.059 | Mean annual rainfall, $MAP$ (mm) | 165 | | |
| Length to catchment centroid, $L_c$ (km) | 0.409 | Catchment parameter, $C$ | 0.104 | | |
| **Midgley & Pitman** | | | | | |
| **Return period, $T$ (years)** | **10** | **20** | **50** | **100** | |
| Constant value of $K_T$ | 0.59 | 0.8 | 1.11 | 1.4 | |
| Peak flow, $Q_T$ (m$^3$/s) | 0.7 | 1.0 | 1.4 | 1.7 | |
| **Kovacs** | | | | | |
| **Return period, $T$ (years)** | **50** | **100** | **200** | **RMF** | |
| $Q_T/Q_{RMF}$ ratios | 0.416 | 0.524 | 0.629 | 1 | |
| Peak flow, $Q_T$ (m$^3$/s) | 7.0 | 8.8 | 10.6 | 16.8 | |

# Rational method for southern channel

| **Physical characteristics** | | | | | | | |
|---|---|---|---|---|---|---|---|
| Size of catchment, $A$ (km$^2$) | | | 0.478 | Weather station name | | Matjiesfontein | |
| Length of longest watercourse, $L$ (km) | | | 0.463 | Weather station number | | 0045134 W | |
| Average slope, $S$ (m/m) | | | 0.060 | Weather station coordinates | | 33°13'S; 20°35'E | |
| Time of concentration, $T_c$ (hours) | | | 0.108 | Mean annual precipitation, $MAP$ (mm) | | | 165 |
| Percentage dolomite area, $D$ (%) | | | 0 | Rainfall for 2-year return period, $M$ (mm) | | | 25 |
| Proportion consisting of rural areas, $\alpha$ | | | 1 | Days of thunder, $R$ (days/year) | | | 16 |
| Proportion consisting of urban areas, $\beta$ | | | 0 | | | | |
| Proportion consisting of lakes, $\gamma$ | | | 0 | | | | |
| **Rural** | | | | **Urban** | | | |
| **Surface slope** | % | Factor | $C_s$ | **Description** | % | Factor | $C_2$ |
| Vleis and pans (<3%) | 0 | 0.01 | 0.000 | **Lawns** | | | |
| Flat areas (3 to 10%) | 5 | 0.06 | 0.003 | Sandy and flat (<2%) | 0 | 0.10 | 0.000 |
| Hilly areas (10 to 30%) | 15 | 0.12 | 0.018 | Sandy and steep (>7%) | 0 | 0.20 | 0.000 |
| Steep areas (>30%) | 80 | 0.22 | 0.176 | Heavy soil and flat (<2%) | 0 | 0.17 | 0.000 |
| **Total** | 100 | | 0.197 | Heavy soil and steep (>7%) | 0 | 0.35 | 0.000 |
| **Permeability** | % | Factor | $C_p$ | **Residential areas** | | | |
| Very permeable | 0 | 0.03 | 0.000 | Houses | 0 | 0.50 | 0.000 |
| Permeable | 0 | 0.06 | 0.000 | Flats | 0 | 0.70 | 0.000 |
| Semi-permeable | 20 | 0.12 | 0.024 | **Industrial areas** | | | |
| Impermeable | 80 | 0.21 | 0.168 | Light industry | 0 | 0.80 | 0.000 |
| **Total** | 100 | | 0.192 | Heavy industry | 0 | 0.90 | 0.000 |
| **Vegetation** | % | Factor | $C_v$ | **Business areas** | | | |
| Thick bush and plantations | 20 | 0.03 | 0.006 | City center | 0 | 0.95 | 0.000 |
| Light bush and farmlands | 40 | 0.07 | 0.028 | Suburban | 0 | 0.70 | 0.000 |
| Grasslands | 30 | 0.17 | 0.051 | Streets | 0 | 0.95 | 0.000 |
| No vegetation | 10 | 0.26 | 0.026 | Maximum flood | 0 | 1.00 | 0.000 |
| **Total** | 100 | | 0.111 | **Total** | 0 | | 0.000 |

| **Run-off coefficient** | | | | | | |
|---|---|---|---|---|---|---|
| **Return period, $T$ (years)** | **2** | **5** | **10** | **20** | **50** | **100** |
| Rural run-off coefficient, $C_1$ | 0.500 | 0.500 | 0.500 | 0.500 | 0.500 | 0.500 |
| Adjustment factor for initial saturation, $F_t$ | 0.75 | 0.8 | 0.85 | 0.9 | 0.95 | 1 |
| Adjusted run-off coefficient, $C_{1T}$ | 0.375 | 0.400 | 0.425 | 0.450 | 0.475 | 0.500 |
| Run-off coefficient, $C_T$ | 0.375 | 0.400 | 0.425 | 0.450 | 0.475 | 0.500 |
| **Rainfall** | | | | | | |
| **Return period, $T$ (years)** | **2** | **5** | **10** | **20** | **50** | **100** |
| Precipitation depth, $P_{t,T}$ (mm) | 4.83 | 8.15 | 10.66 | 13.17 | 16.49 | 19.00 |
| Point intensity, $P_{iT}$ (mm) | 19.33 | 32.60 | 42.65 | 52.69 | 65.97 | 76.01 |
| Area reduction factor, $ARF$ (%) | 100 | 100 | 100 | 100 | 100 | 100 |
| Average rainfall intensity, $I_T$ (mm/hour) | 19.33 | 32.60 | 42.65 | 52.69 | 65.97 | 76.01 |
| **Peak flow** | | | | | | |
| **Return period, $T$ (years)** | **2** | **5** | **10** | **20** | **50** | **100** |
| Peak flow, $Q_T$ (m$^3$/s) | 1.0 | 1.7 | 2.4 | 3.2 | 4.2 | 5.1 |

# Standard design flood method for southern channel

| **Physical characteristics** | | | | | | | |
|---|---|---|---|---|---|---|---|
| Size of catchment, $A$ (km$^2$) | 0.478 | Weather station name | Letjiesbos | | | | |
| Length of longest watercourse, $L$ (km) | 0.463 | Weather station number | 0069483 W | | | | |
| Average slope, $S$ (m/m) | 0.060 | Weather station coordinates | 32°33'S; 22°17'E | | | | |
| Time of concentration, $T_c$ (hours) | 0.108 | Mean annual precipitation, $MAP$ (mm) | 165 | | | | |
| SDF drainage basin (#) | 19 | Rainfall for 2-year return period, $M$ (mm) | 34 | | | | |
| Calibration factor for $T_2$, $C_2$ (%) | 10 | Days of thunder, $R$ (days/year) | 16 | | | | |
| Calibration factor for $T_{100}$, $C_{100}$ (%) | 35 | | | | | | |
| **Run-off coefficient** | | | | | | | |
| **Return period, $T$ (years)** | **2** | **5** | **10** | **20** | **50** | **100** | **200** |
| Return period factors, $Y_T$ | 0 | 0.84 | 1.28 | 1.64 | 2.05 | 2.33 | 2.58 |
| Run-off coefficient, $C_T$ | 0.100 | 0.190 | 0.237 | 0.276 | 0.320 | 0.350 | 0.377 |
| **Rainfall** | | | | | | | |
| **Return period, $T$ (years)** | **2** | **5** | **10** | **20** | **50** | **100** | **200** |
| Point rainfall, $P_{t,T}$ (mm) | 5.981 | 10.089 | 13.198 | 16.306 | 20.414 | 23.522 | 26.631 |
| Area reduction factor, $ARF$ (%) | 100 | 100 | 100 | 100 | 100 | 100 | 100 |
| Average rainfall, $P_{AvgT}$ (mm) | 5.981 | 10.089 | 13.198 | 16.306 | 20.414 | 23.522 | 26.631 |
| Average intensity, $I_T$ (mm/hour) | 55.166 | 93.064 | 121.733 | 150.402 | 188.301 | 216.970 | 245.639 |
| **Peak flow** | | | | | | | |
| **Return period, $T$ (years)** | **2** | **5** | **10** | **20** | **50** | **100** | **200** |
| Peak flow, $Q_T$ (m$^3$/s) | 0.7 | 2.4 | 3.8 | 5.5 | 8.0 | 10.1 | 12.3 |

# Empirical methods for southern channel

| **Physical characteristics** | | | | | |
|---|---|---|---|---|---|
| Size of catchment, $A$ (km$^2$) | 0.478 | Veld type | 5 | | |
| Length of longest watercourse, $L$ (km) | 0.463 | Kovacs region | K4 | | |
| Average slope, $S$ (m/m) | 0.060 | Mean annual rainfall, $MAP$ (mm) | 165 | | |
| Length to catchment centroid, $L_c$ (km) | 0.925 | Catchment parameter, $C$ | 0.274 | | |
| **Midgley & Pitman** | | | | | |
| **Return period, $T$ (years)** | **10** | **20** | **50** | **100** | |
| Constant value of $K_T$ | 0.59 | 0.8 | 1.11 | 1.4 | |
| Peak flow, $Q_T$ (m$^3$/s) | 1.8 | 2.5 | 3.4 | 4.3 | |
| **Kovacs** | | | | | |
| **Return period, $T$ (years)** | **50** | **100** | **200** | **RMF** | |
| $Q_T/Q_{RMF}$ ratios | 0.416 | 0.524 | 0.629 | 1 | |
| Peak flow, $Q_T$ (m$^3$/s) | 13.4 | 16.9 | 20.2 | 32.2 | |

# Appendix C

# Petrographic Results

SAMPLE: Borehole 1

Rock type: Sandstone/Quartzite

MACROSCOPIC ROCK DESCRIPTION

Very fine-grained, light brown to cream-coloured rock fragments.

MICROSCOPIC ROCK DESCRIPTION

Composition: Quartz (95%), Clay minerals and Mica (<5%), Iron oxide (<1%)

Grain size: Fine- to very fine grained (40µm to 100µm)

Sorting: Moderately sorted

Rounding: Rounded to recrystallized

Clast/matrix supported: Clast supported

Other textures: Interlocking

Description: The rock is a sedimentary rock consisting of quartz (95%) set in a clay and mica-rich matrix (<5%). Quartz is rounded to recrystallized as evidenced from the 120º junctions shown by larger quartz grains. The original sedimentary rock was moderately sorted. No preferred orientation was observed in the minerals. Some straining was observed in quartz grains with <20% of all grains showing undulose extinction of average 21.5º indicates an ASR potential.

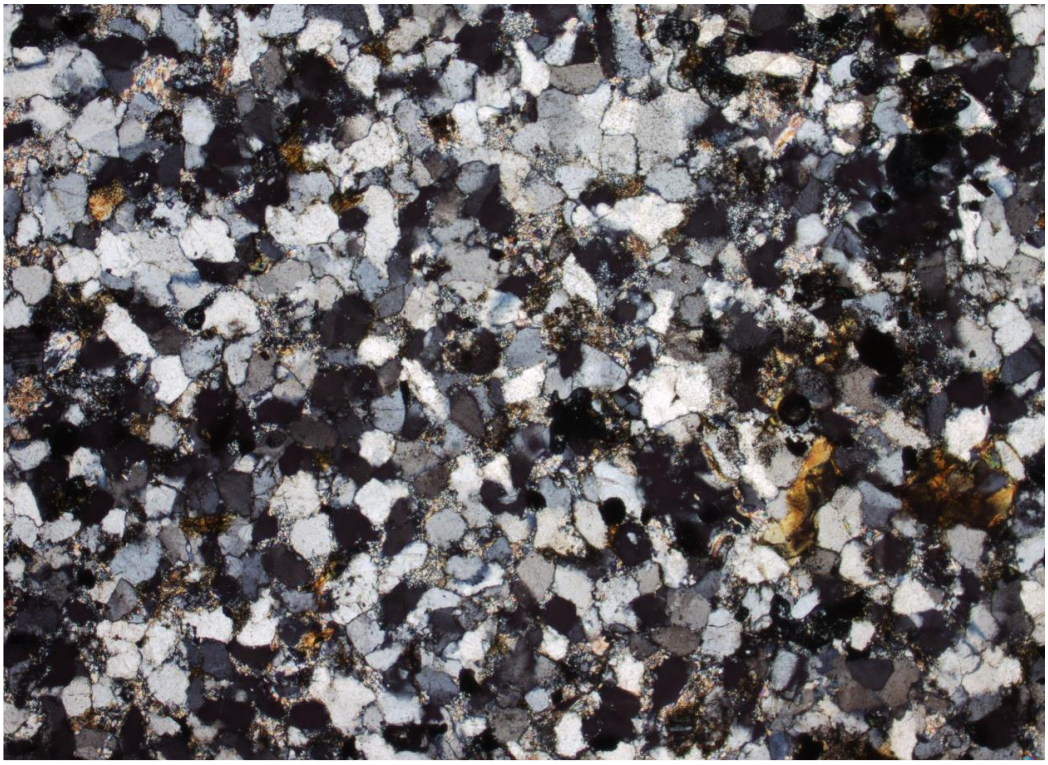

**Photomicrographs of a thin section showing rounded quartz in a clay-mica matrix (5x magnification)**
**Note straining in quartz (crossed polarised light)**

SAMPLE: Borehole 2A

Rock type: Sandstone/Quartzite

MACROSCOPIC ROCK DESCRIPTION

Very fine-grained, light brown to cream-coloured rock fragments.

MICROSCOPIC ROCK DESCRIPTION

Composition: Quartz (90%), Clay minerals and Mica (10%), Iron oxide (<1%)

Grain size: Fine- to medium grained (80µm to 300µm)

Sorting: Moderately to poorly sorted

Rounding: Rounded to recrystallized

Clast/matrix supported: Clast supported

Other textures: Interlocking

Description: The rock is a sedimentary rock consisting of quartz (90%) set in a clay and mica-rich matrix (10%). Quartz is rounded to elongated and recrystallized locally as evidenced from the 120º junctions shown by larger quartz grains. The original sedimentary rock was moderately to poorly sorted. Locally mica and clay minerals form layering which is alternated with more quartz rich interlayers with quartz orientated parallel to the layering in some instances. Some straining was observed in quartz grains with <20% of all grains showing undulose extinction. Some straining was observed in quartz grains with <20% of all grains showing undulose extinction of between 14.5 and 26º according to the Dolar-Mantuani (1975) method, indicating ASR potential.

**Photomicrographs of a thin section showing rounded to elongated quartz interlayers with clay-mica units (5x magnification)**

**Note straining in quartz (crossed polarised light)**

SAMPLE: Borehole 2B

Rock type: Sandstone/Quartzite

MACROSCOPIC ROCK DESCRIPTION

Very fine-grained, light brown to cream-coloured rock fragments.

MICROSCOPIC ROCK DESCRIPTION

Composition: Quartz (95%), Clay minerals and Mica (<5%), Iron oxide (<1%), Feldspar (<1%)

Grain size: Fine- to medium grained (40µm to 500µm)

Sorting: Moderately sorted

Rounding: Rounded to recrystallized

Clast/matrix supported: Clast supported

Other textures: Interlocking

Description: The rock is a sedimentary rock consisting of quartz (95%) set in a clay and mica-rich matrix (<5%). Quartz is recrystallized as evidenced from the 120º junctions shown by quartz grains leading to more angular quartz grains. Micro-crystalline quartz was also observed. In some instances, quartz is interlocked with no matrix between grains, whereas other areas have a higher concentration of clay and mica. The original sedimentary rock was moderately to poorly sorted. Some straining was observed in quartz grains with <20% of all grains showing undulose extinction between 15º and 29º according to the Dolar-Mantuani (1975) method which indicates an ASR potential.

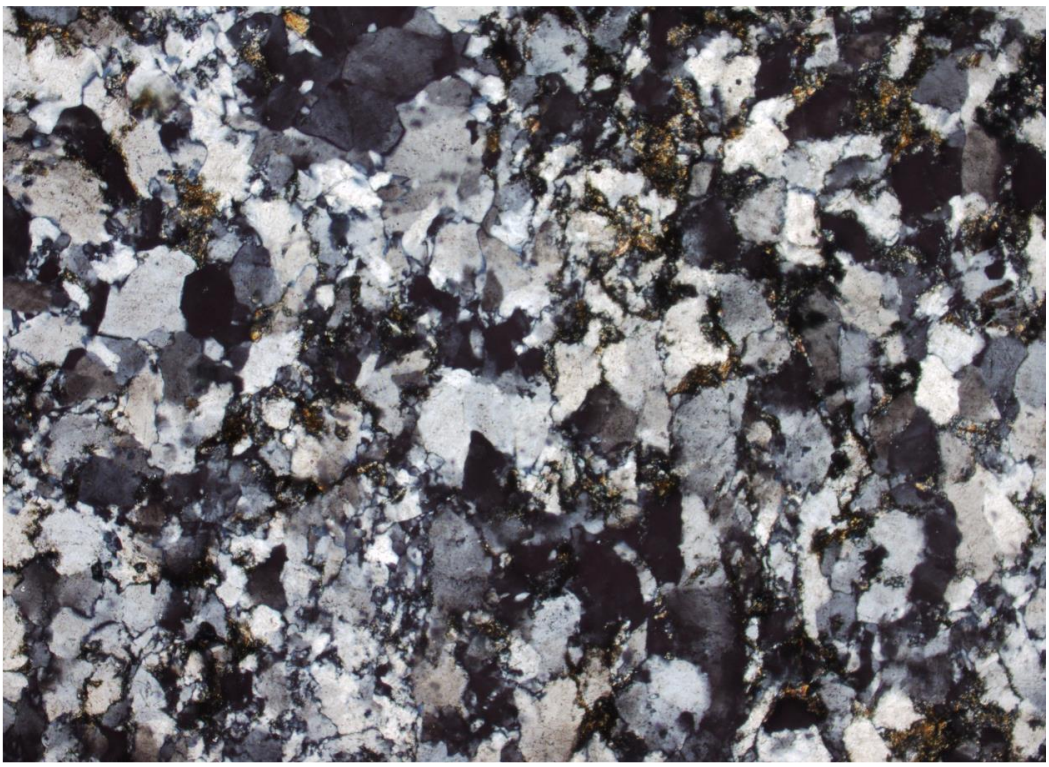

**Photomicrographs of a thin section showing rounded quartz in a clay-mica matrix (5x magnification)**
**Note straining in quartz (crossed polarised light)**

SAMPLE: Borehole 3

Rock type: Mudstone

MACROSCOPIC ROCK DESCRIPTION

Very fine-grained, light brown to cream-coloured rock fragments.

MICROSCOPIC ROCK DESCRIPTION

Composition: Quartz (40%), Clay minerals and Mica (55%), Iron oxide (5%), Feldspar (<1%)

Grain size: Very fine- grained (40µm to 100µm)

Sorting: Poorly sorted

Rounding: Angular to sub-angular

Clast/matrix supported: Matrix supported

Other textures: Foliated

Description: The rock is a sedimentary rock consisting of inhomogeneous alternating layers of containing quartz (40%) set in a clay and mica-rich matrix (55%) and layers consisting entirely of clay minerals and mica with iron oxide staining. Quartz is angular to recrystallized. The original sedimentary layering appears to have been disrupted and shows displacement and kink-banding. Very few quartz grains (<5%) showed undulose extinction, indicating a very low potential for ASR.

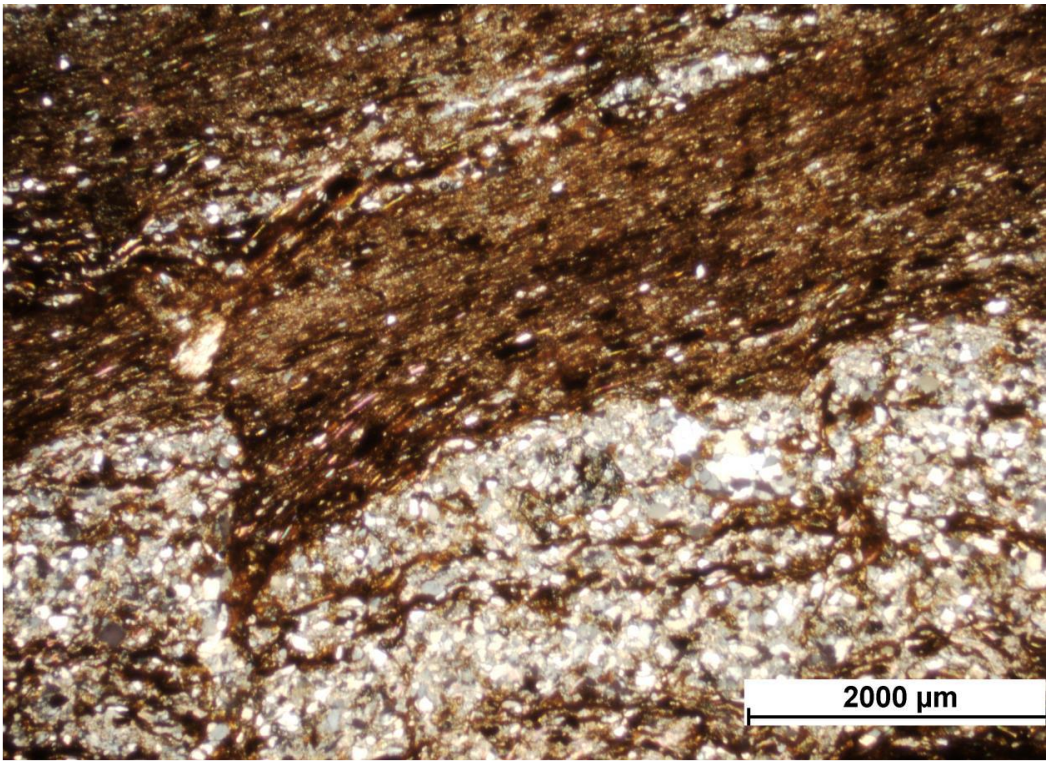


**Photomicrographs of a thin section showing rounded quartz in a clay-mica matrix**

**Note straining in quartz (plain polarised light)**

SAMPLE: Sandstone

Rock type: Sandstone/Quartzite

MACROSCOPIC ROCK DESCRIPTION

Very fine-grained, light brown to cream-coloured rock fragments

MICROSCOPIC ROCK DESCRIPTION

Composition: Quartz (99%), Clay minerals (<1%), Mica (<1%), Iron oxide (<1%)

Grain size: Fine- to medium grained (80µm to 500µm)

Sorting: Moderately sorted

Rounding: Rounded to recrystallized

Clast/matrix supported: Clast supported

Other textures: Interlocking

Description: The rock is a sedimentary rock consisting of quartz (99%) set in a clay and mica-rich matrix (<1%). Quartz rounded to recrystallized as evidenced from the 120º junctions shown by larger quartz grains. The original sedimentary rock was moderately sorted. Some straining was observed in quartz grains with <20% of all grains showing undulose extinction of average 12.3º according to the Dolar-Mantuani (1975) method which falls within the limits for rocks indicating a low ASR potential.

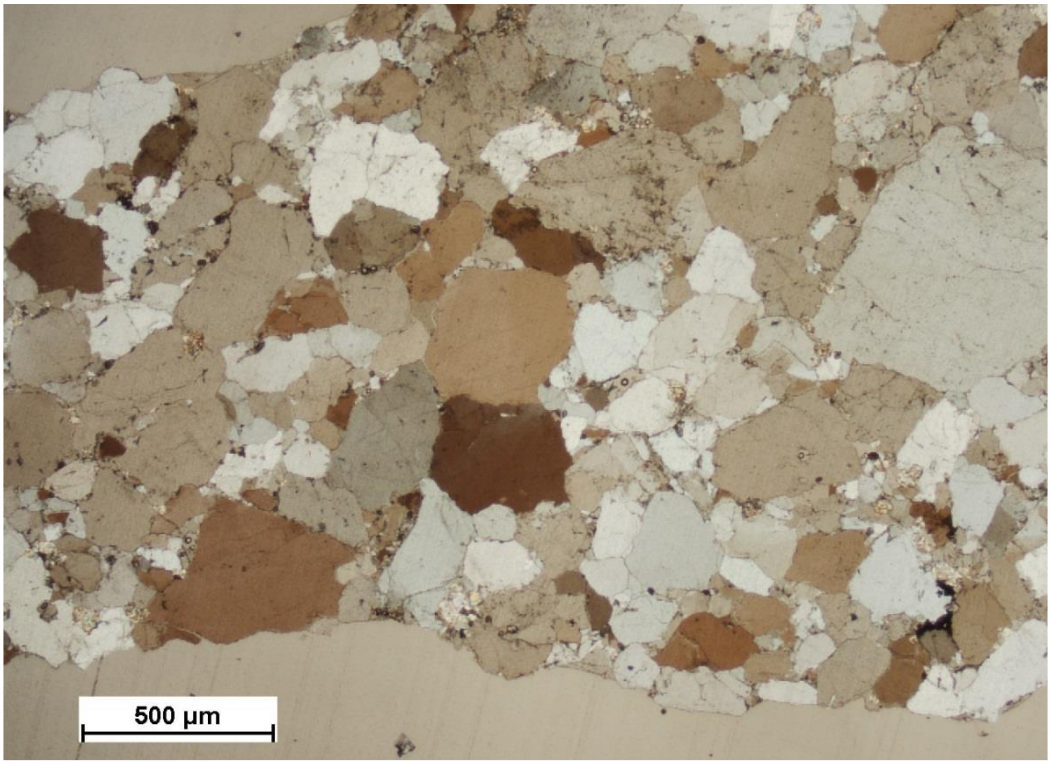


**Photomicrographs of a thin section showing rounded quartz in a clay-mica matrix**
**Note straining in quartz (crossed polarised light)**

SAMPLE: Tillite

Rock type: Tillite

MACROSCOPIC ROCK DESCRIPTION

Very fine-grained, brown rock with angular rock fragments.

MICROSCOPIC ROCK DESCRIPTION

Composition: Quartz (80%), Rock flour (Clay minerals and Mica (20%)), Iron oxide (<1%), Feldspar (<1%)

Rock fragments (80%)

Grain size: Fine- to locally coarse grained (40µm to 1000µm)

Sorting: Moderately to poorly sorted

Rounding: Angular to sub-angular

Clast/matrix supported: Fragments are matrix supported

Other textures:

Description: The rock is a tillite consisting of rock fragments and individual quartz grains (80%) set in a rock flour (clay and mica-rich matrix). Quartz is angular to sub-angular and is moderately sorted. Some straining was observed in quartz grains with ~30% of all grains showing an undulose extinction angle between 9º and 25º according to the Dolar-Mantuani (1975) method which indicates an ASR potential.

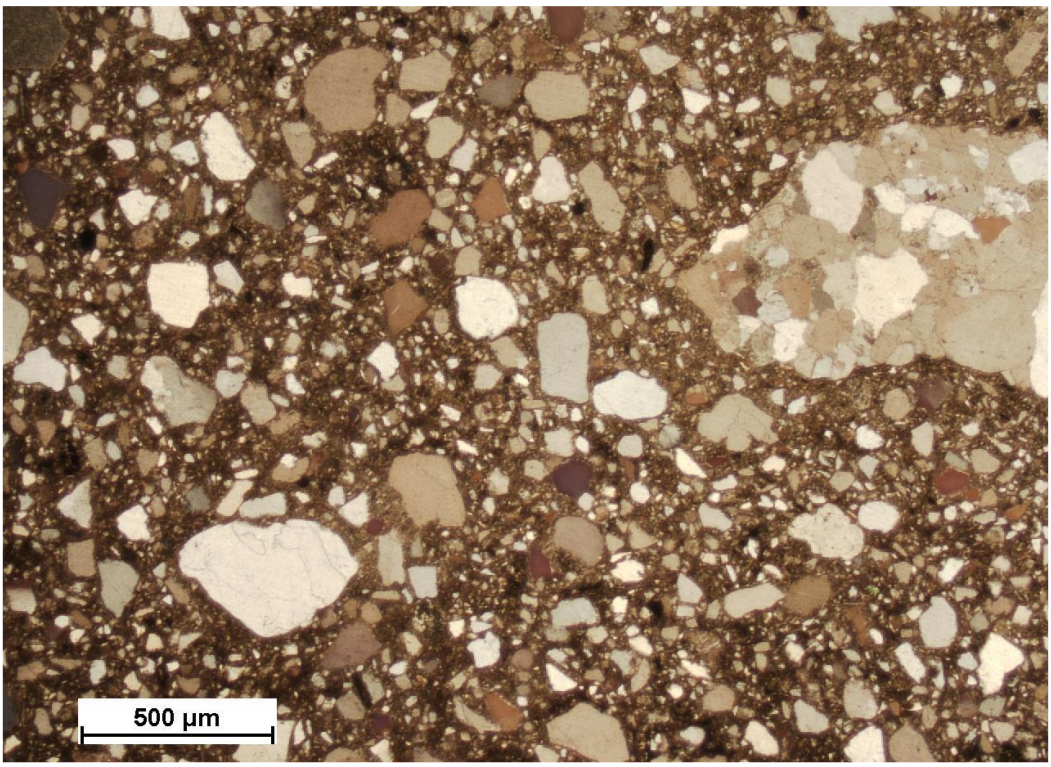


**Photomicrographs of a thin section showing angular to sub-angular quartz in rock flour matrix**
**Note straining in some quartz (crossed polarised light)**

SAMPLE: Sandstone mortar-bar

Rock type: Sandstone

MACROSCOPIC ROCK DESCRIPTION

Very fine-grained, light brown to cream-coloured rock

MICROSCOPIC ROCK DESCRIPTION

Composition: Quartz (95%), Clay minerals and Mica (5%), Iron oxide (<1%), Feldspar (<%)

Grain size: Fine- to very fine-grained (60µm to 140µm)

Sorting: Poorly sorted

Rounding: Angular to unrounded

Clast/matrix supported: Matrix supported

Other textures: This sample is a mortar-bar consisting of rock material in a cement matrix

Description: The rock is a sandstone consisting of individual quartz grains and rock fragments dominated by quartz (95%) and minor feldspar (<1%) set in very fine grained clay and mica-rich matrix (5%). Quartz is angular to unrounded and some grains show undulose extinction representing straining and potential ASR. Some straining was observed in quartz grains with <20% of all grains showing undulose extinction of average 11.2º according to the Dolar-Mantuani (1975) method which falls within the limits for rocks indicating a low ASR potential.

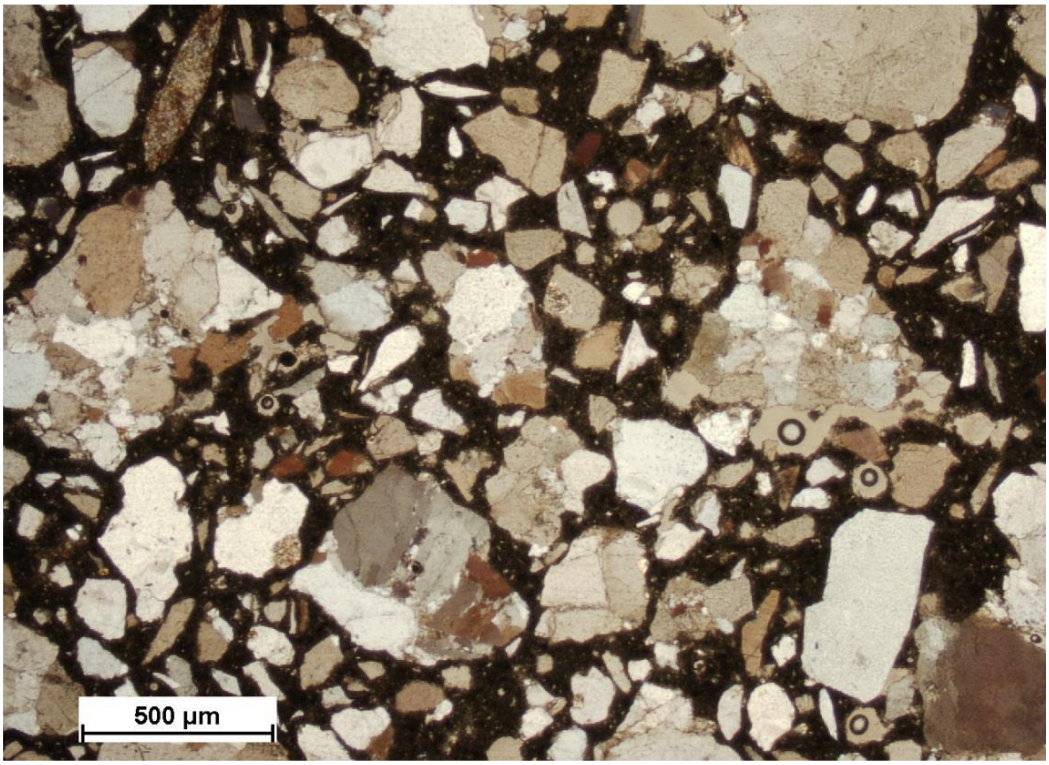


**Photomicrographs of a thin section showing angular quartz grains and rock fragments in a clay-mica matrix/rock four**

**Note straining in quartz (Crossed polarised light)**

SAMPLE: Tillite mortar-bar

Rock type: Tillite

MACROSCOPIC ROCK DESCRIPTION

Very fine-grained, brown rock with angular rock fragments

MICROSCOPIC ROCK DESCRIPTION

Composition: Quartz (60%), Rock flour (Clay minerals and Mica (40%)), Iron oxide (<1%), Feldspar (<1%)

Rock fragments (80%)

Grain size: Fine- to locally coarse grained (50µm to 1000µm)

Sorting: Very poorly sorted

Rounding: Angular to sub-angular

Clast/matrix supported: Fragments are matrix supported

Other textures: This sample is a mortar bar consisting of rock material in a cement matrix

Description: The rock is a tillite consisting of rock fragments and individual quartz grains (60%) set in a rock flour (clay and mica-rich matrix). Quartz is angular to sub- angular and is very poorly sorted. Small fractures were observed filled with iron oxide. Some straining was observed in quartz grains with <5% of all grains showing undulose extinction.

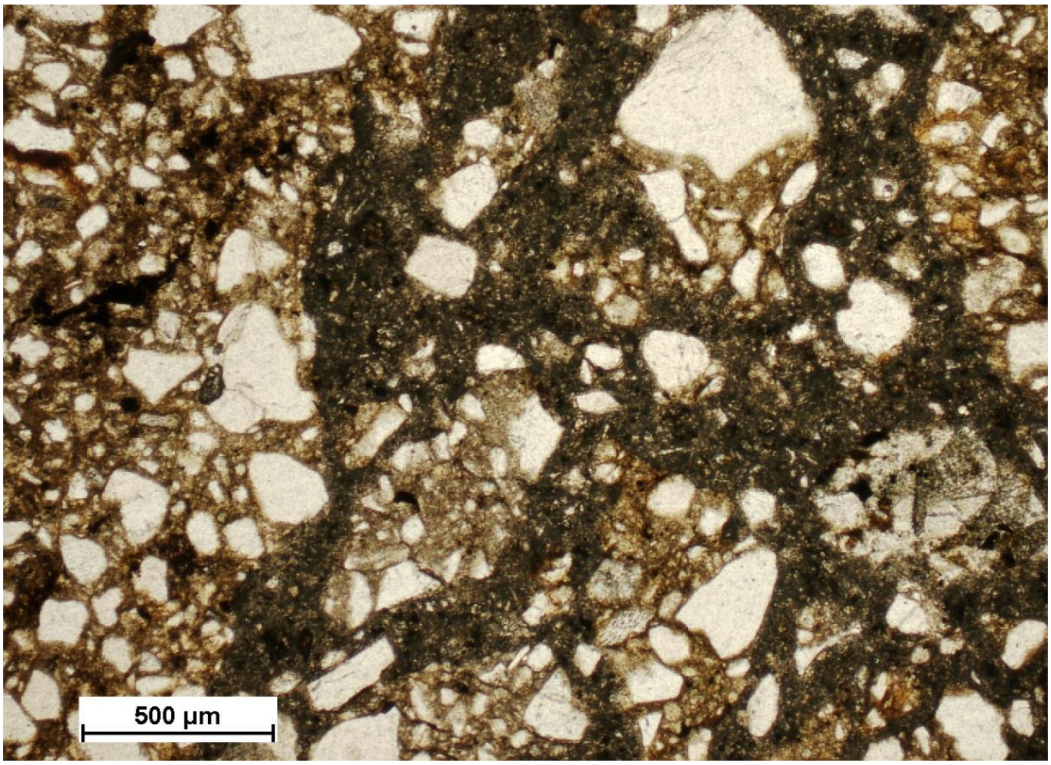


**Plain polarised light**

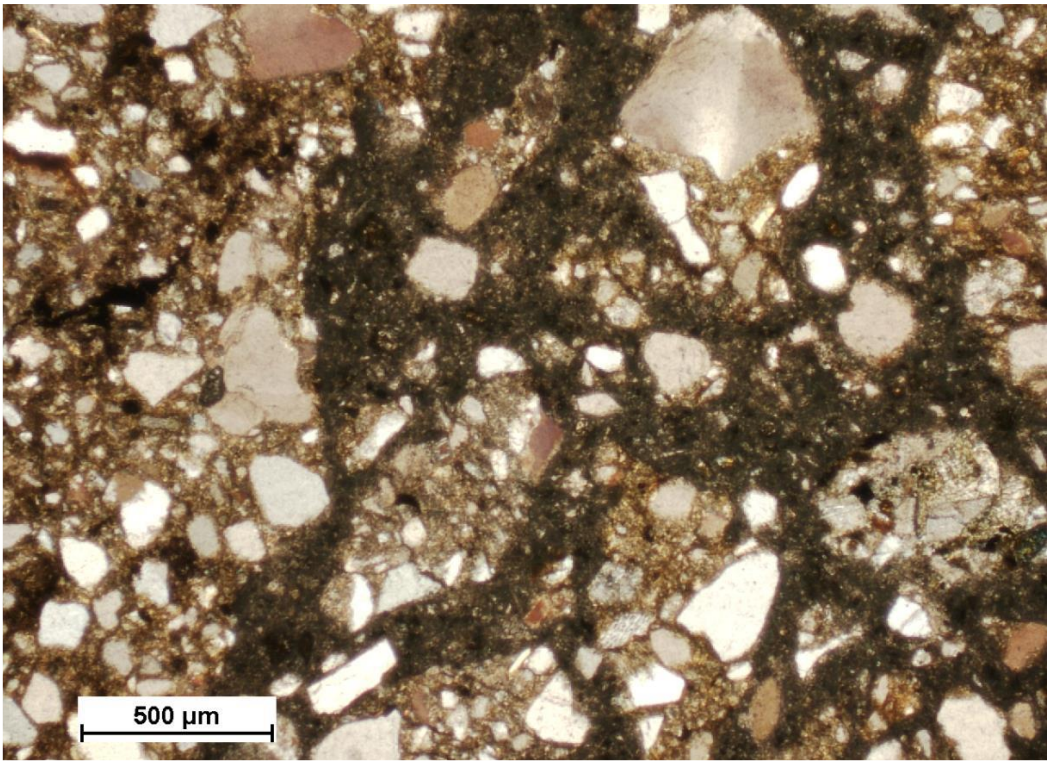


**Crossed polarised light**

**Photomicrographs of a thin section showing angular to sub-angular quartz in rock flour matrix**

**Note straining in some quartz**

# Appendix D

# Miscellaneous Results

## Sieve results of material ≥ 0.425mm

| Size (mm) | Mass retained (g) | | | | | | Mass retained (%) | | | | | | Cumulative passing sieve (%) | | | | | |
|---|---|---|---|---|---|---|---|---|---|---|---|---|---|---|---|---|---|---|
| | S1 | S2 | S3 | S4 | S5 | S6 | S1 | S2 | S3 | S4 | S5 | S6 | S1 | S2 | S3 | S4 | S5 | S6 |
| 37.5 | 0.0 | 0.0 | 0.0 | 0.0 | 0.0 | 0.0 | 0.0 | 0.0 | 0.0 | 0.0 | 0.0 | 0.0 | 100.0 | 100.0 | 100.0 | 100.0 | 100.0 | 100.0 |
| 28.0 | 36.9 | 0.0 | 0.0 | 0.0 | 0.0 | 0.0 | 2.8 | 0.0 | 0.0 | 0.0 | 0.0 | 0.0 | 97.2 | 100.0 | 100.0 | 100.0 | 100.0 | 100.0 |
| 20.0 | 32.6 | 0.0 | 0.0 | 0.0 | 0.0 | 0.0 | 2.5 | 0.0 | 0.0 | 0.0 | 0.0 | 0.0 | 94.7 | 100.0 | 100.0 | 100.0 | 100.0 | 100.0 |
| 14.0 | 36.0 | 27.1 | 11.7 | 0.0 | 0.0 | 0.0 | 2.8 | 2.1 | 0.9 | 0.0 | 0.0 | 0.0 | 91.9 | 97.9 | 99.1 | 100.0 | 100.0 | 100.0 |
| 5.0 | 142.2 | 31.1 | 141.7 | 15.3 | 156.0 | 17.5 | 10.9 | 2.4 | 11.2 | 1.3 | 9.7 | 1.2 | 81.1 | 95.5 | 87.9 | 98.7 | 90.3 | 98.8 |
| 2.0 | 56.8 | 81.7 | 360.8 | 19.6 | 275.8 | 34.2 | 4.3 | 6.4 | 28.4 | 1.6 | 17.1 | 2.4 | 76.7 | 89.1 | 59.5 | 97.1 | 73.2 | 96.4 |
| 0.425 | 109.9 | 258.2 | 628.0 | 178.0 | 915 | 486.2 | 8.4 | 20.1 | 49.4 | 14.7 | 56.9 | 33.6 | 68.3 | 69.0 | 10.1 | 82.5 | 16.3 | 62.8 |
| Pan | 894.2 | 886.0 | 128.4 | 1001.7 | 262.6 | 909.6 | 68.3 | 69.0 | 10.1 | 82.5 | 16.3 | 62.8 | 0.0 | 0.0 | 0.0 | 0.0 | 0.0 | 0.0 |
| Total | 1308.6 | 1284.1 | 1270.6 | 1214.6 | 1609.4 | 1447.5 | 100.0 | 100.0 | 100.0 | 100.0 | 100.0 | 100.0 | - | - | - | - | - | - |

## Sieve results of material < 0.425mm

| Size (mm) | Mass retained (g) | | | | | | Mass retained (%) | | | | | | Cumulative passing sieve (%) | | | | | |
|---|---|---|---|---|---|---|---|---|---|---|---|---|---|---|---|---|---|---|
| | S1 | S2 | S3 | S4 | S5 | S6 | S1 | S2 | S3 | S4 | S5 | S6 | S1 | S2 | S3 | S4 | S5 | S6 |
| 0.250 | 17.4 | 40.3 | 65.9 | 5.0 | 33.5 | 28.4 | 11.9 | 27.8 | 6.7 | 4.2 | 5.5 | 17.9 | 56.4 | 41.2 | 3.4 | 78.3 | 10.9 | 45.0 |
| 0.150 | 27.9 | 30.8 | 21.2 | 16.9 | 36.2 | 52.4 | 19.1 | 21.3 | 2.1 | 13.9 | 5.9 | 32.9 | 37.4 | 19.9 | 1.3 | 64.4 | 5.0 | 12.1 |
| 0.075 | 26.8 | 20.6 | 7.1 | 5.5 | 6.2 | 7.6 | 18.3 | 14.2 | 0.7 | 4.5 | 1.0 | 4.7 | 19.1 | 5.7 | 0.6 | 59.8 | 3.9 | 7.3 |
| Pan | 27.9 | 8.3 | 5.8 | 72.6 | 24.1 | 11.7 | 19.1 | 5.7 | 0.6 | 59.8 | 3.9 | 7.3 | 0.0 | 0.0 | 0.0 | 0.0 | 0.0 | 0.0 |
| Total | 100.0 | 100.0 | 100.0 | 100.0 | 100.0 | 100.0 | 68.3 | 69.0 | 10.1 | 82.5 | 16.3 | 62.8 | - | - | - | - | - | - |

## Sieve results for river sand

| Size (mm) | Mass retained (g) | | | | | | Mass retained (%) | | | | | | Cumulative passing sieve (%) | | | | | |
|---|---|---|---|---|---|---|---|---|---|---|---|---|---|---|---|---|---|---|
| | S3 | S5 | S6 | Mix | Fine | Coarse | S3 | S5 | S6 | Mix | Fine | Coarse | S3 | S5 | S6 | Mix | Fine | Coarse |
| 4.75 | 0.0 | 0.0 | 0.0 | 0.0 | - | - | 0.0 | 0.0 | 0.0 | 0.0 | - | - | 100.0 | 100.0 | 100.0 | 100.0 | 100.0 | 90.0 |
| 2.36 | 252.2 | 275.8 | 34.2 | 286.4 | - | - | 20.4 | 19.0 | 2.4 | 10.7 | - | - | 79.6 | 81.0 | 97.6 | 89.3 | 100.0 | 80.0 |
| 1.18 | 313.9 | 404.1 | 72.8 | 386.7 | - | - | 25.3 | 27.8 | 5.1 | 14.5 | - | - | 54.3 | 53.2 | 92.5 | 74.8 | 85.0 | 50.0 |
| 0.60 | 363.9 | 371.7 | 194.0 | 557.9 | - | - | 29.4 | 25.6 | 13.6 | 20.9 | - | - | 25.0 | 27.6 | 79.0 | 53.9 | 60.0 | 25.0 |
| 0.30 | 243.5 | 227.1 | 477.8 | 721.3 | - | - | 19.6 | 15.6 | 33.4 | 27.0 | - | - | 5.3 | 12.0 | 45.5 | 26.9 | 40.0 | 15.0 |
| 0.15 | 51.1 | 95.0 | 476.5 | 527.6 | - | - | 4.1 | 6.5 | 33.3 | 19.8 | - | - | 1.2 | 5.5 | 12.2 | 7.1 | 25.0 | 10.0 |
| Pan | 14.6 | 79.7 | 174.7 | 189.3 | - | - | 1.2 | 5.5 | 12.2 | 7.1 | - | - | 0.0 | 0.0 | 0.0 | 0.0 | 0.0 | 0.0 |
| Total | 1239.2 | 1453.4 | 1430.0 | 2669.2 | - | - | 100.0 | 100.0 | 100.0 | 100.0 | - | - | - | - | - | - | - | - |

## Hydrometer readings

| Parameter description | Sample 1 | | | Sample 2 | | | Sample 3 | | | Sample 4 | | |
|---|---|---|---|---|---|---|---|---|---|---|---|---|
| | 18sec | 40sec | 1hr | 18sec | 40sec | 1hr | 18sec | 40sec | 1hr | 18sec | 40sec | 1hr |
| Temperature recorded (°C) | 21.5 | 21.5 | 21.6 | 21.5 | 21.5 | 20.6 | 21.5 | 21.5 | 21.2 | 21.0 | 21.0 | 21.0 |
| Hydrometer reading at indicated time | 20.0 | 19.0 | 15.0 | 22.5 | 22.0 | 19.0 | 23.0 | 22.5 | 19.0 | 58.5 | 43.5 | 16.5 |
| Adjustment for temperature from TMH | +0.5 | +0.5 | +0.6 | +0.5 | +0.5 | +0.2 | +0.5 | +0.5 | +0.4 | +0.4 | +0.4 | +0.4 |
| Adjusted hydrometer reading | 20.5 | 19.5 | 15.6 | 23.0 | 22.5 | 19.2 | 23.5 | 23.0 | 19.4 | 58.9 | 43.9 | 16.9 |

## Determination of liquid limit

| Parameter description | Sample 1 | | | Sample 2 | | | Sample 3 | | | Sample 4 | | |
|---|---|---|---|---|---|---|---|---|---|---|---|---|
| Number of ticks, $N$ | 30 | 24 | 18 | 32 | 26 | 18 | 35 | 22 | 18 | 28 | 22 | 16 |
| Mass of container with wet soil, $a$ (g) | 16.39 | 17.42 | 18.30 | 20.13 | 21.53 | 22.33 | 14.16 | 15.48 | 15.43 | 12.72 | 11.81 | 11.40 |
| Mass of container with dry soil, $b$ (g) | 16.06 | 16.94 | 17.69 | 19.70 | 20.86 | 21.53 | 13.74 | 15.06 | 15.00 | 11.91 | 10.97 | 10.47 |
| Mass of empty container, $c$ (g) | 14.09 | 14.1 | 14.1 | 17.64 | 17.70 | 17.85 | 11.28 | 12.68 | 12.62 | 9.73 | 8.92 | 8.41 |
| Moisture content, $\omega$ (%) | 16.8 | 16.9 | 17.0 | 20.9 | 21.2 | 21.7 | 17.1 | 17.6 | 18.1 | 37.2 | 41.0 | 45.1 |

## Determination of plastic limit

| Parameter description | Sample 1 | | Sample 2 | | Sample 3 | | Sample 4 | |
|---|---|---|---|---|---|---|---|---|
| Mass of container with wet soil, $a$ (g) | 27.79 | 28.09 | 31.24 | 30.96 | - | - | 20.60 | 15.75 |
| Mass of container with dry soil, $b$ (g) | 26.09 | 26.49 | 29.59 | 29.41 | - | - | 20.34 | 15.37 |
| Mass of empty container, $c$ (g) | 13.97 | 14.17 | 17.77 | 17.53 | - | - | 18.90 | 13.50 |
| Moisture content, $\omega$ (%) | 14.0 | 13.0 | 14.0 | 13.0 | NP | NP | 18.1 | 20.3 |

# Determination of maximum dry density and optimum moisture content

| Sample | Specimen | Mass (g) | Water (%) | Water (g) | Container ID | $a$ (g) | $b$ (g) | $c$ (g) | $d$ (%) | $W'$ (g) | $W$ (g) | $D$ (kg/m$^3$) |
|---|---|---|---|---|---|---|---|---|---|---|---|---|
| 1 | 1 | 7 000 | 4 | 280 | 1A | 702.6 | 671.9 | 81.1 | 5.2 | 9 682 | 4 862 | 1 994 |
| | 2 | 7 000 | 5 | 350 | 1B | 673.6 | 639.2 | 84.7 | 6.2 | 9 800 | 4 980 | 2 023 |
| | 3 | 7 000 | 6 | 420 | 1C | 694.5 | 652.8 | 88.9 | 7.4 | 9 894 | 5 074 | 2 038 |
| | 4 | 7 000 | 7 | 490 | 1D | 700.2 | 653.4 | 75.2 | 8.1 | 9 882 | 5 062 | 2 020 |
| | 5 | 7 000 | 8 | 560 | 1E | 632.5 | 586.1 | 82.0 | 9.2 | 9 862 | 5 042 | 1 992 |
| 2 | 1 | 7 000 | 3 | 210 | 2A | 698.6 | 657.5 | 78.4 | 7.1 | 9 711 | 4 891 | 1 970 |
| | 2 | 7 000 | 4 | 280 | 2B | 684.5 | 638.5 | 77.1 | 8.2 | 9 876 | 5 056 | 2 016 |
| | 3 | 7 000 | 5 | 350 | 2C | 589.6 | 546.2 | 82.1 | 9.4 | 9 994 | 5 174 | 2 041 |
| | 4 | 7 000 | 6 | 420 | 2D | 568.4 | 524.0 | 88.8 | 10.2 | 9 960 | 5 140 | 2 020 |
| | 5 | 7 000 | 7 | 490 | 2E | 640.9 | 584.2 | 79.6 | 11.2 | 9 913 | 5 093 | 1 975 |
| 3 | 1 | 7 000 | 2 | 140 | 3A | 712.4 | 686.3 | 78.2 | 4.3 | 9 476 | 4 656 | 1 926 |
| | 2 | 7 000 | 3 | 210 | 3B | 742.6 | 709.6 | 75.5 | 5.2 | 9 621 | 4 801 | 1 969 |
| | 3 | 7 000 | 4 | 280 | 3C | 681.2 | 645.7 | 82.0 | 6.3 | 9 743 | 4 923 | 1 998 |
| | 4 | 7 000 | 5 | 350 | 3D | 781.4 | 733.6 | 79.2 | 7.3 | 9 697 | 4 877 | 1 961 |
| | 5 | 7 000 | 6 | 420 | 3E | 668.6 | 622.6 | 82.6 | 8.5 | 9 647 | 4 827 | 1 919 |

| | | | | | |
|---|---|---|---|---|---|
| $a$ | Mass of the container and wet material (g) | $W$ | Mass of the wet material (g) | | |
| $b$ | Mass of the container and dry material (g) | $D$ | Dry density (kg/m$^3$) | | |
| $c$ | Mass of the container (g) | $M$ | Mass of the mould (g) | 4 820 | |
| $d$ | Moisture content expressed as a percentage of the dry material (%) | $V$ | Volume of the mould (g) | 2 318 | |
| $W'$ | Mass of the mould and wet material (g) | $F$ | Mould factor | 43.1 | |

## Determination of hygroscopic moisture content

| Parameter description | Sample 1 | | Sample 2 | | Sample 3 | |
|---|---|---|---|---|---|---|
| | 1 | 2 | 1 | 2 | 1 | 2 |
| Mass of container with wet soil, $a$ (g) | 669.5 | 660.5 | 635.8 | 585.5 | 764.5 | 783.3 |
| Mass of container with dry soil, $b$ (g) | 663.6 | 654.7 | 608.7 | 564.3 | 748.3 | 768.8 |
| Mass of empty container, $c$ (g) | 75.5 | 76.1 | 76.6 | 82.9 | 71.5 | 77.3 |
| Hygroscopic moisture content, $\omega$ (%) | 1.0 | 1.0 | 5.1 | 4.4 | 2.4 | 2.1 |

## Determination of water required for optimum moisture

| Parameter description | Sample 1 | Sample 2 | Sample 3 |
|---|---|---|---|
| Hygroscopic moisture content, $x$ (%) | 1.0 | 4.7 | 2.2 |
| Required moisture content, $y$ (%) | 7.0 | 9.1 | 6.0 |
| Total mass of sample material, $z$ (g) | 21 000 | 20 750 | 20 700 |
| Mass of water required, $W$ (g) | 1 247 | 862 | 760 |

## Verification of moisture content

| Parameter description | Sample 1 | Sample 2 | Sample 3 |
|---|---|---|---|
| Mass of container with wet soil, $a$ (g) | 641.4 | 531.1 | 821.2 |
| Mass of container with dry soil, $b$ (g) | 603.6 | 494.2 | 776.7 |
| Mass of empty container, $c$ (g) | 78.2 | 88.9 | 82.0 |
| Moisture content, $\omega$ (%) | 7.2 | 9.1 | 6.4 |

## Determination of dry densities

| Parameter description | Sample 1 | | | Sample 2 | | | Sample 3 | | |
|---|---|---|---|---|---|---|---|---|---|
| | MOD | NRB | STD | MOD | NRB | STD | MOD | NRB | STD |
| Mass of mould, $M$ (g) | 4 926 | 4 897 | 3 161 | 4 800 | 5 409 | 4 955 | 5 053 | 4 967 | 4 907 |
| Mass of the mould and wet material, $W'$ (g) | 10 041 | 9 744 | 7 767 | 10 000 | 10 322 | 9 627 | 9 994 | 9 656 | 9 365 |
| Mass of the wet material, $W$ (g) | 5 115 | 4 847 | 4 606 | 5 200 | 4 913 | 4 672 | 4 941 | 4 689 | 4 458 |
| Volume of mould, $V$ (mℓ) | 2 332 | 2 321 | 2 330 | 2 327 | 2 315 | 2 337 | 2 330 | 2 316 | 2 321 |
| Mould factor, $F$ | 42.9 | 43.1 | 42.9 | 43.0 | 43.2 | 42.8 | 42.9 | 43.2 | 43.1 |
| Dry density, $\rho_d$ (kg/m$^3$) | 2 046 | 1 948 | 1 844 | 2 048 | 1 945 | 1 832 | 1 993 | 1 903 | 1 805 |
| Relative compaction (%) | 100.2 | 95.4 | 90.3 | 100.3 | 95.3 | 89.7 | 99.7 | 95.2 | 90.3 |

## Determination of swelling

| Parameter description | Sample 1 | | | Sample 2 | | | Sample 3 | | |
|---|---|---|---|---|---|---|---|---|---|
| | MOD | NRB | STD | MOD | NRB | STD | MOD | NRB | STD |
| Reading before material has soaked, $L$ (mm) | 5.00 | 5.00 | 5.00 | 5.00 | 5.00 | 5.00 | 5.00 | 5.00 | 5.00 |
| Reading after material has soaked for four days, $k$ (mm) | 5.01 | 5.03 | 5.05 | 5.04 | 5.07 | 5.10 | 5.00 | 5.01 | 5.02 |
| Swelling as percentage of initial height, $S$ (%) | 0.01 | 0.02 | 0.04 | 0.03 | 0.06 | 0.08 | 0.00 | 0.01 | 0.02 |

# Penetration results

| Penetration depth (mm) | Sample 1 | | | Sample 2 | | | Sample 3 | | |
|---|---|---|---|---|---|---|---|---|---|
| | MOD | NRB | STD | MOD | NRB | STD | MOD | NRB | STD |
| 0.000 | 0.00 | 0.00 | 0.00 | 0.00 | 0.00 | 0.00 | 0.00 | 0.00 | 0.00 |
| 0.635 | 0.60 | 0.44 | 0.22 | 0.29 | 0.10 | 0.05 | 0.60 | 0.22 | 0.10 |
| 1.270 | 1.09 | 0.87 | 0.34 | 0.64 | 0.36 | 0.16 | 1.40 | 0.44 | 0.30 |
| 1.905 | 1.93 | 1.21 | 0.69 | 1.00 | 0.46 | 0.26 | 2.73 | 0.76 | 0.56 |
| 2.540 | 2.87 | 1.79 | 1.05 | 1.29 | 0.56 | 0.40 | 4.03 | 1.23 | 0.86 |
| 3.175 | 3.84 | 2.39 | 1.43 | 1.52 | 0.60 | 0.45 | 5.38 | 1.84 | 1.20 |
| 3.810 | 4.79 | 2.99 | 1.85 | 1.73 | 0.70 | 0.53 | 6.25 | 2.51 | 1.70 |
| 4.445 | 5.71 | 3.56 | 2.28 | 1.90 | 0.72 | 0.59 | 7.19 | 3.11 | 2.39 |
| 5.080 | 6.48 | 4.03 | 2.74 | 2.05 | 0.88 | 0.66 | 8.03 | 3.57 | 2.84 |
| 5.715 | 7.16 | 4.58 | 3.56 | 2.17 | 0.94 | 0.70 | 8.81 | 4.03 | 3.28 |
| 6.350 | 7.78 | 4.95 | 3.90 | 2.31 | 1.01 | 0.82 | 9.55 | 4.46 | 3.66 |
| 6.985 | 8.30 | 5.46 | 4.20 | 2.42 | 1.10 | 0.89 | 10.23 | 4.86 | 3.90 |
| 7.620 | 8.72 | 6.01 | 4.80 | 2.53 | 1.18 | 0.95 | 10.95 | 5.22 | 4.20 |
| 8.255 | 9.06 | 7.31 | 5.20 | 2.63 | 1.29 | 0.99 | 11.65 | 5.58 | 4.64 |
| 8.890 | 9.44 | 8.16 | 5.80 | 2.74 | 1.40 | 1.05 | 12.33 | 5.95 | 4.96 |
| 9.525 | 9.74 | 8.60 | 6.19 | 2.83 | 1.50 | 1.10 | 12.95 | 6.27 | 5.17 |

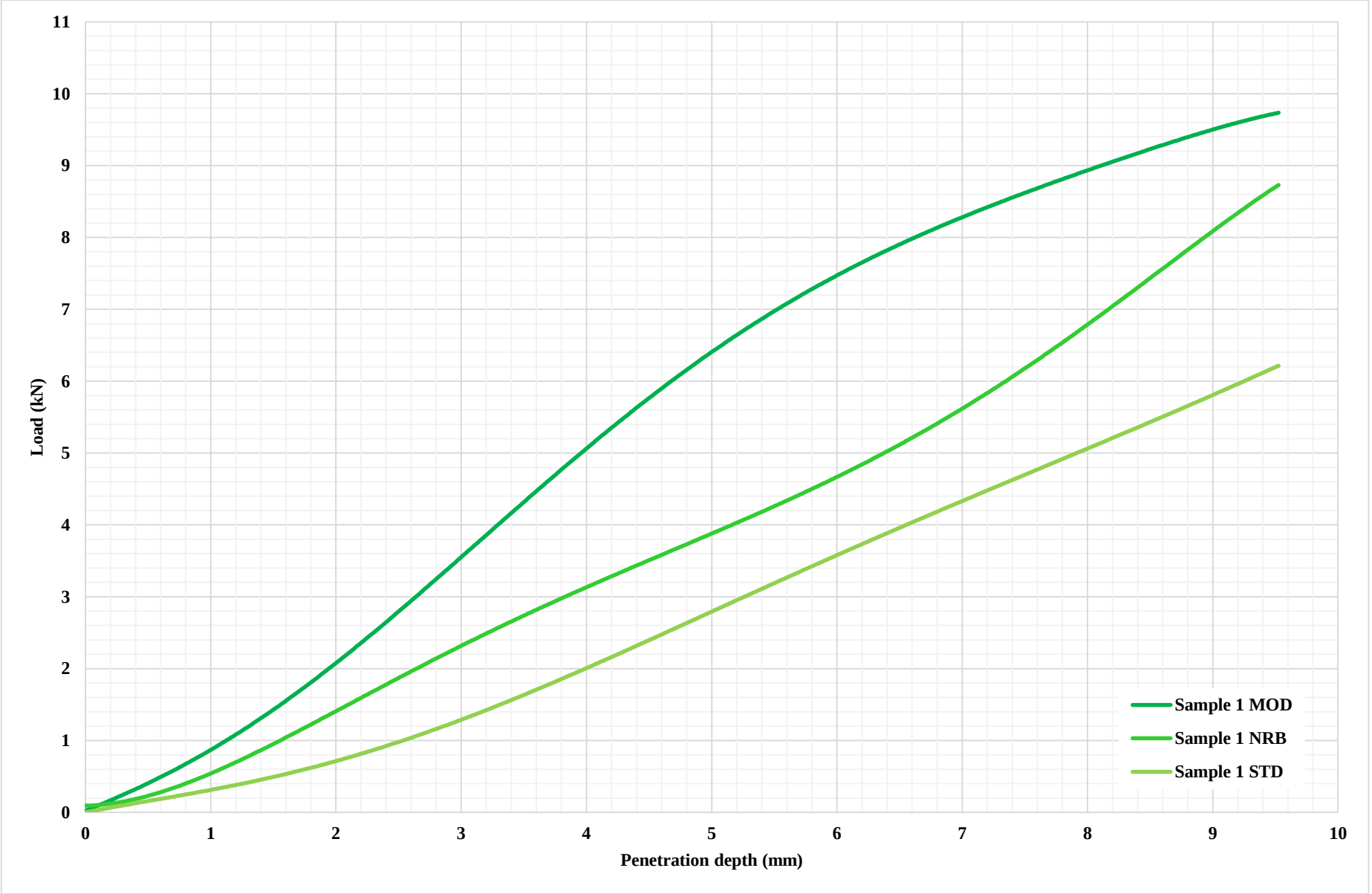

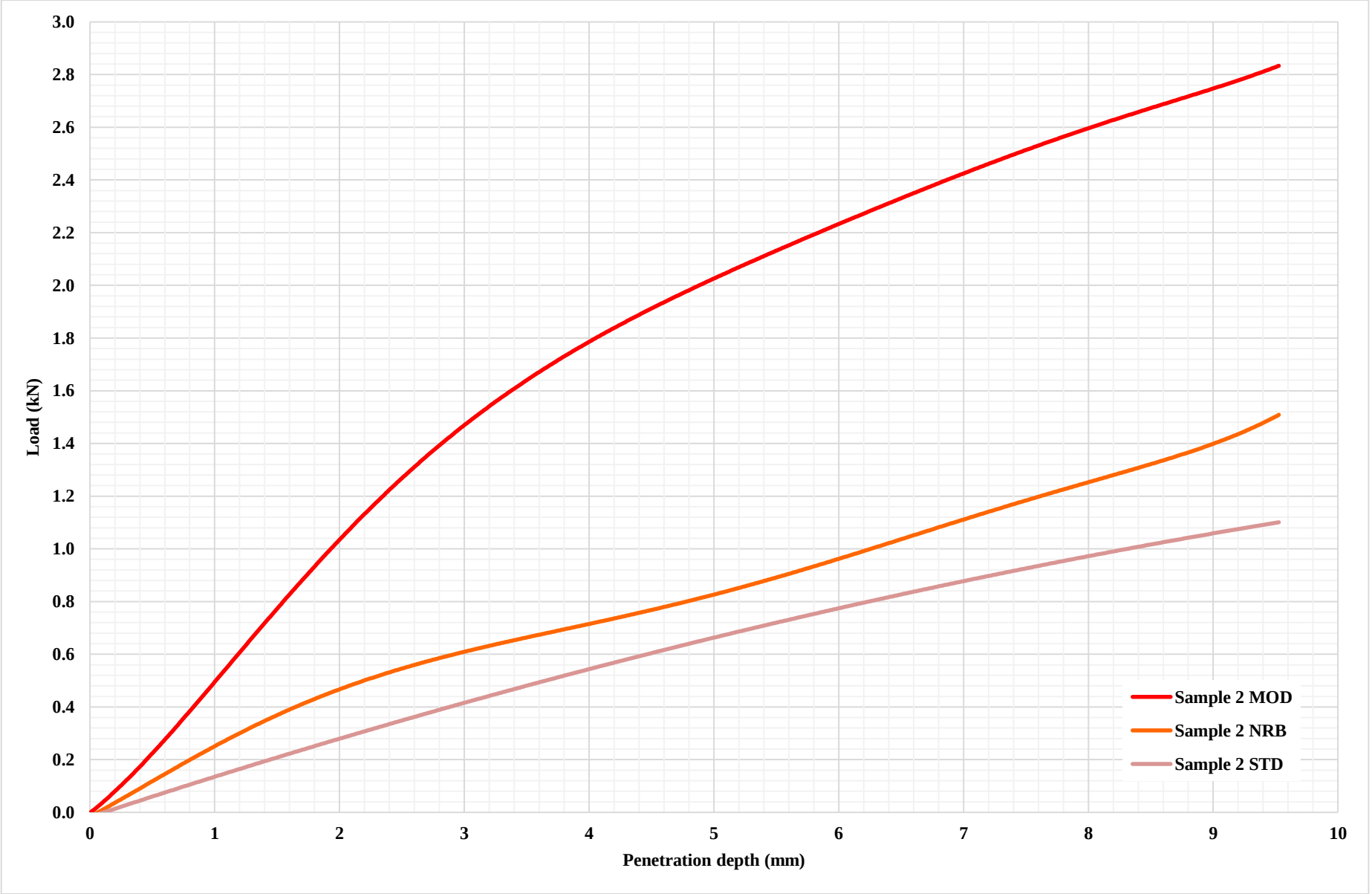

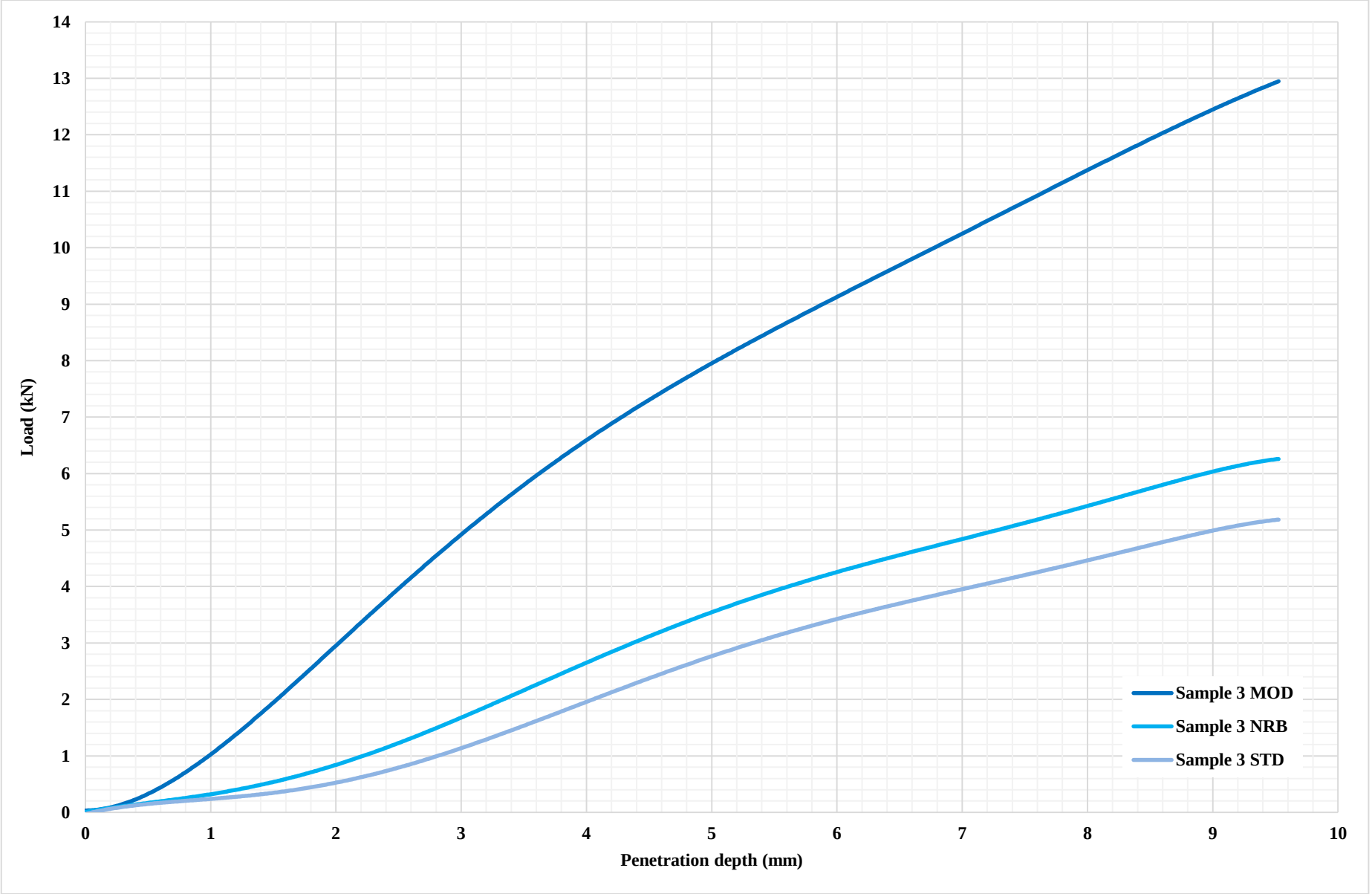

## Determination of UCS for sandstone

| Specimen | Length, $L$ (mm) | Diameter, $d$ (mm) | $L/d$ ratio | Load, $F$ (kN) | Cross sectional area, $A$ (mm$^2$) | UCS, $\sigma$ (MPa) |
|---|---|---|---|---|---|---|
| 1 | 92.5 | 44.2 | 2.1 | 118.0 | 1534.4 | 76.9 |
| 2 | 91.0 | 44.2 | 2.1 | 89.0 | 1534.4 | 58.0 |
| 3 | 92.3 | 44.4 | 2.1 | 117.0 | 1548.3 | 75.6 |
| 4 | 92.3 | 44.4 | 2.1 | 111.5 | 1548.3 | 72.0 |
| 5 | 93.6 | 44.2 | 2.1 | 169.0 | 1534.4 | 110.1 |
| 6 | 91.4 | 44.4 | 2.1 | 84.0 | 1548.3 | 54.3 |
| Average | 92.2 | 44.3 | 2.1 | 114.8 | 1541.3 | 74.5 |

## Determination of UCS for tillite

| Specimen | Point load, $P$ (kN) | Point load index, $I_S$ (MPa) | UCS, $\sigma$ (MPa) |
|---|---|---|---|
| 1 | 7.0 | 3.6 | 85.1 |
| 2 | 7.5 | 3.8 | 91.2 |
| 3 | 3.0 | 1.5 | 36.5 |
| 4 | 4.0 | 2.0 | 48.6 |
| 5 | 7.0 | 3.6 | 85.1 |
| 6 | 6.5 | 3.3 | 79.0 |
| Average | 5.8 | 3.0 | 70.9 |

## Determination of particle and relative densities

| Parameter description | Sandstone | Tillite |
|---|---|---|
| Mass of the pycnometer, $m_a$ (g) | 492.0 | 492.0 |
| Mass of the pycnometer with aggregate, $m_b$ (g) | 970.7 | 980.8 |
| Mass of the saturated surface-dry aggregate, $m_c$ (g) | 478.7 | 488.8 |
| Mass of the pycnometer, aggregate and water, $m_d$ (g) | 2 087.4 | 2 095.7 |
| Mass of the pycnometer filled with water (g) | 1 790.5 | 1 790.5 |
| Mass of the container (g) | 92.2 | 89.2 |
| Mass of the container with dry aggregate (g) | 569.6 | 573.7 |
| Mass of the oven-dried aggregate (g) | 477.4 | 484.5 |

## Mortar-bar test readings

| Reading | Mortar-bars with sandstone as fine aggregate | | | | | |
|---|---|---|---|---|---|---|
| | 1 | 2 | 3 | 4 | 5 | 6 |
| Zero | 818 | 835 | 823 | 827 | 864 | 878 |
| Initial | 898 | 910 | 901 | 900 | 938 | 950 |
| 2nd | 900 | 915 | 904 | 905 | 946 | 961 |
| 3rd | 903 | 916 | 908 | 906 | 946 | 966 |
| 4th | 904 | 918 | 919 | 911 | 946 | 966 |
| 5th | 908 | 918 | 919 | 911 | 946 | 966 |

| Reading | Mortar-bars with tillite as fine aggregate | | | | | |
|---|---|---|---|---|---|---|
| | 1 | 2 | 3 | 4 | 5 | 6 |
| Zero | 847 | 932 | 881 | 804 | 773 | 872 |
| Initial | 904 | 965 | 954 | 872 | 839 | 929 |
| 2nd | 905 | 913 | 954 | 873 | 846 | 938 |
| 3rd | 909 | 915 | 950 | 873 | 847 | 942 |
| 4th | 912 | 901 | 952 | 875 | 847 | 940 |
| 5th | 912 | 901 | 952 | 875 | 847 | 941 |

## Mortar-bar test readings

| Time of reading | Q1 | Q2 | Q3 | Q4 | Q5 | Q6 | Avg | Length, ΔL (mm) | Strain, ε (%) |
|---|---|---|---|---|---|---|---|---|---|
| Initial reading at 24 hours from cast | 0 | 0 | 0 | 0 | 0 | 0 | 0 | 0.000 | 0.000 |
| 1 day in water at 80˚C | 80 | 75 | 78 | 73 | 74 | 72 | 75 | 0.122 | 0.061 |
| Strain at 16 days | 85 | 81 | 85 | 79 | 82 | 88 | 83 | 0.135 | 0.068 |
| Strain due to ASR after 14 days | 5 | 6 | 7 | 6 | 8 | 16 | 8 | 0.013 | 0.006 |

| Time of reading | T1 | T2 | T3 | T4 | T5 | T6 | Avg | Length, ΔL (mm) | Strain, ε (%) |
|---|---|---|---|---|---|---|---|---|---|
| Initial reading at 24 hours from cast | 0 | ~~0~~ | ~~0~~ | 0 | 0 | 0 | 0 | 0.000 | 0.000 |
| 1 day in water at 80˚C | 57 | ~~33~~ | ~~73~~ | 68 | 66 | 57 | 62 | 0.100 | 0.050 |
| Strain at 16 days | 62 | ~~-17~~ | ~~69~~ | 69 | 74 | 70 | 69 | 0.111 | 0.056 |
| Strain due to ASR after 14 days | 5 | ~~-50~~ | ~~-4~~ | 1 | 8 | 13 | 7 | 0.011 | 0.005 |

# Appendix E

# Design Calculations

# Input data

| Foundation property | Dimension | Superstructure loads acting on foundation | Nominal loads, $Q_n$ | |
|---|---|---|---|---|
| | | | ULS | SLS |
| Foundation diameter, $D$ (m) | 5.5 | Vertical force, $F_Z$ (kN) | 603 | 474 |
| Foundation height, $H$ (m) | 1.0 | Bending moment, $M_R$ (kNm) | 1 398 | 440 |
| Pedestal diameter, $d$ (m) | 2.5 | Radial force, $F_R$ (kN) | 158 | 20 |
| Pedestal height, $h$ (mm) | 75 | Torsional moment, $M_Z$ (kNm) | 126 | 30 |
| TOC crossfall, $s$ (%) | 2.0 | Equivalent shear force, $F_R{}'$ (kN) | 266 | 49 |
| Depth to water table, $z$ (m) | 0.0 | The equivalent shear force takes account of the interaction between the radial force and torsional moment | | |
| Total foundation height, $e_H$ (m) | 1.105 | | | |

| $P(x;y)$ | A | B | C | D | E | F | G | H |
|---|---|---|---|---|---|---|---|---|
| $x$ | 0 | 0 | 1.5 | 1.5 | 4 | 4 | 5.5 | 5.5 |
| $y$ | 0 | 1 | 1.03 | 1.105 | 1.105 | 1.03 | 1 | 0 |

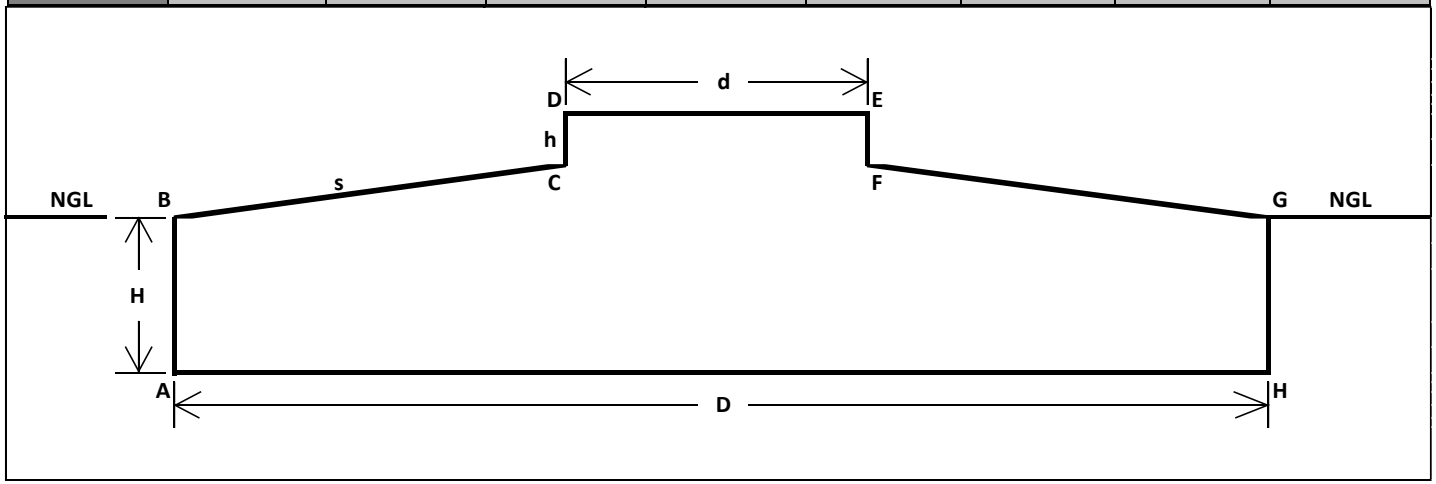

## Overall stability

| **Parameters for overall stability calculations** | | | |
|---|---|---|---|
| Density of concrete, $\rho$ (kg/m$^3$) | 2 500 | | |
| Unit weight of water, $\gamma_w$ (kN/m$^3$) | 9.8 | | |
| Unit weight of concrete, $\gamma_c$ (kN/m$^3$) | 24.525 | | |
| Volume of foundation, $V$ (m$^3$) | 24.521 | | |
| **Superstructure loads acting on foundation (ULS)** | **Nominal loads, $Q_n$** | **Partial load factors, $\gamma_f$** | **Design loads, $Q_d$** |
| Vertical force, $F_Z$ (kN) | 603 | 0.9 | 543 |
| Radial force, $F_R$ (kN) | 158 | 1.3 | 205 |
| Bending moment, $M_R$ (kNm) | 1 398 | 1.3 | 1 817 |
| Weight of foundation, $W$ (kN) | 601 | 0.9 | 541 |
| Buoyancy force, $F_B$ (kN) | -233 | 1.0 | -233 |
| **Moment equilibrium** | | | |
| Stabilizing moments, $M_{stb}$ (kNm) | 2 341 | | |
| Destabilizing moments, $M_{dst}$ (kNm) | 2 044 | | |
| $M_{stb}/M_{dst} \geq 1$ | 1.145 | | |

## Sliding resistance

| **Material parameters** | **Characteristic material properties, $f_k$** | **Partial material factors, $\gamma_m$** | **Design resistance, $R_d$** |
|---|---|---|---|
| Friction angle, $\varphi$ (deg) | 29 | 1.25 | 24 |
| **Superstructure loads acting on foundation (ULS)** | **Nominal loads, $Q_n$** | **Partial load factors, $\gamma_f$** | **Design loads, $Q_d$** |
| Vertical force, $F_Z$ (kN) | 603 | 0.9 | 543 |
| Equivalent shear force, $F_R$ (kN) | 266 | 1.3 | 346 |
| Weight of foundation, $W$ (kN) | 601 | 0.9 | 541 |
| Buoyancy force, $F_B$ (kN) | -233 | 1.0 | -233 |
| **Horizontal force equilibrium** | | | |
| Vertical design force, $V_d$ (kN) | 851 | | |
| Stabilizing force, $V_d \tan \varphi_d$ (kN) | 377 | | |
| Destabilizing force, $H_d$ (kN) | 346 | | |
| $V_d \tan \varphi_d / H_d \geq 1$ | 1.092 | | |

# Bearing resistance

| **Parameters for bearing capacity calculations** | |
|---|---|
| Eccentricity of normal force, $e$ (m) | 2.104 |
| Elliptical area, $A'$ (m$^2$) | 3.129 |
| Elliptical width, $B_e$ (m) | 1.292 |
| Elliptical length, $L_e$ (m) | 3.541 |
| Effective width, $B'$ (m) | 1.068 |
| Effective length, $L'$ (m) | 2.929 |

| **Material parameters** | **Characteristic material properties, $f_k$** | **Partial material factors, $\gamma_m$** | **Design resistance, $R_d$** |
|---|---|---|---|
| Cohesion, $c$ (kPa) | 234 | 1.25 | 187 |
| Friction angle, $\varphi$ (deg) | 29 | 1.25 | 24 |
| **Unit weight of overburden material** | | | |
| Bulk unit weight, $\gamma$ (kN/m$^3$) | 18 | 1.0 | 18 |
| Saturated unit weight, $\gamma_{sat}$ (kN/m$^3$) | 21 | 1.0 | 21 |
| Submerged unit weight, $\gamma'$ (kN/m$^3$) | 11 | 1.0 | 11 |
| **Unit weight of founding material** | | | |
| Bulk unit weight, $\gamma$ (kN/m$^3$) | 26 | 1.0 | 26 |
| Saturated unit weight, $\gamma_{sat}$ (kN/m$^3$) | 26 | 1.0 | 26 |
| Submerged unit weight, $\gamma'$ (kN/m$^3$) | 16 | 1.0 | 16 |
| **Superstructure loads acting on foundation (ULS)** | **Nominal loads, $Q_n$** | **Partial load factors, $\gamma_f$** | **Design loads, $Q_d$** |
| Vertical force, $F_Z$ (kN) | 603 | 1.0 | 603 |
| Radial force, $F_R$ (kN) | 158 | 1.3 | 205 |
| Bending moment, $M_R$ (kNm) | 1 398 | 1.3 | 1 817 |
| Weight of foundation, $W$ (kN) | 601 | 1.0 | 601 |
| Buoyancy force, $F_B$ (kN) | -233 | 1.0 | -233 |

| **Design loads, $Q_d$** | |
|---|---|
| Design vertical force, $V_d$ (kN) | 972 |
| Design horizontal force, $H_d$ (kN) | 205 |
| Design moment, $M_d$ (kNm) | 2 044 |

| **Bearing capacity terms, $x$** | **Bearing capacity factors, $N_x$** | **Shape factors, $s_x$** | **Inclination factors, $i_x$** |
|---|---|---|---|
| Cohesion ($c$) | 19.210 | 1.165 | 0.832 |
| Surcharge ($q$) | 9.519 | 1.148 | 0.850 |
| Weight density ($\gamma$) | 7.555 | 0.891 | 0.774 |

| **Bearing resistance** | |
|---|---|
| Cohesion term (kN/m$^2$) | 3 487 |
| Surcharge term (kN/m$^2$) | 104 |
| Weight density term (kN/m$^2$) | 44 |
| Bearing pressure, $R_d/A'$ (kN/m$^2$) | 3 636 |
| Bearing resistance, $R_d$ (kN) | 11 374 |
| Vertical force, $V_d$ (kN) | 972 |
| $R_d/V_d \geq 1$ | 12 |

## Settlement

| **Parameters for settlement calculations** | |
|---|---|
| Area, $A$ (m$^2$) | 23.758 |
| Distance furthest from NA, $y$ (m) | 2.750 |
| Moment of inertia, $I$ (m$^4$) | 44.918 |
| Maximum pressure, $q_{max}$ (kPa) | 73.554 |
| Minimum pressure, $q_{min}$ (kPa) | 16.972 |

| **Material parameters** | **Characteristic material properties, $f_k$** | **Partial material factors, $\gamma_m$** | **Design resistance, $R_d$** |
|---|---|---|---|
| Elastic modulus, $E$ (GPa) | 10.00 | 1.0 | 10.00 |
| Shear modulus, $G$ (GPa) | 4.76 | 1.0 | 4.76 |
| Poisson's ratio, $\nu$ | 0.05 | 1.0 | 0.05 |
| **Superstructure loads acting on foundation (SLS)** | **Nominal loads, $Q_n$** | **Partial load factors, $\gamma_f$** | **Design loads, $Q_d$** |
| Vertical force, $F_Z$ (kN) | 474 | 1.0 | 474 |
| Radial force, $F_R$ (kN) | 20 | 1.0 | 20 |
| Bending moment, $M_R$ (kNm) | 440 | 1.0 | 440 |
| Weight of foundation, $W$ (kN) | 601 | 1.0 | 601 |

| **Design loads, $Q_d$** | |
|---|---|
| Design vertical force, $V_d$ (kN) | 1 075 |
| Design moment, $M_d$ (kNm) | 462 |
| **Stiffness, displacement and rotation** | |
| Vertical stiffness, $k_z$ ($10^4$ kN/mm) | 5.514 |
| Displacement, $\delta$ (mm) | 0.020 |
| Rotational stiffness, $k_\theta$ ($10^8$ kNm/rad) | 2.780 |
| Rotation, $\theta$ (arcseconds) | 0.343 |

# Appendix F

# Drawings

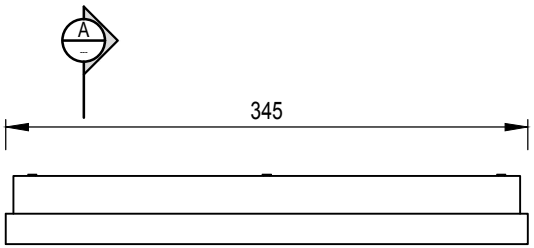


ELEVATION
SCALE 1:5

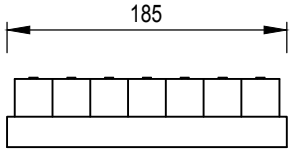


SIDE VIEW
SCALE 1:5

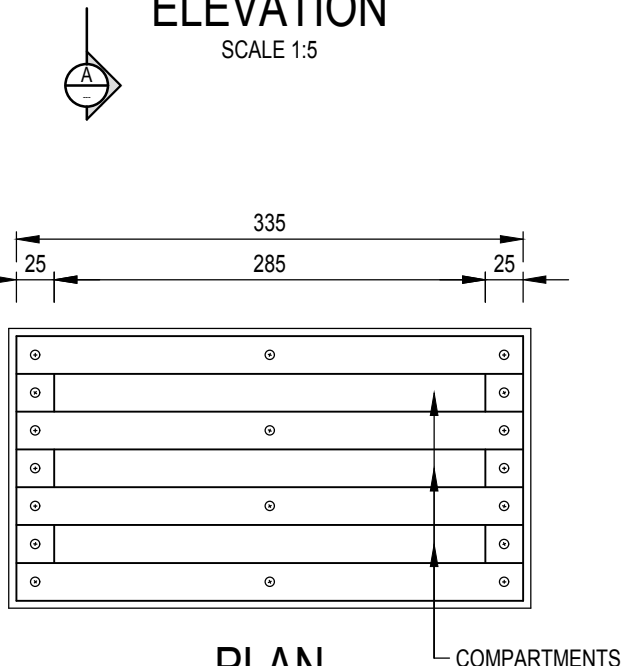


PLAN
SCALE 1:5

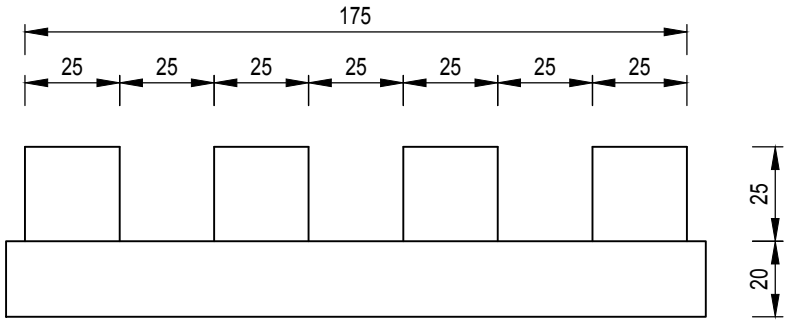


SECTION A-A
SCALE 1:2

| | | | | |
|---|---|---|---|---|
| DESIGNED BY | | THESIS TITLE | | DRAWING TITLE |
| CJT JANSE VAN RENSBURG | | SITE CHARACTERIZATION AND FOUNDATION DESIGN FOR THE EMPLACEMENT OF RADIO TELESCOPE ANTENNAS AT THE MATJIESFONTEIN SPACE GEODESY OBSERVATORY | | MOULD DETAILS |
| REVIEWED BY | | | | DRAWING DESCRIPTION |
| J VAN DER MERWE | | | | MOULDS TO BE CONSTRUCTED FOR THE MORTAR-BAR TEST |
| DRAWN BY | | | | |
| CJT JANSE VAN RENSBURG | | | | |

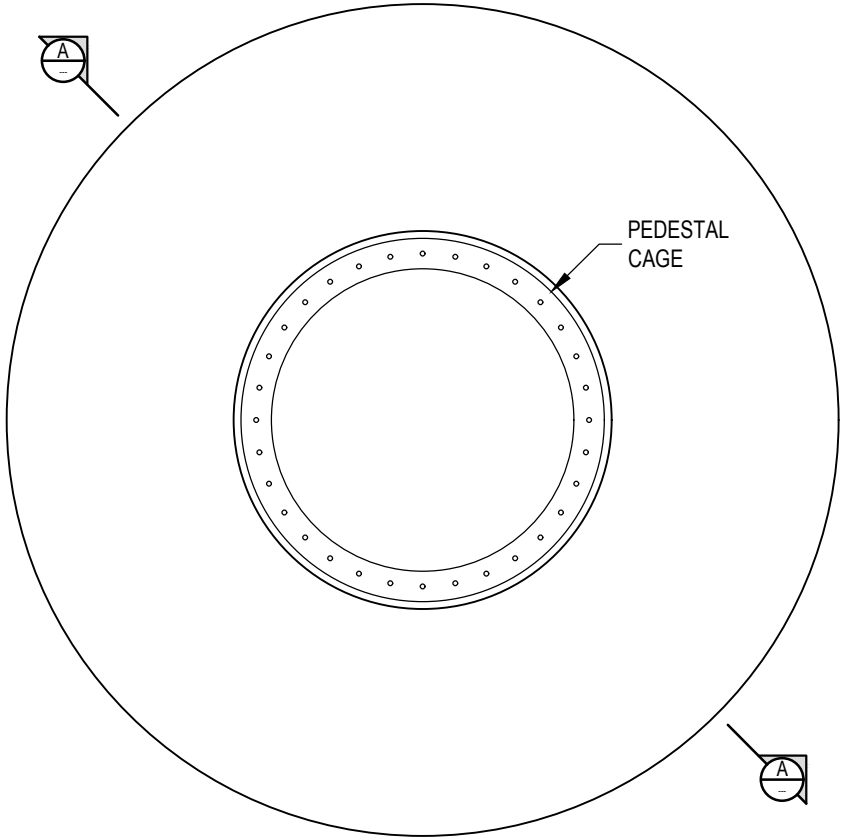


PLAN
SCALE 1:50

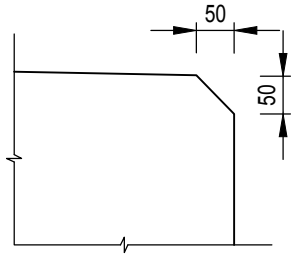


CHAMFER DETAIL
SCALE 1:10

NOTES

1. CONCRETE CLASS TO BE W40/19
2. TOP OF CONCRETE TO HAVE A SMOOTH SURFACE FINISH
3. LOAD CONCENTRATION FACTORS CAN BE USED FOR DETERMINING THE REQUIRED RADIAL AND CONCENTRIC REINFORCEMENT
4. REINFORCEMENT TO BE TIED IN WITH THE PEDESTAL CAGE TO ENSURE ADEQUATE LOAD TRANSFER
5. COVER TO REINFORCEMENT 75mm
6. PROVISION NEEDS TO BE MADE FOR THE RADIO-TELESCOPE TO BE ADEQUATELY EARTHED AGAINST LIGHTNING

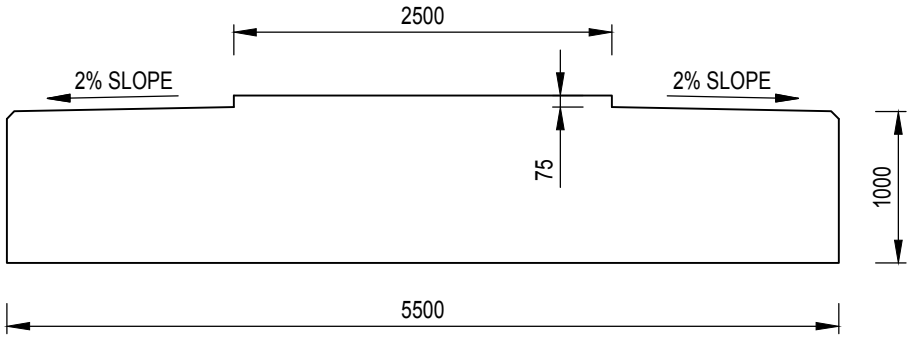


SECTION A-A
SCALE 1:50

| | | | | |
|---|---|---|---|---|
| DESIGNED BY | | THESIS TITLE | | DRAWING TITLE |
| CJT JANSE VAN RENSBURG | | SITE CHARACTERIZATION AND FOUNDATION DESIGN FOR THE EMPLACEMENT OF RADIO TELESCOPE ANTENNAS AT THE MATJIESFONTEIN SPACE GEODESY OBSERVATORY | | FOUNDATION DETAILS |
| REVIEWED BY | | | | DRAWING DESCRIPTION |
| PW DAY | | | | DETAILS FOR A SKA-TYPE RADIO TELESCOPE AT THE MSGO |
| DRAWN BY | | | | |
| CJT JANSE VAN RENSBURG | | | | |

# Appendix G

# Photo Report

**View of site entrance to the north**

**View over main study area**

**View over main study area**

**View of mountain to the south**


**Setting up the drilling equipment**

**Extensions added for next drill run**

**Beginning of drill run**

**Maximum depth of core recovered**

**Northern channel upstream view**

**Southern channel upstream view**

**Northern channel downstream view**

**Southern channel downstream view**

**Mortar-bar mould**


**Dial gauge used for measuring expansion**


**Perspex containers**

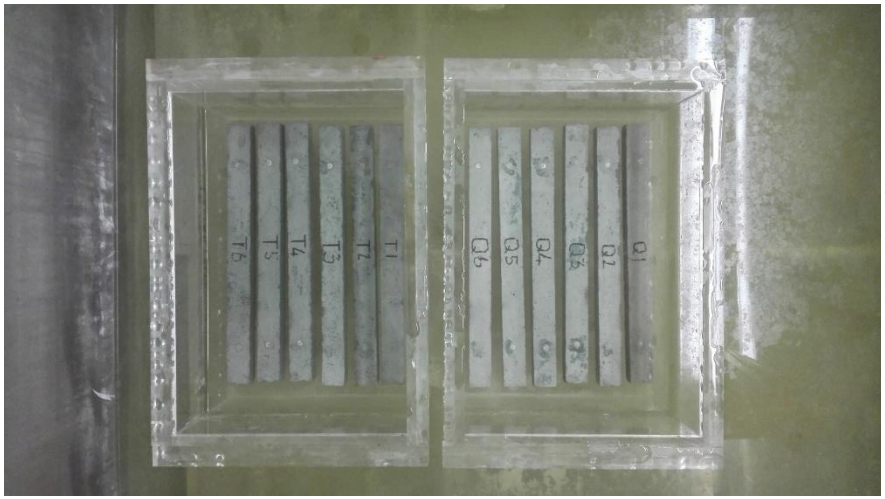


**Mortar-bars inside containers in tank**